**NTNU – Trondheim**
Norwegian University of
Science and Technology

# The Efficiency of a Mewis Duct in Waves

Rolf Arild Topphol

Marine Technology (2 year)
Submission date: June 2013
Supervisor: Sverre Steen, IMT

Norwegian University of Science and Technology
Department of Marine Technology

NTNU
Norwegian University of Science and Technology
Department of Marine Technology

# MASTER THESIS

| **Title:** | **Delivered:** |
|---|---|
| **The Efficiency of a Mewis Duct in Waves** | 06.06.2013 |
| | **Availability:** |
| | Open |
| **Student:** | **Number of pages:** |
| Rolf Arild Topphol | 72 |

**Abstract:**

In this thesis, the efficiency of a Mewis Duct in waves has been investigated with the use of model tests in the large towing tank at MARINTEK in Trondheim. A "load-varying" self-propulsion method was used, allowing for calculations without the need for results from a resistance test. Still water, regular and irregular wave conditions have been tested. The vessel model used, M3030 A, was originally used to test the Mewis Duct in still water.

Results in still water have been compared to the original test results. Deviations from the original tests have been found, which could be due to increased resistance of the model and bias in the tow force and thrust measurements.

Results in regular waves show a consistent increase in the effective wake with the Mewis Duct fitted, but the thrust deduction contains a high amount of scatter. This results in scatter in the hull efficiency, and further in the propulsive efficiency.

Uncertainty analysis has been carried out and shows that scatter in the tow force are probably the reason for inaccurate results. It indicates the necessity of accurate measurements of the tow force with the load-varying self-propulsion method.

**Keyword:**

| |
|---|
| Mewis-Duct |
| Efficiency |
| Wake |

**Advisor:**

Sverre Steen

Address:
NTNU
Department of Marine Technology
N-7491 Trondheim

Location
Marinteknisk Senter
O. Nielsens vei 10

Tel. +47 73 595501
Fax +47 73 595697

## Sammendrag

I denne avhandlingen, har effekten av en “Mewis Duct” i bølger blitt undersøkt ved hjelp av modellforsøk i den store modelltanken ved MARINTEK i Trondheim. En "last-varierende" propulsjonsmetode ble tatt i bruk, som gjør at beregninger kan bli foretatt uten behovet for data fra motstandstester. Propulsjon i stille vann, regelmessige og uregelmessige bølgeforhold har blitt foretatt. Modellen benyttet, M3030 A, ble opprinnelig brukt til modellforsøk av “Mewis Duct” i stille vann.

Resultater fra stille vann har blitt sammenlignet med de opprinnelige testresultatene. Avvik fra de originale testene har blitt funnet, noe som kan skyldes økt motstand av modellen og bias i thrust- og momentmålinger.

Resultater i regulære bølger viser en konsekvent økning i medstrøm med “Mewis Duct” montert, mens thrustreduksjonen inneholder høy spredning. Dette resulterer i spredning i skrogvirkningsgraden, og videre i propulsjonsvirkningsgraden.

En usikkerhetsanalyse er gjennomført og viser at spredning i slepekraften trolig er årsaken til unøyaktige resultater. Det indikerer nødvendigheten av nøyaktige målinger av slepekraft med den last-varierende testmetoden.

# MASTER THESIS IN MARINE TECHNOLOGY

## SPRING 2013

## FOR

## Rolf Arild Topphol

## The efficiency of a Mewis duct in waves

Both due to environmental concerns and increasing fuel prices there is an increasing demand for energy saving in the international shipping fleet. Thus, there is a renewed interest in so-called energy saving devices. There is a large sub-group of these devices which are related to the propeller and the area around the propeller, and the current project focus on this sub-group. An example of such a device, which has gotten quite a lot of attention and some popularity in the market recently, is the so-called Mewis duct, which is a combination of a wake-equalizing duct and pre-swirl fins. Power-saving in the order of 5% is reported, but mainly in calm water. The most reliable estimates of power saving are obtained in very carefully executed model tests, and so far these have been performed only in calm water. However, it is known that when the ship operates in waves the flow into the propeller changes quite significantly. Thus, it is expected that waves might influence the efficiency of the Mewis duct. Therefore, the objective of the master thesis is to investigate and document through model testing how the efficiency of a Mewis duct change when subject to waves. The primary activity will be a model test of one particular vessel, belonging to Solstad Shipping. The model test will be carried out in the spring term, as part of the master thesis. The master thesis is a part of the research project Energy Management in Practice II (EMIP II).

The master thesis should address the following issues:

- Give a short introduction to the Mewis duct, and how it compares to other energy devices. Document what is known about efficiency gain with use of Mewis duct.
- Discuss how speed loss and change of propulsive factors due to waves can be assessed, in general and in particular by using model tests.
- Make a detailed plan for the model tests
- Co-operate with the workshop and laboratories at MARINTEK in the preparations for the tests.
- Perform the model tests with assistance from technicians from MARINTEK and/or NTNU.
- Analyze the model test results to determine the influence of waves on the efficiency of the Mewis duct. Also determine the efficiency of the duct in calm water with the current set-up as a necessary reference.
- Discuss and conclude regarding how waves influence the efficiency of a Mewis duct.

In the thesis the candidate shall present his personal contribution to the resolution of problem within the scope of the thesis work.

Theories and conclusions should be based on mathematical derivations and/or logic reasoning identifying the various steps in the deduction.

The candidate should utilize the existing possibilities for obtaining relevant literature.

The thesis should be organized in a rational manner to give a clear exposition of results, assessments, and conclusions. The text should be brief and to the point, with a clear language. Telegraphic language should be avoided.

The thesis shall contain the following elements: A text defining the scope, preface, list of contents, summary, main body of thesis, conclusions with recommendations for further work, list of symbols and acronyms, reference and (optional) appendices. All figures, tables and equations shall be numerated.

The supervisor may require that the candidate, in an early stage of the work, present a written plan for the completion of the work. The plan should include a budget for the use of computer and laboratory resources that will be charged to the department. Overruns shall be reported to the supervisor.

The original contribution of the candidate and material taken from other sources shall be clearly defined. Work from other sources shall be properly referenced using an acknowledged referencing system.

The thesis shall be submitted in the DAIM portal http://daim.idi.ntnu.no/
The submitted thesis shall be:

- Signed by the candidate
- The text defining the scope included
- Drawings, computer code and other deliverables that don't fit in the thesis can be uploaded as electronic appendices.

Supervisor : Professor Sverre Steen
Start : 14.01.2013
Deadline : 10.06.2013

Trondheim, 18.01.2013

Sverre Steen
Supervisor

## Preface

This master thesis is a part of the fulfillment requirements to obtain the degree of Master of Science in Marine Technology from the Norwegian University of Science and Technology (NTNU). The work was carried out in the spring semester in 2013.

The thesis is allso part of the research program Energy Management in Practice II (EMIP II) which seeks to reduce fuel consumption and thus CO2 emission through improving energy efficient ships in a practical and cost efficient way. I would like to thank the participants for providing information regarding the Mewis Duct and for the constructive feedback in the session in the middle of the semester.

I would like to thank the students who I share office space with, who are all in the same situation and responsible for a positive work environment. They have also helped with technical insight of the softwares used in the thesis, MATLAB, Excell and Word.

The technicians I worked with for the model tests in the MARINTEK towing tank have been helpful, and I want to thank them for an interesting, educational and pleasant stay.

Last I would like to thank my supervisor Prof. Sverre Steen for all the help and constructive feedback he have given me during the semester.

Trondheim, June 6th, 2013

_____

Rolf Arild Topphol

# Contents

1 Introduction ..... 1

2 Working Principles of Energy Saving Devices ..... 3

2.1 Energy Loss around a Rotating Propeller ..... 3

2.1.1 Axial Loss ..... 3

2.1.2 Rotational Loss ..... 4

2.1.3 Frictional Loss ..... 4

2.1.4 Hull Interaction Losses ..... 4

2.2 Energy Saving Devices ..... 5

2.2.1 Ducts and Tunnels ..... 5

2.2.2 Fins and Fin Systems ..... 5

2.2.3 Rudder Bulbs ..... 6

2.2.4 Rotating Devices ..... 6

2.2.5 Combination of Principles ..... 6

3 The Mewis-Duct ..... 7

3.1 Design ..... 7

3.2 Power Saving ..... 8

3.3 Model Test Results ..... 9

3.4 Full Scale Trial Results ..... 10

4 Speed Loss and Propulsive Factors due to Waves ..... 11

4.1 Change of Open Water Characteristics ..... 11

4.2 Change of the Wake ..... 12

4.3 Change of Thrust Deduction ..... 12

4.4 Change of Relative Rotative Efficiency ..... 13

4.5 Speed Loss and Propulsive Factors in Waves using Model Test Results ..... 14

5 Model Test Procedure ..... 15

5.1 Open Water Test ..... 15

5.1.1 Data Reduction Equations ..... 15
5.2 Propulsion Tests ..... 17
5.2.1 Load Varying Self-Propulsion Test ..... 17
5.2.2 Thrust and Torque Correction ..... 17
5.2.3 External Tow Force ..... 18
5.2.4 Propeller Hull Interaction ..... 20
5.3 Seakeeping Tests ..... 24
5.3.1 Test Requirements ..... 24
5.3.2 Test Procedure ..... 24
5.4 Resistance Test ..... 25
6 Model Test of Becker Mewis Duct ..... 26
6.1 Test Set-Up ..... 26
6.1.1 Test Arrangement ..... 26
6.1.2 Hull Model ..... 27
6.1.3 Becker Mewis Duct Model ..... 29
6.1.4 Propeller Model ..... 30
6.2 Instrumentation ..... 31
6.3 Environmental Conditions ..... 31
6.3.1 Wave Calibration ..... 31
6.4 Test Program ..... 33
6.4.1 Decay Tests ..... 33
6.4.2 Calm Water Propulsion ..... 33
6.4.3 Propulsion in Regular Waves ..... 34
6.4.4 Propulsion in Irregular Waves ..... 35
7 Results and Analysis ..... 36
7.1 Surge Decay Test ..... 36
7.2 Calm Water Propulsion ..... 37

7.2.1 Initial Results ..... 37
7.2.2 Propulsive Factors ..... 40
7.2.3 Propulsive Efficiency ..... 42
7.2.4 Powering Prediction ..... 43
7.3 Propulsion in Regular Waves ..... 45
7.3.1 Pitch and Heave Motion in Regular Waves ..... 45
7.3.2 Initial Results ..... 47
7.3.3 Propulsive Factors ..... 49
7.3.4 Propulsive Efficiency ..... 53
7.3.5 Powering Prediction ..... 56
7.4 Propulsion in Irregular Waves ..... 59
7.4.1 Initial Results ..... 59
7.4.2 Propulsive Efficiency ..... 60
7.4.3 Influence of Thrust Deduction ..... 61
7.5 Repeatability ..... 63
7.5.1 Precision Limit ..... 63
7.5.2 Error Propagation in the calculated thrust deduction ..... 66
8 Discussion of Error Sources ..... 69
9 Conclusion and Recommendations ..... 70

## List of Figures

Figure 1 Principle sketch of the Mewis-Duct, Mewis and Guiard (2011) ..... 7
Figure 2: Possible power reductions by the PSD, Mewis (2009) ..... 8
Figure 3: Power savings with Mewis Duct from propulsion tests, Mewis (2012) ..... 9
Figure 4: Open Water Diagram for P-1099, reproduction from Alterskjær (2012). ..... 16
Figure 5: Plotted polynomial for torque correction ..... 18
Figure 6: Plotted polynomial for thrust correction ..... 18
Figure 7: Plotted polynomial for J versus Kt ..... 21
Figure 8: Plotted polynomial for Kq versus J ..... 21
Figure 9: T-F diagram including severe overloading, Holtrop (2001) ..... 22
Figure 10: Schematic of model test set-up, Steen (2012). ..... 26
Figure 11: Force transducers located at each beam end ..... 26
Figure 12: Model M3030 A, aft view ..... 28
Figure 13: Becker Mewis Duct model ..... 29
Figure 14: Becker Mewis Duct model fitted to M3030 A ..... 29
Figure 15: Stock propeller P-1099 ..... 29
Figure 16: T-F diagram illustrating the linearity between thrust and tow force ..... 38
Figure 17: Model resistance calculated with Becker Mewis Duct in calm water ..... 38
Figure 18: Model resistance calculated without Becker Mewis Duct in calm water ..... 39
Figure 19: Wake fraction versus model velocity in calm water ..... 41
Figure 20: Thrust deduction versus model velocity in calm water ..... 41
Figure 21: Propulsive efficiency versus model velocity in calm water ..... 43
Figure 22: Difference in brake power in still water with and without Becker Mewis Duct fitted ..... 44
Figure 23: RAO for heave ..... 45
Figure 24: RAO for pitch ..... 46
Figure 25: Thrust deduction versus wave length for $V_S$=15 [knots] ..... 50
Figure 26: Effective wake versus wave length for Vs=15 [knots] ..... 50
Figure 27: Thrust deduction versus wave length for Vs=17 [knots] ..... 52
Figure 28: Effective wake versus wave length for Vs=17 [knots] ..... 52
Figure 29: Propulsive efficiency versus wave length to ship length ratio in regular waves at Vs = 15 [knots] ..... 54

Figure 30: Propulsive efficiency versus wave length to ship length ratio in regular waves at Vs = 17 [knots] ..... 55
Figure 31: Brake power versus wave length to ship length ratio for H = 4.03 [m] at VS = 15 [knots]..... 57
Figure 32: Brake power versus wave length to ship length ratio for H = 4.03 [m] at VS = 17 [knots]..... 58
Figure 33: Influence of thrust deduction on the propulsive efficiency ..... 62
Figure 34: The weight t for estimating confidence intervals using Student's t distribution, Steen (2012) ..... 64

## Nomenclature

### Symbols

| | |
|---|---|
| $\eta_D$ | Propulsive efficiency |
| $\eta_0$ | Open water efficiency |
| $\eta_H$ | Hull efficiency |
| $\eta_R$ | Relative rotative efficiency |
| $\eta_i$ | Ideal efficiency |
| $\eta_r$ | Efficiency accounting for fluid rotation |
| $\eta_f$ | Efficiency accounting for blade friction |
| $\zeta_{mom}$ | Momentum loss |
| $C_T$ | Thrust loading coefficient |
| $T$ | Thrust |
| $Q$ | Torque |
| $P$ | Power |
| $K_T$ | Thrust coefficient |
| $K_Q$ | Torque coefficient |
| $n$ | Propeller revolutions |
| $w$ | Wake fraction |
| $w_p$ | Potential wake |
| $t$ | Thrust deduction |
| $t^*$ | "True" thrust deduction |
| $k$ | Form factor |
| $J_A, J_0, J$ | Advance ratio |
| $A_P$ | Propeller disk area |
| $D$ | Propeller diameter |
| $R$ | Propeller radius |
| $V$ | Velocity in general |
| $U$ | Velocity in general |
| $F_D, F$ | Tow-rope force |
| $R_T$ | Resistance |
| $L$ | Length unit |
| $\lambda$ | Scaling factor |
| $\Delta p$ | Pressure gradient |
| $\eta_i$ | Motion amplitude in degree of freedom i |
| $C_B$ | Block coefficient |
| $h$ | Distance between propeller shaft center and water surface |
| $\beta$ | Thrust diminution factor |
| $\eta_{R\zeta}$ | Relative vertical motion amplitude |
| $F_n$ | Froude number |
| $R_n$ | Reynolds number |
| $m$ | Empirical constant |
| $r$ | Radius of gyration |
| $\rho$ | Mass density |
| $g$ | Acceleration of gravity |

### Wave data

| | |
|---|---|
| $\zeta_a$ | Wave amplitude |
| $\lambda$ | Wave length |
| $\omega$ | Circular frequency |
| $\omega_0$ | Wave circular frequency |

| | |
|---|---|
| $\omega_e$ | Circular frequency of encounter |
| $k$ | Wave number $\frac{\omega^2}{g}$ |
| $H$ | Wave height |
| $T$ | Period |

**Symbols in uncertainty analysis**

| | |
|---|---|
| s | Standard deviation |
| n | Number of observations |
| $q_k$ | Observed quantity |
| $\bar{q}$ | Mean value |
| P | Precision limit |
| t | Weight from Student's t distribution |
| X | True value for which uncertainty is sought |
| $Y_i$ | Parameters which X depends on |
| $\Delta Y_i$ | Error of parameter $Y_i$ |
| $X$ | Resultfromthe measurement |
| $\kappa_i$ | Influence coefficient |
| $e_i$ | Elemental error |
| e | Combined error |

**Sub-indices**

| | |
|---|---|
| m | Model |
| s | Ship |

# 1 Introduction

Considering the continuously rising fuel oil prices and the increasing awareness of the environmental conditions, energy saving is of high priority, and Energy Saving Devices (ESD) for propellers and propulsors has gained renewed attention. ESD's are flow-directing devices placed near or at the propeller. These can either be active systems, such as contra-rotating propellers and the Grim vane wheel, or passive systems such as various ducts and tunnels, fins and fin systems and rudder bulbs.

The Mewis Duct is an ESD placed in front of the propeller, and is targeting individual loss factors by combining two different principals to reduce the energy loss. The duct is built up by two components; a wake-equalizing duct for equalization of the flow created by the hull towards the propeller, and a set of pre-swirl fins to generate a swirl in the flow in the opposite direction of the propeller to reduce the rotational losses. The duct to propeller radii is also optimized to create a higher loading at the inner radii of the propeller area to reduce the hub-vortices.

The Mewis Duct have been model tested in several model tank facilities, and energy savings in the order of 5% have been reported depending on vessel type and loading condition. Former tests have only been conducted in still water conditions, and due to what is known about added resistance, speed loss and change of propulsive factors in waves it have been questioned whether such benefit is present in waves. Especially the modification of the wake field in waves is expected to be of importance as it is an important part of the Mewis Duct. Full scale trials of the Mewis Duct have also been carried out, with varying or inconclusive results, which can either come from inaccurate measurements, or that there is a cancelation of the efficiency gain in waves. In an attempt to aquire accurate data regarding the efficiency in waves, model self-propulsion tests is conducted, with and without the Mewis Duct fitted, in the large towing tank at MARINTEK in Trondheim, Norway.

Since the expected energy saving with the Mewis Duct is in the order of 5% and could be smaller or even canceled in waves, a careful execution of the model test setup is of importance. The conditions tested should be as equal as possible with and without the Mewis Duct fitted to obtain comparable results.

This master thesis is part of the project Energy Management in Practice  phace II (EMIP II), which stand for the financing of the model tests conducted at MARINTEK. The EMIP II project is controlled by the socalled WG 5 cooperation, consisting of 5 shipping companies; Klavness Ship Management AS, Wilh. Wilhelmsen AS, BW Gas AS, Grieg Star Shipping AS and Solvang ASA. The project group have also joined forces with MARINTEK. It is a User controlled Innovation Project (UIP) supported by the Research Council of Norway, with a budget of 10.5 MNOK and the period of execution started September 2011 and is planned finished September 2013. The goal of the project is to reduce fuel consumption and thus CO2 emission through improving energy efficient ships in a practical and cost efficient way as a contribution towards the NSA environmental vision “zero harmful emissions to air and sea”.

# 2 Working Principles of Energy Saving Devices

A more comprehensive literature study of the topic in this section was carried out in the project thesis in the fall semester of 2012, Topphol (2012).

## 2.1 Energy Loss around a Rotating Propeller

To understand the working principles of the Mewis Duct and other energy saving devices in general, knowledge of the energy losses the devices target to improve is needed. Around a working propeller behind the stern of a ship there are many factors contributing to energy loss, and hence a loss of propulsive efficiency. The losses around a rotating propeller can be divided in axial losses considering the ideal efficiency, rotational losses in the slip-stream rotation, hub vortices and tip vortices, frictional losses due to the roughness of the propeller blades and other propulsor parts and appendages and the losses related to the propeller to hull interaction effects.

According to Molland et al. (2011) the effects on the various components of the quasi-propulsive coefficient $\eta_D$ need to be considered:

$$\eta_D = \eta_0 \eta_H \eta_R \tag{2.1}$$

where $\eta_0$ is the open water efficiency, $\eta_H$ is the hull efficiency and $\eta_R$ is the relative rotative efficiency.

$\eta_0$ can be considered made up of:

$$\eta_0 = \eta_i \eta_r \eta_f \tag{2.2}$$

Here $\eta_r$ accounts for losses due to fluid rotation induced by the propeller, and $\eta_f$ accounts for losses due to blade friction drag. The breakdown of the components will indicate where savings can be made.

### 2.1.1 Axial Loss

For high propeller loadings, the axial loss is the largest factor, and is due to the axial velocity increase required for thrust generation. The axial loss is calculated according to Steen (2012):

$$\zeta_{mom} = 1 - \eta_i \tag{2.3}$$

Based on axial momentum theory the loss expressed through the ideal efficiency is derived as:

$$\eta_i = \frac{2}{1+\sqrt{1+C_T}} \tag{2.4}$$

where the thrust loading coefficient $C_T$ is defined as:

$$C_T = \frac{T}{\frac{1}{2}\rho A_p V^2} \tag{2.5}$$

where $A_p$ is the propeller disk area and $T$ is the thrust.

### 2.1.2 Rotational Loss

Rotational losses are due to the induced tangential and swirling velocities in the slip-stream of the propeller which leads to lost kinetic energy. These losses can be reduced by reducing the swirl, either by pre-swirling the flow in the opposite direction towards the propeller, or to convert the swirling velocities behind the propeller to axial velocities and by that generating thrust.

### 2.1.3 Frictional Loss

Frictional losses are due to the frictional resistance of the propeller blades and other components, like ducts or fins. The losses from frictional resistance on the blades are a significant contribution due to the high velocities involved. It is important to consider especially when the propeller loadings are low.

### 2.1.4 Hull Interaction Losses

Hull interactional losses are a very complex and not very precise form of loss contribution, and more or less results in the three types of losses described above. The most important contributions to this are the thrust deduction and the wake from the hull. The average wake tends to increase the propeller efficiency, but inhomogeneous wake will be a problem because it will lead to an uneven propeller loading which again can lead to cavitation and vibration. An uneven wake will also lead to losses because the acceleration of the flow through the propeller disk will be uneven, which relates to momentum losses. It also requires a larger margin against cavitation, which is typically requiring a larger blade area and hence increased frictional resistance.

## 2.2 Energy Saving Devices

An “Energy Saving Device” (ESD) for propulsion is a device placed at or near the propeller to increase its efficiency by targeting the energy losses explained in the previous section. There are a large variety of such devices on the market, and a brief discussion of the most common follows in this section.

### 2.2.1 Ducts and Tunnels

Various ducts and tunnels are a common form of ESD. The Schneekluth Wake-Equalizing Duct, Schneekluth (1986), is placed immediately in front of the propeller. It aims to reduce the amount of separation over the after body, by accelerating the flow in the upper part of the propeller disc which establish a more uniform inflow, and attempting to minimize the tangential velocity components in the wake field. The main effect on more slender ships is homogenous flow and vibration reduction. Power savings up to 4% have been registered for $C_T$=5, Mewis (2010). Stern tunnels, the Hitachi Zosen nozzle and integrated ducted propeller are other examples of devices developed to target improvement of the wake field, Carlton (2007). Originally, ducts were not applied to increase the efficiency, but to reduce the propeller induced vibrations by reducing the wake peak effect of pronounced V-form hulls. Ducts can also be subcategorized in axisymmetric ducts and asymmetric ducts (to compensate for uneven and inhomogeneous wake).

A propeller duct placed at the propeller increases the efficiency of highly loaded propellers, but also increases the risk of cavitation. Its frictional resistance also means that it is inefficient on low propeller loadings. Decelerating ducts are also used to reduce the risk of cavitation.

### 2.2.2 Fins and Fin Systems

Fins and fin systems are placed either in front of the propeller or on the rudder. They aim to convert vertical velocity to thrust, reducing the rotational losses. placed immediately in front of the propeller. Fins placed behind the propeller on the rudder, the boss cap or a rudder bulb aim to reduce the hub vortex losses. Thrusting fins placed on the rudder, such as the Hyundai Thrust Fin system, reduces the hub vortex losses, but can also reduce the overall tangential velocities. Fins and fin systems in front reduces the rotational losses by pre-swirling the flow into the propeller. The SVA-Pre Swirl Fin, the DSME-Pre Swirl System and reaction fins are such devices. Reaction fins is a system normally built up of six radially located fins reinforced by a slim ring nozzle. Propeller tip end-plates, Carlton (2007), suppress the tip vortices, but at

the cost of high drag due to the high tip-velocity of propellers, and it are not certain that the concept will increase the efficiency. The Kappel propeller utilizes this concept, Mewis (2009).

### 2.2.3 Rudder Bulbs

Rudder bulbs behind the propeller aim to reduce the hub vortex losses and also increase the thrust due to the displacement effect of the bulb, which eliminates the drag force on the hub and gives increased velocity in the slip-stream. Examples of rudder bulbs are the Costa-bulb, Mewis (2010), the Propac rudder with bulb from Värtsilä and the Promas system, Rolls Royce (2009), from Rolls-Royce Marine. The Promas system is also integrated with a twisted rudder to reduce the rotational losses. Efficiency gains up to 10% have been registered for such devices.

### 2.2.4 Rotating Devices

The contra-rotating propeller, Mewis (2010), developed in 1836 is a very efficient device to regain the tangential velocities in the slipstream. The downside of it is that it is very costly. Power savings up to 14% for $C_T$=5 have been registered.

The Grim vane wheel, Carlton (2007), from 1966 uses the rotational velocity in the slip-stream to run a “turbine”, which also has a propeller portion on the tips of the turbine wheel for generation of extra thrust. The device increases the total diameter of the propeller, and the turbine wheels are easily damaged due to the long and slender form.

### 2.2.5 Combination of Principles

Often the various energy-loss sources can be handled independent by combining different principles to develop new devices. Some of the above mentioned devices are such combinations. Examples are boss cap fins, the Grim vane wheel, the counter rotating propeller and the Promas system. The Mewis Duct tested in this thesis is also a combination of principles.

# 3 The Mewis-Duct

The Pre-Swirl Duct (PSD) marketed under the trademark “Mewis Duct” is named after the developer Friedrich Mewis, and developed in cooperation with Becker Marine Systems in Hamburg. It is an energy-saving device placed in front of the propeller, and a combination of a wake equalizing duct and a pre-swirl fin system. It is suited to single-screw vessels with high block coefficient and speeds up to 20 knots, such as tankers and bulk carriers of all sizes, and multi-purpose carriers and container-feeder vessels. A principle sketch of the PSD is shown in Figure 1 below.

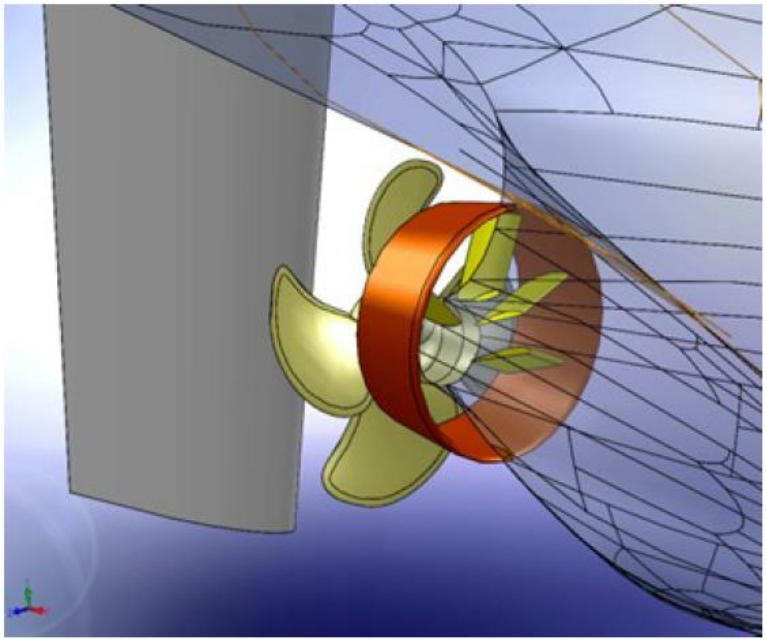

Figure 1 Principle sketch of the Mewis-Duct, Mewis and Guiard (2011)

## 3.1 Design

The purpose of the PSD is to target and improve three components of the propeller flow:

1. Equalization of the wake inflow
2. Reduction of rotational losses in the slipstream
3. Higher load at the inner radii of the propeller for reduction of the hub-vortices

The duct component equalizes the wake created by the ship hull. It is vertically offset, above the propeller shaft axis to distribute the wake equally in the upper region of the propeller area, and to distribute the wake race of the duct through a wider range towards the propeller. The duct component works as an endplate for the fins, suppressing tip-vortices from them. The effect from the increased loading on the inner radii of the propeller increases with the hub to propeller diameter ratio.

The pre-swirl fin system reduces the rotational losses. It is set up with asymmetrical arranged fins to consider the shape of the ships wake. An upward turning blade will mainly work with the wake flow, and downward turning blades are working against it, hence to get the desired pre-swirl it is required more blades turning upwards than downwards.

## 3.2 Power Saving

The best possibilities for improvement are present when the thrust coefficient $C_T$ is high and the velocity of the ship is relatively low, as can be seen from in Figure 2 taken from Mewis (2009).

The thrust coefficient is defined as:

$$C_T = \frac{T}{\frac{1}{2}\rho A_p V^2} \tag{3.1}$$

where $T$ is the thrust, $\rho$ is the water density, $A_p$ is the propeller disk area and $V$ is the velocity of the vessel.

Because of that, the PSD is best suited for smaller container vessels, small vessels with high block coefficient, such as multi-purpose carriers, and bulk carriers and tankers of all sizes. At the present stage of development the PSD is not well suited for high speed vessels, including large container vessels.

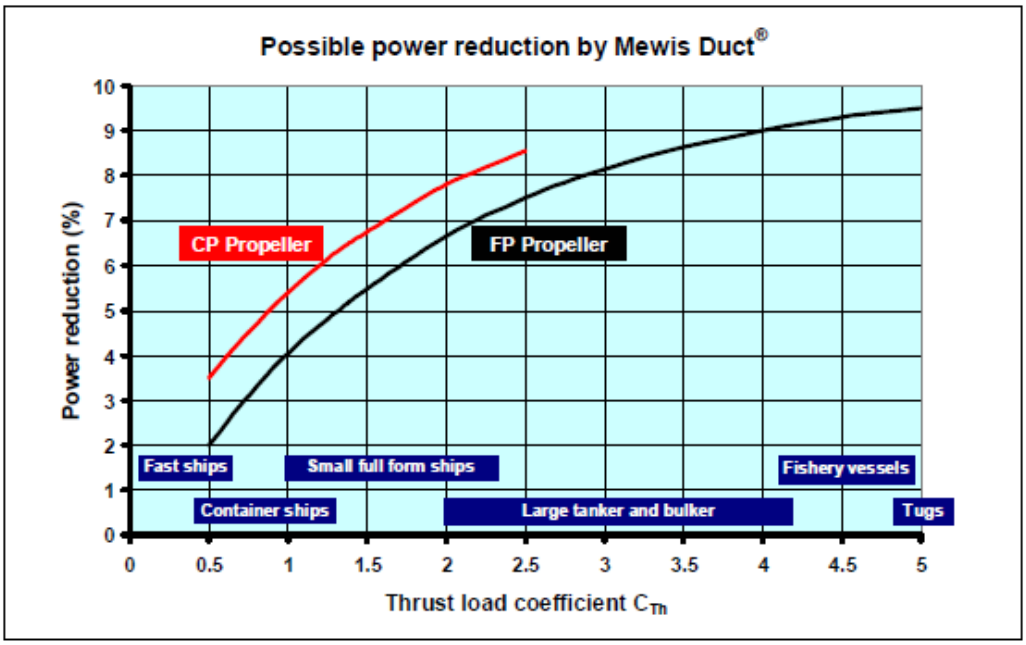


Figure 2: Possible power reductions by the PSD, Mewis (2009)

## 3.3 Model Test Results

Up until May 2012, as many as 48 projects in 8 model tanks was conducted with and without the Mewis Duct, with an average power-saving of 6.3%, Mewis (2012). Figure 3 below presents the power savings obtained from these propulsion tests, including design draught and ballast draught. The tabulated results can be found in appendix E.

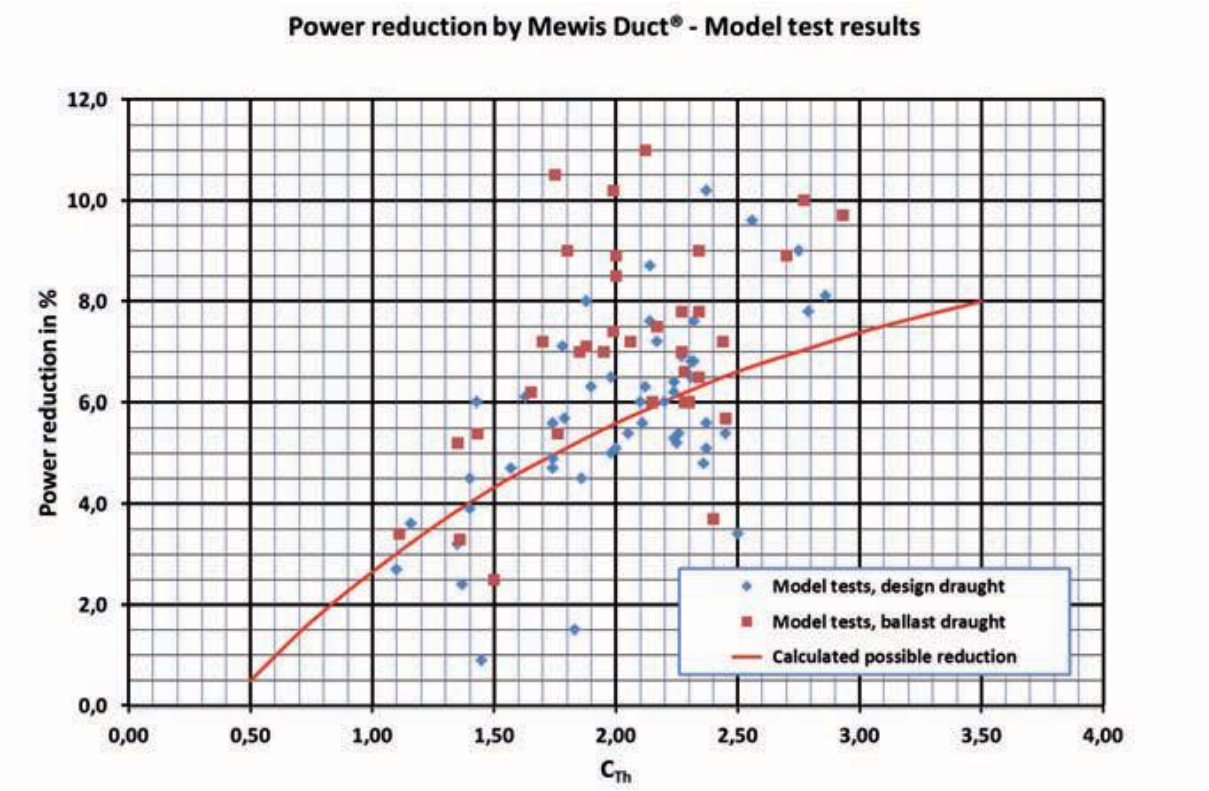


Figure 3: Power savings with Mewis Duct from propulsion tests, Mewis (2012)

## 3.4 Full Scale Trial Results

Full scale trials has also been conducted with the Mewis Duct. These have not all shown conclusive results. It has been discussed if this could be due to cancelation of the effect in waves, but might be a result of high uncertainty in the measurements.

Full scale trial results without and with the Mewis Duct was conducted in October 2010 for a bulk carrier new building, AS VINCENTIA, within 5 days of each other and under ideal comparable conditions, Mewis and Guiard (2011). 6.5% power reduction, or 0.25 [knots] higher speed at constant power was observed in this case.

In January/February 2013, results from speed trials for the sister vessels Star Istind, fitted with the Mewis Duct, and Star Ismeme, without the Mewis Duct, was executed. The two vessels was tested at near optimum comparable conditions. The conclusion was that Star Istind with the Mewis Duct fitted had a power saving in the magnitude of 6% compared to Star Ismeme in weather condition Beufort 3 or lower, Langeland (2013).

# 4 Speed Loss and Propulsive Factors due to Waves

A more comprehensive literature study of the topic in this section was carried out in the project thesis in the fall semester of 2012, Topphol (2012).

## 4.1 Change of Open Water Characteristics

When analyzing propulsion factors based on resistance and propulsion tests in waves, it is common to fit data into open water propeller diagram derived from tests with deeply immersed propeller. But the open water propeller diagram is a function of submergence, especially for h/R<1.5, where h is the distance between the propeller shaft center and the water surface and R is the propeller radius. When the propeller is oscillating in waves it might be in instantaneous positions where h/R<1.5, in particular for a ship in ballast condition, which indicates that it might be physically wrong to use an open water propeller diagram for deeply immersed propeller. It may lead to wrong conclusions about effective wake, relative rotatory efficiency and propeller efficiency. Faltinsen et al. (1980)

According to Faltinsen et al. (1980), when the propeller is working close to the free surface, it will set up a steady wave motion, which leads to a reduction in the propeller thrust. This reduction is a function of the propeller loading, and the Froude number.

Thrust and torque coefficients can be corrected for reductions in propeller submergence due to waves and ship motions with to the approximations according to Faltinsen et al. (1980):

$$K_T = \beta \cdot K_{T0} \tag{4.1}$$

$$K_Q = \beta^m \cdot K_{Q0} \tag{4.2}$$

where $K_{T0}$ and $K_{Q0}$ are thrust and torque coefficients for deeply submerged propeller, m is a factor between 0.8 and 0.85 and $\beta$ is the thrust diminution factor which can be approximated according to ITTC (2008) by

$$\beta = \begin{Bmatrix} 1 - 0.675 \cdot (1 - 0.769 \cdot h/R)^{1.258}, h/R < 1.3 \\ 1, h/R \geq 1.3 \end{Bmatrix} \tag{4.3}$$

With the submergence in still water $h_0$ and the relative vertical motion amplitude between the shaft and the water surface $\eta_{R\zeta}$ the instantaneous value of the submergence ratio can be approximated, disregarding the wave diffraction:

$$h / R = h_0 / R + (\eta_{R\zeta} \sin(\omega_e t + \varepsilon)) / R \tag{4.4}$$

Averaging $\beta$ and $\beta^m$ over one wave cycle the averaged values of thrust and torque coefficients can be written, according to Faltinsen et al. (1980), as:

$$K_T = \overline{\beta} \cdot K_{T0} \tag{4.5}$$

$$K_Q = \overline{\beta^m} \cdot K_{Q0} \tag{4.6}$$

The relative motion amplitude $\eta_{R\zeta}$ can be found both from calculation and model tests in waves.

## 4.2 Change of the Wake

Nakamura and Naito (1975), have shown that the wave induced motions of the ship is increasing the velocities of the wake. They showed in regular waves that the wake velocities increased with the wave height and that the change was more noticeable around the natural period of pitch. They also performed tests of forced motion in pitch, and could show that the velocities increased with pitch angle and frequency. Faltinsen et al. (1980) has shown a theoretical approach to help understanding this qualitatively by examining the influence of the wave induced motions on the mean pressure along the ship. Considering a flat plate as a rough model of the ship bottom and the plate is pitching harmonically. It is then possible to make a rough approximation of the mean pressure at a fixed point in the fluid due to oscillatory fluid motion

$$\Delta\overline{p} \sim -\frac{\rho}{4} \omega_e^2 \, |\eta_5|^2 \, x^2 \tag{4.7}$$

where $\omega_e$ is the circular frequency of encounter and $\eta_5$ is motion in pitch. This indicates a pressure drop from the middle of the ship towards the stern because of the pitching motion. This will cause the flow to get sucked towards the stern of the ship and hence increase the flow velocities to the propeller. Some of the consequences of this velocity increase are that the boundary layer thickness is reduced, the shear forces on the ship are changed and the separation point is delayed.

## 4.3 Change of Thrust Deduction

Nakamura and Naito (1975) made observations that the thrust deduction decreases in waves compared to still water, with a minimum around the pitch natural period. They also found that

for increasing wave height the thrust deduction decreases, but this was relatively a small change. According to Faltinsen et al. (1980), Nowacki and Sharma came to a simplified equation for the potential thrust deduction fraction in still water, by neglecting the wave induced wake and assuming uniform source distribution over the propeller disc area.

$$t = \frac{2}{1+\sqrt{1+C_T}} \frac{w_p}{1-w} \tag{4.8}$$

where

$$C_T = \frac{T_p}{\frac{\rho}{2} V_a{}^2 \pi R^2} \tag{4.9}$$

w is the effective wake, $w_p$ is the potential wake, R is the propeller radius and $V_a$ is the advance velocity

$$V_a = U(1-w) \tag{4.10}$$

If this equation is used in waves, and use the information about propeller loading in waves compared with calm water, a decrease in the thrust deduction can be found of the same order which has been measured by model testing.

## 4.4 Change of Relative Rotative Efficiency

It have been shown by Nakamura and Naito (1975), that the relative rotative efficiency $\eta_R$ sometimes may change in severe sea conditions compared to still water, with both increasing and decreasing values reported. According to Faltinsen et al. (1980), the change can sometimes be a false change because of use of open water diagram for deeply submerged propeller, but it might be real changes due to change in the wake field and propeller loading. This has been showed both theoretically and experimentally.

## 4.5 Speed Loss and Propulsive Factors in Waves using Model Test Results

In order to assess the differences in speed and propulsive coefficients in waves by model testing, propulsion tests in waves can be carried out for the same speeds as for calm water and for several wave conditions. Procedures for conducting model tests are explained in section 5.

According to ITTC (2011_1), the measurements to find the difference in the propulsive characteristics can be done by conducting self-propulsion tests in two runs with constant carriage speed:

- Estimation of the self-propulsion point in still water at a certain speed.
- Estimation of the corresponding SPP in waves.

The differences in the propulsive characteristics required to maintain the constant speed is obtained as the difference in averaged values from still water and in regular waves. Speed loss by this method can be assessed by interpolation in the results at different test conditions.

# 5 Model Test Procedure

Propulsion in still water, regular waves and irregular waves was conducted for the model M3030 A, see details of the model in section 6.1.2. Open water test results from previous model tests by MARINTEK, Alterskjær (2012), with the same stock propeller, P-1099, was used in the analysis in this thesis.

## 5.1 Open Water Test

To measure the performance of the propeller alone an open water test needs to be carried out. Propeller open water characteristics are required for use in the analysis of propulsion tests and the estimation of required power.

### 5.1.1 Data Reduction Equations

The results of the open water test are presented as dimensionless data reduction equations and presented in an open water diagram as shown in Figure 4. This is the diagram for the stock propeller P-1099, produced based on the data from the previous tests by MARINTEK, Alterskjær (2012). The reduction equations is defined according to Steen and Minsaas (2012):

$$K_T = \frac{T}{\rho n^2 D^4} \quad \text{Thrust coefficient} \tag{5.1}$$

$$K_Q = \frac{Q}{\rho n^2 D^5} \quad \text{Torque coefficient} \tag{5.2}$$

$$J_A = \frac{V_A}{nD} \quad \text{Advance coefficient} \tag{5.3}$$

$$\eta_0 = \frac{JK_T}{2\pi K_Q} = \frac{TV_A}{2\pi nQ} \quad \text{Open water efficiency} \tag{5.4}$$

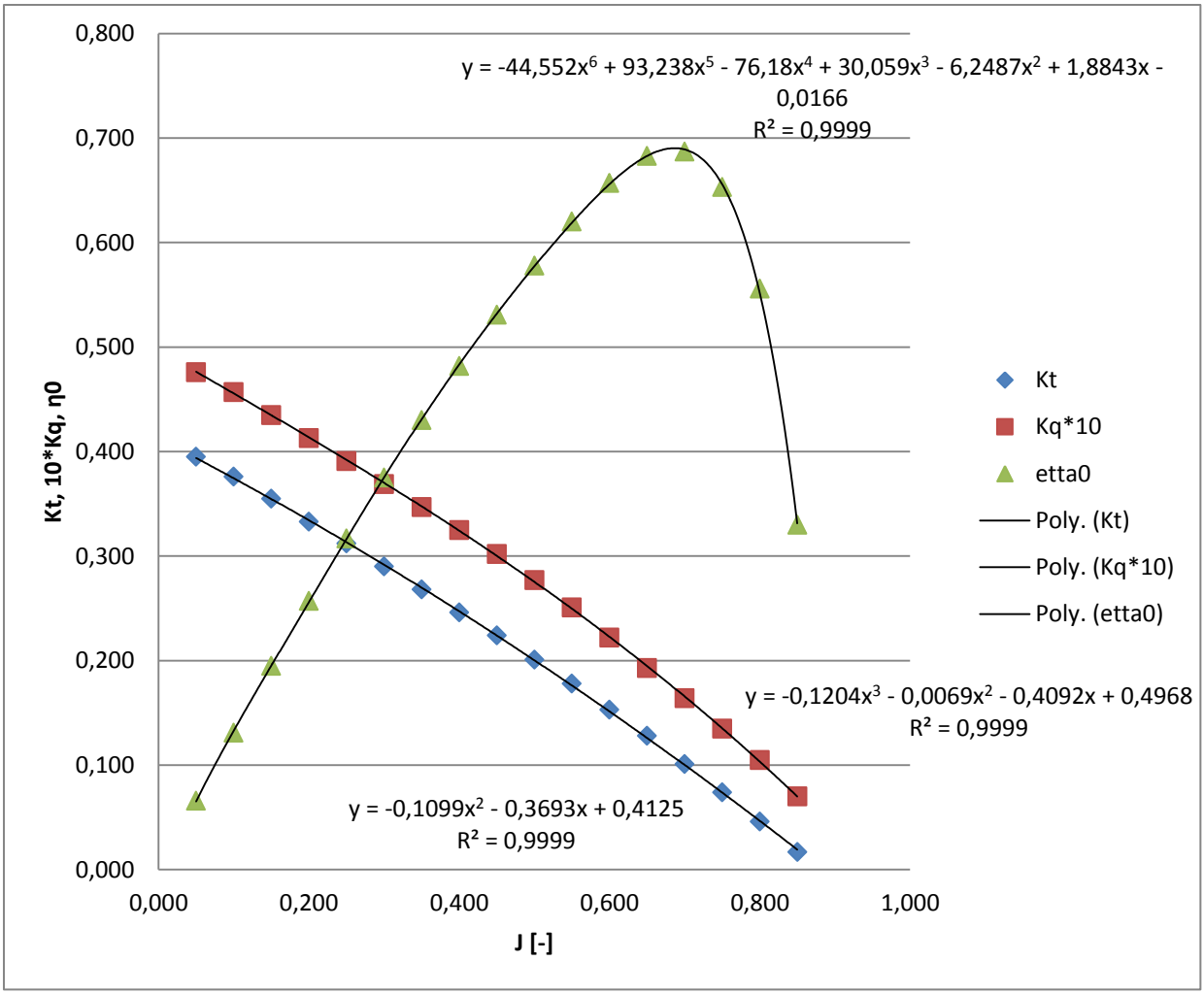


Figure 4: Open Water Diagram for P-1099, reproduction from Alterskjær (2012).

## 5.2 Propulsion Tests

A geometrically scaled propeller model is fitted and driven by an electric motor mounted inside the hull. Dynamometers are fitted inboard for measurements of thrust T, torque Q and rate of revolutions n of the propeller.

### 5.2.1 Load Varying Self-Propulsion Test

The procedure used for testing the Mewis Duct was a load varying self-propulsion procedure (constant speed). The load varying self-propulsion extrapolation procedure, proposed by Holtrop (2001), seeks to predict delivered power and propulsion factors without the need to conduct resistance tests for the model. For each constant speed at least two different constant propeller revolution settings are tested and hence two values for thrust T, torque Q and towing force $F_D$ are measured allowing for a minimum for interpolation in the results. The values at the tow force that gives the self propulsion point (SPP) corresponding to the full scale SPP is found by interpolation in the results. The rates of revolutions are chosen so that one value of the tow force are below the self propulsion point and the other is above.

### 5.2.2 Thrust and Torque Correction

Since the propeller dynamometer is fitted inside the hull for conventional shafted propellers, the friction of bearings and seals will influence the measurement of torque. This can be corrected for by measurements of idle torque for several propeller speeds, which is the measured torque with a dummy boss with identical weight as the model propeller, and then later on make corrections to the measured propeller torque by interpolation. A plot of the torque polynomial used is presented in Figure 5 below:

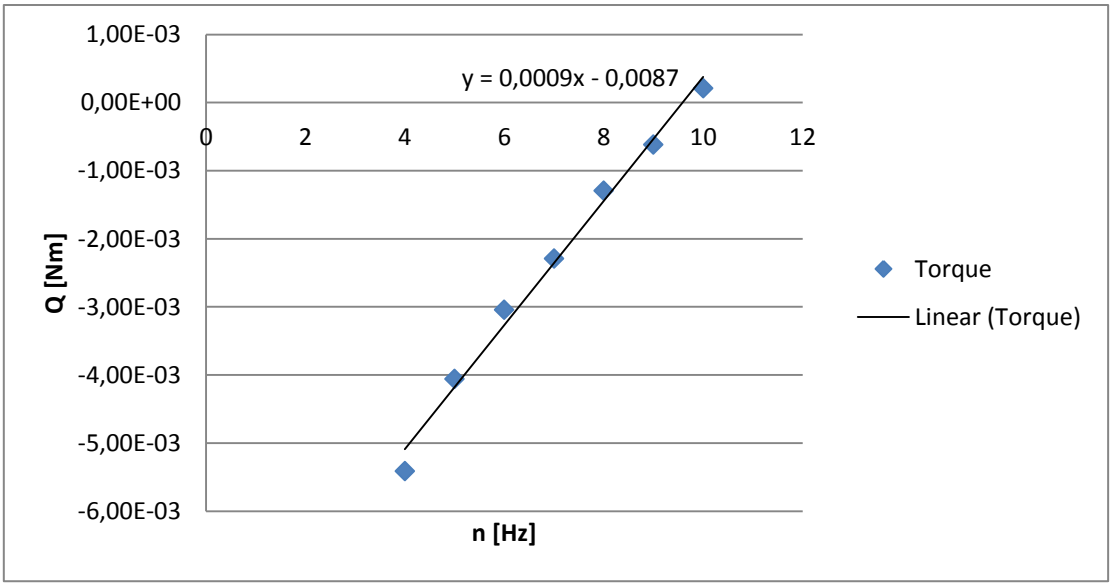


Figure 5: Plotted polynomial for torque correction

Thrust correction considers the effect the weight of the shaft and drag on the propeller hub. As with the torque correction, a dummy boss cap is placed instead of the propeller. The tests are performed at constant propeller speed and the vessel speed is varied. Torque and thrust correction has been applied in all calculations. A plot of the thrust polynomial is presented in Figure 6 below:

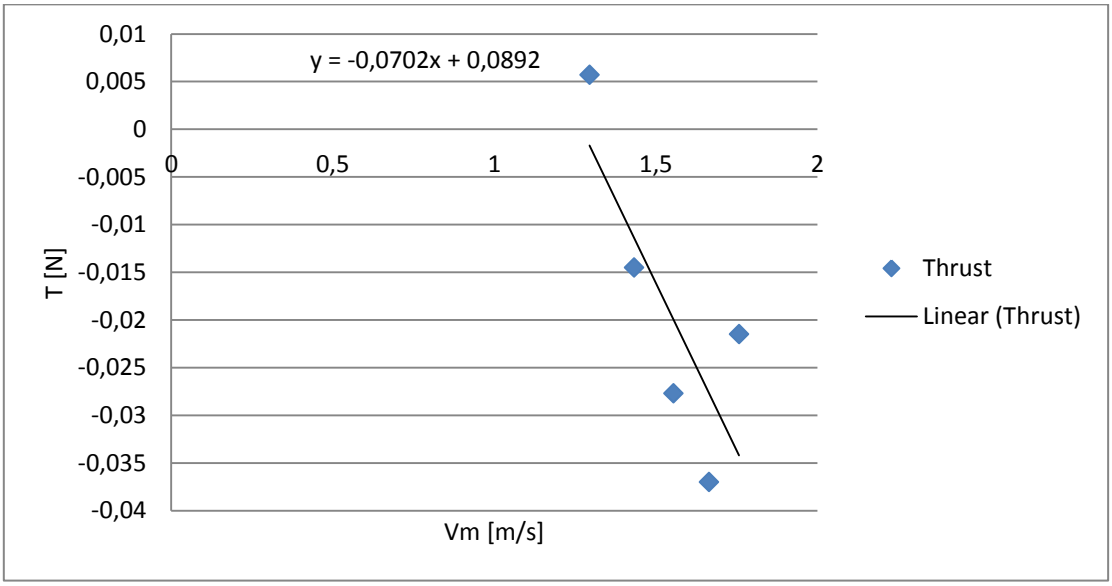


Figure 6: Plotted polynomial for thrust correction

### 5.2.3 External Tow Force

The frictional resistance coefficient is larger in model scale than in full scale. Hence a correction for this must be applied in the set-up to obtain the correct loading condition for the propeller. An external tow force $F_D$ has to be applied. Depending on the experimental

procedure adopted, the model can either be towed by a resistance dynamometer to measure the unknown external towing force during each run, “British method”, or a preselected tow force can be directly applied as a constant load, “Continental method”. In the model tests conducted for this analysis, a method alike the “British Method” was used in the way explained in section 5.2.1. The basis for the interpolasion was the calculated tow force $F_D$ from the previous tests by MARINTEK, Alterskjær (2012).

The tow force was calculated as:

$$F_D = C_S \cdot \frac{\rho_M}{2} \cdot V_M{}^2 \cdot S_M \tag{5.5}$$

where

$$C_S = (C_{Fm} - C_{Fs} - \Delta C_F) \cdot (1+k) - C_A + (C_{BDm} - C_{BDs}) + (C_{Appm} - C_{Apps}) \tag{5.6}$$

and the frictional resistance coefficients $C_{Fm}$ and $C_{Fs}$ are calculated according to the ITTC57 correlation line:

$$C_{F-ITTC57} = \frac{0.075}{(\log(R_N) - 2)^2} \tag{5.7}$$

$C_{BD}$ are the transom stern resistance coefficients and $C_{App}$ are appendage resistance coefficients.

The roughness allowance $\Delta C_F$ was calculated as:

$$\Delta C_F = (110.31 \cdot (HV_s)^{0.21} - 403.33) \cdot C_{Fs}^2 \tag{5.8}$$

where $H$ is the hull surface roughness in $\mu$($10^{-3}$mm).

The value of the correlation factor $C_A$ is the standard for the ship based on previous model tests performed in the specific facility.

The tow force should where possible be applied at $X_{CB}$ and $Z_{CB}$ to avoid artificial trim due to the force.

### 5.2.4 Propeller Hull Interaction

The interaction effects between the propeller and hull, except the thrust deduction t, is found by using the propeller open water test results in combination with the propulsion test and the resistance test if conducted. In this particular case only propulsion tests were conducted, and as mentioned in the previous section, earlier open water test results were used in the analysis. $w$, $t$, $\eta_R$ and $\eta_H$ are calculated as following:

The effective wake is the difference between the ship velocity and the apparent velocity and is defined as:

$$w = 1 - \frac{V_A}{V} = 1 - \frac{J_0}{J} \tag{5.9}$$

where $V_A$ is the apparent velocity, $V$ is the ships velocity, $J_0$ is the advance coefficient found by using "thrust identity" in the open water diagram. $K_Q$, $K_T$ and $J = \frac{V}{nD}$ values are calculated for the propulsion test. $K_T$ is entered in the open water diagram to obtain corresponding $J_0$ and $K_{Q0}$ values. The effective wake can now be rewritten as:

$$w = 1 - \frac{J_0 nD}{V} \tag{5.10}$$

Below follows plots of J and $K_Q$ polynomials used to find $J_0$ and $K_{Q0}$ from the propulsion test using thrust identity, Figure 7 and Figure 8:

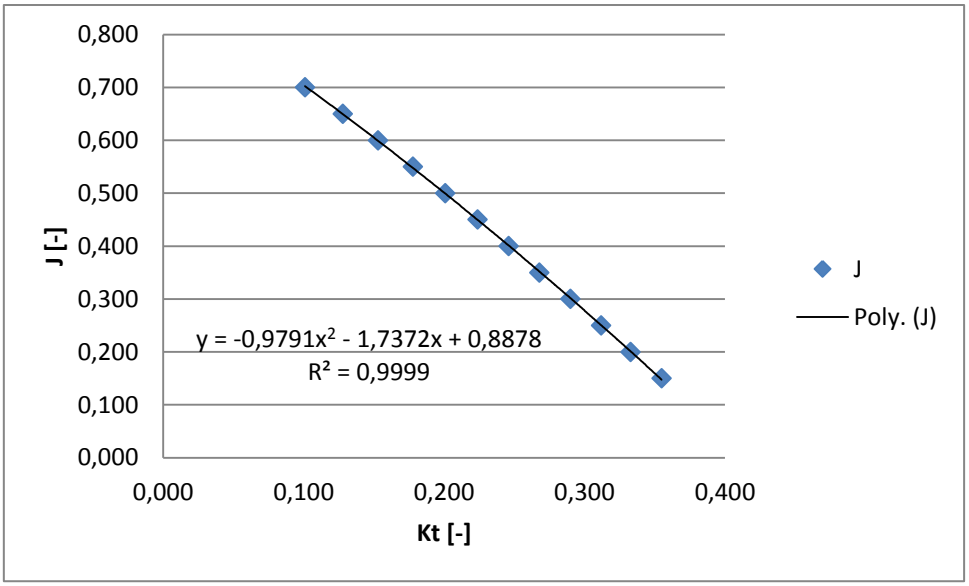


Figure 7: Plotted polynomial for J versus Kt

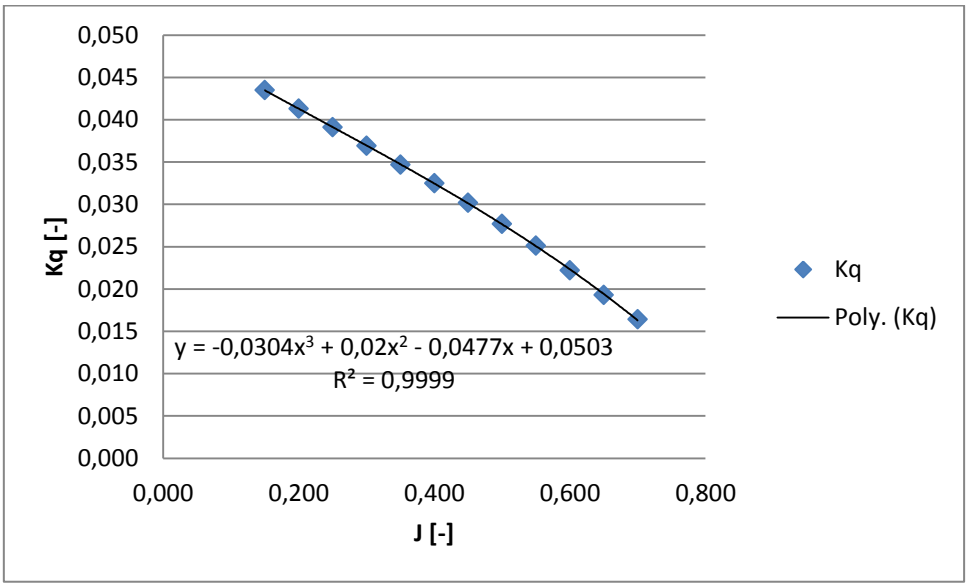


Figure 8: Plotted polynomial for Kq versus J

The thrust deduction represents a difference between the thrust and the resistance of the ship due to the fact that the propeller creates suction behind the hull, and as a consequence increases the velocities in the after body. It is defined in model scale as:

$$t = 1 - \frac{R_{Tm} - F_D}{T_m} \tag{5.11}$$

where $R_{Tm}$ is the model resistance found from a resistance test or calculated from the zero thrust condition, $F_{T=0}$, from the load-varying propulsion test which was the method adopted in this thesis. From the load-varying propulsion test the tow force F can be plotted against the total thrust. According to Holtrop (2001), the linearity between T and F is nearly always preserved as long as the towing force is in the forward direction, and applies to all kinds of hull forms and propulsors. This is shown in Figure 9 below for different ship speeds and in bollard pull condition (V=0). The plot also includes the condition of severe overloading.

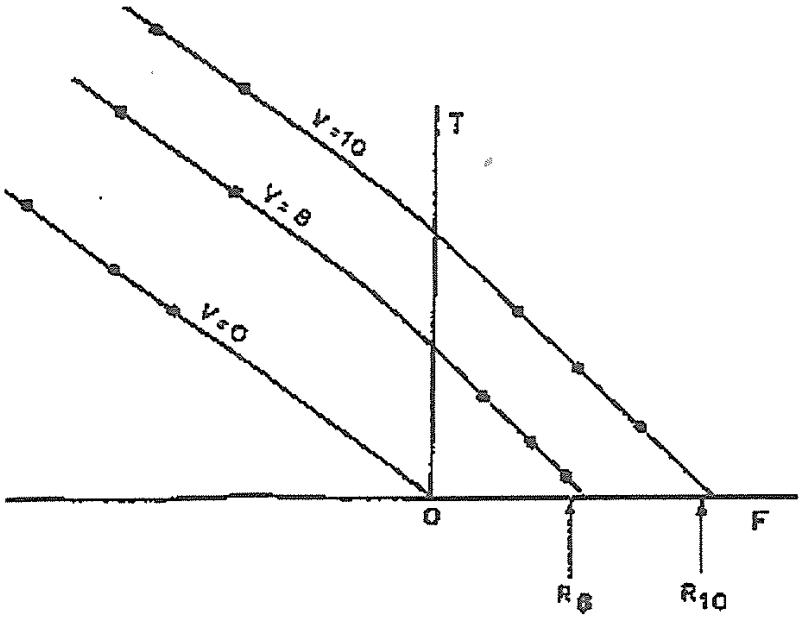


Figure 9: T-F diagram including severe overloading, Holtrop (2001)

Knowing this a coefficient t* can be defined as:

$$t^* = 1 - \frac{(F_{T=0} - F)}{T} = 1 - \frac{\delta F}{\delta T} \tag{5.12}$$

This assumes that the thrust deduction fraction is not influenced by the loading contrary to the classical thrust deduction. Applying t*, the $F_{T=0}$ can be found for each velocity:

$$F_{T=0} = F + T(1 - t^*) \tag{5.13}$$

Examination of many model test results show that the resistance R found from conventional resistance tests is in almost all cases 1-4% lower than $F_{T=0}$, Holtrop (2001). If $F_{T=0} / R$ is larger than 1, t will always be larger than t*, and also implies a dependency of the propeller loading where t decreases for increasing loading.

The relative rotative efficiency $\eta_R$ is an expression for the fact that the propeller operates in a non-homogenous wake field in front of a rudder. This gives variable propeller blade forces and may decrease or increase the lift/drag ratio of the propeller blades compared to the open water test. The relative rotative efficiency is expressed as:

$$\eta_R = \frac{Q_0}{Q_m} = \frac{K_{Q0}}{K_{Qm}} \tag{5.14}$$

The hull efficiency $\eta_H$ is determined from the thrust deduction and the effective wake according to:

$$\eta_H = \frac{1-t}{1-w} \tag{5.15}$$

The open water efficiency of the propeller $\eta_0$ is found with use of the data from a propulsion test according to:

$$\eta_0 = T_m(1-w)\cdot\frac{V}{2\pi Q_0 n} \tag{5.16}$$

Finally the quasi-propulsive efficiency $\eta_D$ is determined as:

$$\eta_D = \eta_H \eta_0 \eta_R \tag{5.17}$$

This is an expression for the relationship between the effective power and power developed by the propeller.

## 5.3 Seakeeping Tests

Seakeeping are the general term used for model testing in wave conditions. It can be carried out in a towing tank equipped with a wave maker, limiting it to head and following sea, or in a seakeeping basin/ocean laboratory, where arbitrary wave headings can be covered. A towing tank procedure was used in this case.

### 5.3.1 Test Requirements

In wave conditions, gravity forces are the governing force contribution, hence Froude scaling must be applied, Steen (2012). This implies that the scaling of wave height follows the geometrical scaling ratio and the period follows the square root of the scale ratio.

The dynamic motions of the model are the key to the obtained results and hence the inertia forces will be important. This implies that the mass distribution of the model needs to be scaled correctly. The following requirements need to be satisfied:

- Total mass
- Moment of inertia expressed in terms of the gyration radii $r_{xx}$, $r_{yy}$ and $r_{zz}$
- Longitudinal and vertical center of gravity

To determine the position of the center of gravity and momentum of inertia it is common to perform a pendulum test. The model is arranged in a pendulum, free to rotate around a fixed point. In the set-up for the tests with the Mewis Duct, only pendulum test in pitch was of relevance. The results from the test can be found in appendix A.

### 5.3.2 Test Procedure

Self-propelled model tests in both regular and irregular waves were conducted for the M3030 A. Propulsion tests in waves are usually performed by applying one of the following procedures according to Steen (2012):

- At constant propulsion power, adjusting the carriage speed to follow the model
- At constant carriage speed, adjusting the propulsion power to follow the carriage

For the M3030 A, the load-varying propulsion procedure explained in section 5.2.1 was used, following the same calculation procedures for the hull-propeller interaction. The runs was initiated after the waves was fully developed and the model was accelerated after the wave front had passed the model.

In irregular waves the model was accelerated with the spectra fully developed, and run three times through the tank distance with a constant time interval between each run. To get long measurements only one rate of revolution was applied attempting to get a tow rope force as close as possible to the one required for the SPP. As no resistance test was conducted the thrust deduction t cannot be calculated directly, hence a mean value of t from either the regular waves with approximately the same wave length λ, or values from still water is used in the analysis.

## 5.4 Resistance Test

Model resistance tests are conducted to provide data from which the model resistance can be determined for any desired speed. The results from a resistance test may be used as part of performance predictions.The original tests of M3030 A and the Mewis Duct performed by MARINTEK used the MARINTEK standard procedure for the extrapolation from model scale to full scale values, and hence resistance tests was performed on the hull, Alterskjær (2012). Resistance tests was not concucted for the current setup, and is therefore not further discussed.

# 6 Model Test of Becker Mewis Duct

Model testing regarding the efficiency of the Mewis Duct in waves was carried out in the large towing tank at MARINTEK, Trondheim, Norway in February/March of 2013.

## 6.1 Test Set-Up

### 6.1.1 Test Arrangement

The seakeeping carriage in the towing tank was used to tow the model. The model was fastened to the carriage in a system of springs and pre-tensioned wires as can be seen in Figure 10 below taken from Steen (2012). The springs were located between the connections to the carriage and the wires. A beam located amidships connected the model to the wires, with force transducers in each end for measurements of the towrope force, shown in Figure 11 below.

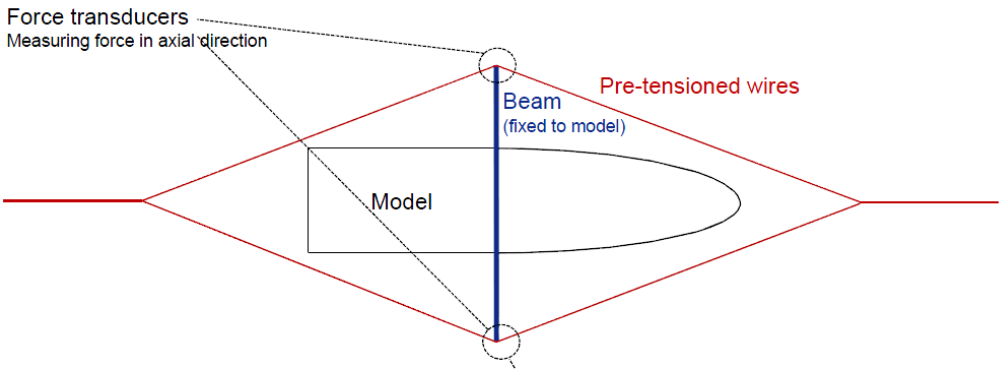


Figure 10: Schematic of model test set-up, Steen (2012).

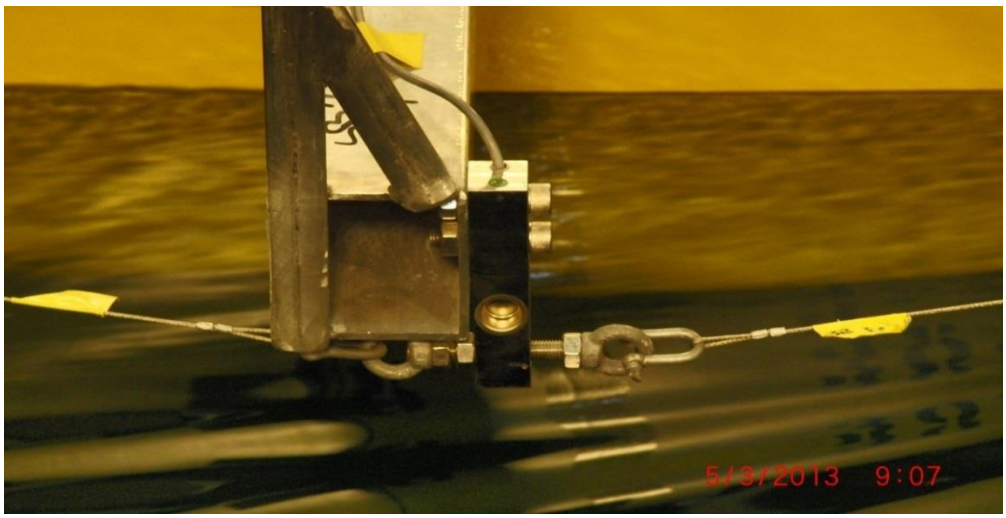


Figure 11: Force transducers located at each beam end

### 6.1.2 Hull Model

The hull model used in the test was M3030 A, seen in Figure 12, which is a model representing the 84 k LPG carrier, and is in scale 1:31.005. The hull model is made from Divinycell and reinforced with wood and coated with paint for a hydro dynamically smooth finish. The test was performed at the Design Waterline (DWL) 11.6/11.6 [m] in full scale.

The model went through its original model tests in 2012, conducted by the MARINTEK staff, which included resistance tests and propulsion tests in calm water with and without the Mewis Duct model fitted, for DWL and Ballast Waterline (WL1) 7.8/5.8 [m]. The MARINTEK report from these tests, Alterskjær (2012) was available and has been used both for comparison and directly for calculations in this report.

Since these tests the hull model has been through repairing of some cracks on the surface which may influence the resistance of the model. It is known that due to ageing the resistance of models tend to increase with time, mainly due to detoriation of surface finish. An increase in the order of 2% could be observed, but this is clearly not known exactly.

The model was first prepared for testing at the ballast waterline, where the largest difference of brake power was calculated from the original tests in still water. A decision to first conduct the regular wave tests was made to observe if the propeller ventilated during the runs, which would have had a large influence on the measured data. Both visible and audible indications of air suction from the surface were observed, and the model was hence prepared for the design waterline by the technicians at MARINTEK. This was done by adding weight without taking the model out of the tank, to physically reach the waterline, and a pendulum test to determine the location of vertical center of gravity and longitudinal radius of gyration was performed after the propulsion tests due to the time schedule.

Due to confidentiality agreements drawings are not included in the report.

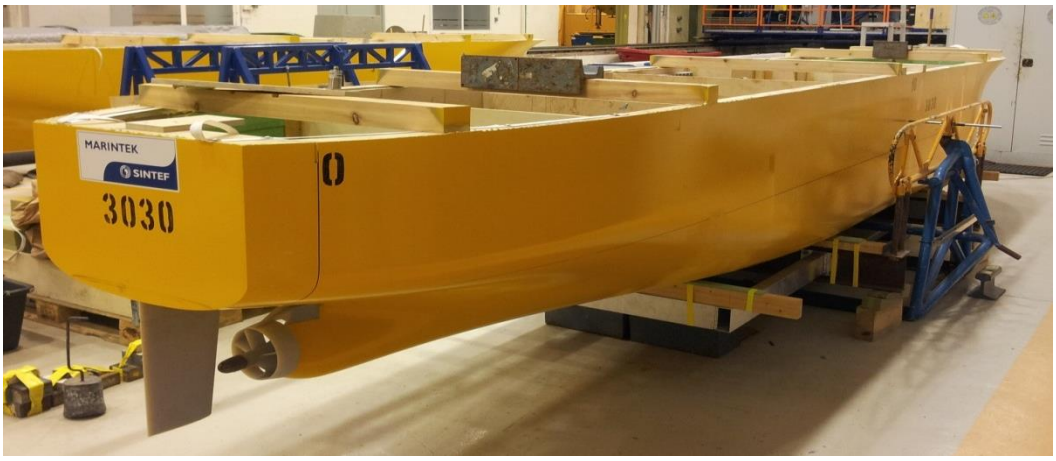


Figure 12: Model M3030 A, aft view

Hull main dimensions and characteristics, obtained from Alterskjær (2012), are presented in Table 1 below:

Table 1: M3030 A hull main dimensions and properties

| | Symbol | Unit | Full scale | Model scale |
|---|---|---|---|---|
| Length overall | $L_{OA}$ | [m] | 225.001 | 7.257 |
| Length on designed waterline | $L_{WL}$ | [m] | 212.198 | 6.844 |
| Length between perp. | $L_{PP}$ | [m] | 220.000 | 7.096 |
| Breadth molded | B | [m] | 36.615 | 1.181 |
| Breadth waterline | $B_{WL}$ | [m] | 36.608 | 1.181 |
| Depth to 1st deck | D | [m] | 24.212 | 0.781 |
| Draught at LPP/2 | T | [m] | 11.600 | 0.374 |
| Draught at FP | $T_{FP}$ | [m] | 11.600 | 0.374 |
| Draught at AP | $T_{AP}$ | [m] | 11.600 | 0.374 |
| Trim (pos. aft) | t | [m] | 0 | 0 |
| Volume Displacement | $\nabla$ | $m^3$ | 69033.9 | 2.316 |
| Displacement | $\Delta$ | t | 71173.8 | 2.314 |
| Block Coefficient | $C_B$ | - | 0.7388 | 0.7388 |
| Wetted Surface | S | $m^2$ | 10963.05 | 11.404 |
| Wetted Surf. of Transom Stern | $A_T$ | $m^2$ | 2.59 | 0.003 |

### 6.1.3 Becker Mewis Duct Model

The Becker Mewis Duct model, shown in Figure 13 and Figure 14, is made of a plastic material using a 3D printer. The accuracy of the printer is 16 µm, Alterskjær (2012).

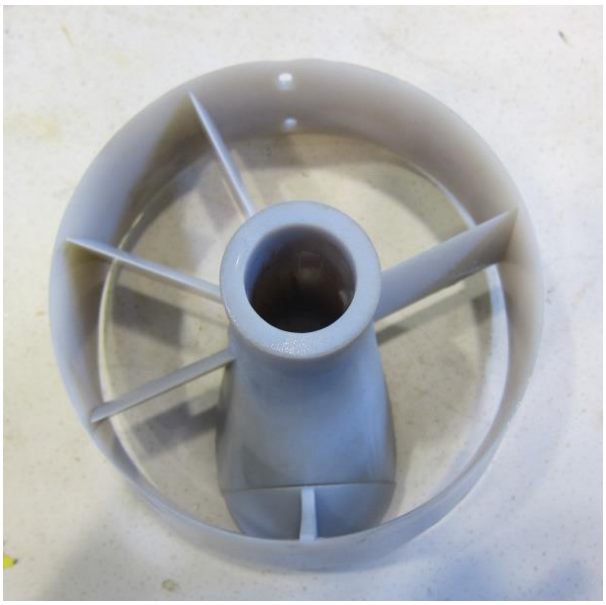

Figure 13: Becker Mewis Duct model

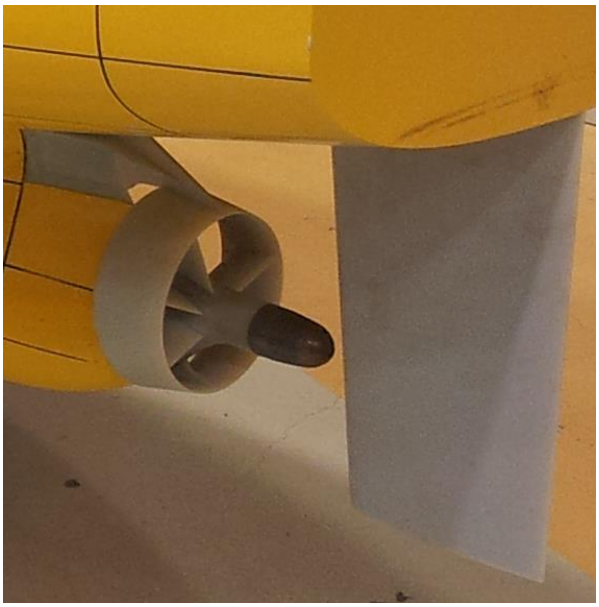

Figure 14: Becker Mewis Duct model fitted to M3030 A

Figure 15: Stock propeller P-1099

### 6.1.4 Propeller Model

The propeller model used in the test was the stock propeller P-1099, seen in Figure 15, which has the characteristics, obtained from Alterskjær (2012), presented in Table 2 below:

Table 2: P-1099 main characteristics

| | Symbol | Unit | Model |
|---|---|---|---|
| Diameter | D | [mm] | 238,67 |
| Pitch ratio | $P/D_{mean}$ | [-] | 0,833 |
| EAR | $A_E/A_0$ | [-] | 0,555 |
| Number of blades | Z | [-] | 4 |
| Hub diameter ratio | d/D | [-] | 0,163 |

## 6.2 Instrumentation

The following instrumentation was mounted:

- Ocus mast (6 DoF optical position measurement)
- Vertical acceleration at FP, CoG, AP.
- Longitudinal acceleration at CoG
- Tow force measurements (one transducer at each beam end)
- Wave probe on the carriage, at the longitudinal position of FP
- Relative wave probe at the propeller position
- Propeller torque, thrust and rate of revolution (conventional propeller dynamometer)

Details of the calibration can be found in appendix B.

## 6.3 Environmental Conditions

The tests were performed for calm water, regular waves and irregular waves. No wind or current was present. A water density of $\rho_m = 999.14$ [kg/m$^3$] was assumed in the calculations. Dimensions of the towing tank, obtained from Steen (2012), are shown in Table 3 below:

Table 3: Dimensions of the towing tank

| | Symbol | Unit | Tank |
|---|---|---|---|
| Width | B | [m] | 10.5 |
| Length | L | [m] | 175 |
| Depth | D | [m] | 5.6 |

### 6.3.1 Wave Calibration

For the test, 7 regular waves and 2 irregular spectra was calibrated. The calibration was done without the model present in the tank to avoid disturbance from reflections. Wave 8999 was a standard test wave for the calibration. Waves 8200-8260 are regular waves with length $\lambda$ ranging from 0.6-1.5 of the ship length $L_{OA}$. Waves 8000 and 8010 are irregular spectra of the Pierson-Moskowitz type. Details of the calibration of the irregular spectra can be found in appendix C. A numerical spectra was first simulated and used to create the physical wave spectra in model scale. The approximation as given in DNV (2010) is fulfilled for both spectra:

$$5 \leq T_P / \sqrt{H_S} \tag{6.1}$$

Data from the wave calibration is presented in Table 4 below:

Table 4: Data from wave calibration

| Wave | l/L | Wave data M | Wave data F | Meas. H [m] | ΔH [%] | Meas. T [s] | ΔT [%] |
|---|---|---|---|---|---|---|---|
| 8999 | | H0.25-T2 | | | | | |
| 8200 | 0.6 | H0.13-T1.670 | H4.03-T9.3 | 0.13831 | 6 | 1.666 | -0.24 |
| 8210 | 0.8 | H0.13-T1.928 | H4.03-T10.7 | 0.12841 | -1.23 | 1.932 | 0.21 |
| 8220 | 1 | H0.13-T2.156 | H4.03-T12.0 | 0.12586 | -3.18 | 2.152 | -0.19 |
| 8230 | 1 | H0.17-T2.156 | H5.27-T12.0 | 0.16631 | -2.17 | 2.158 | 0.09 |
| 8240 | 1.1 | H0.13-T2.261 | H4.03-T12.6 | 0.12529 | -3.62 | 2.270 | 0.4 |
| 8250 | 1.3 | H0.13-T2.458 | H4.03-T13.7 | 0.1308 | 0.61 | 2.453 | -0.2 |
| 8260 | 1.5 | H0.13-T2.640 | H4.03-T14.7 | 0.1345 | 3.34 | 2.645 | 0.2 |
| 8000 | | Hs0.113-Tp2.156 | Hs3.5-Tp12.0 | | | | |
| 8010 | | Hs0.161-Tp2.156 | Hs5.0-Tp12.0 | | | | |

## 6.4 Test Program

### 6.4.1 Decay Tests

Decay tests was performed for surge and roll motion. This was done by physically setting motion to the model in the respective degree of freedom. The test program is presented in Table 5 below.

Table 5: Decay tests

| TEST NO. | INFORMATION | Tn [s] |
|---|---|---|
| 9007 | Surge | 13,6 |
| 9008 | Roll | 1,95 |

### 6.4.2 Calm Water Propulsion

The calm water propulsion was performed for 3 speeds and 2 different propeller revolution settings at each speed with and without the Mewis Duct fitted. The test program is presented in Table 6 below. The propeller revs. in the table are the measured mean values, so there are slight differences with and without the duct fitted.

Table 6: Test program in still water

| With Mewis Duct Fitted | | | | |
|---|---|---|---|---|
| TEST NO. | Vs [knots] | Vm [m/s] | n1 | n2 |
| 6100 | 15 | 1,386 | 6,658 | 7,992 |
| 6110 | 16 | 1,478 | 7,154 | 10,013 |
| 6120 | 17 | 1,571 | 7,651 | 9,038 |
| 6111 | 16 | 1,478 | 7,154 | 8,487 |
| Without Mewis Duct Fitted | | | | |
| 6200 | 15 | 1,386 | 6,660 | 7,995 |
| 6210 | 16 | 1,478 | 7,156 | 8,490 |
| 6220 | 17 | 1,571 | 7,653 | 9,027 |

### 6.4.3 Propulsion in Regular Waves

Propulsion in regular waves was performed for 2 speeds with 2 different propeller revolution settings for the 7 waves presented in section 6.3.1 with and without the Mewis Duct fitted. The test program is presented in Table 7 for the Mewis Duct fitted and Table 8 without the Mewis Duct fitted below.

Table 7: Test program in regular waves with Becker Mewis Duct fitted

| With Mewis Duct Fitted | | | | | |
|---|---|---|---|---|---|
| TEST NO. | WAVE NO. | Vs [knots] | Vm [m/s] | n1 | n2 |
| 2200 | 8200 | 15 | 1,386 | 6,66 | 8,19 |
| 2210 | 8200 | 17 | 1,571 | 7,652 | 8,934 |
| 2220 | 8210 | 15 | 1,386 | 6,66 | 9,023 |
| 2230 | 8210 | 17 | 1,571 | 7,652 | 9,38 |
| 2240 | 8220 | 15 | 1,386 | 6,659 | 9,375 |
| 2250 | 8220 | 17 | 1,571 | 7,652 | 10,01 |
| 2260 | 8230 | 15 | 1,386 | 6,659 | 10,6972 |
| 2270 | 8230 | 17 | 1,571 | 7,651 | 10,8 |
| 2280 | 8240 | 15 | 1,386 | 6,658 | 10,0096 |
| 2290 | 8240 | 17 | 1,571 | 7,6514 | 10,9957 |
| 2300 | 8250 | 15 | 1,386 | 6,6585 | 9,5024 |
| 2310 | 8250 | 17 | 1,571 | 7,6517 | 10,0146 |
| 2320 | 8260 | 15 | 1,386 | 6,7083 | 7,993 |
| 2330 | 8260 | 17 | 1,571 | 7,6518 | 8,8346 |
| 2251 | 8220 | 17 | 1,571 | 9,0201 | 10,3103 |
| 2271 | 8230 | 17 | 1,571 | 9,0247 | 11,4873 |

Table 8: Test program in regular waves without Becker Mewis Duct fitted

| Without Mewis Duct Fitted | | | | | |
|---|---|---|---|---|---|
| TEST NO. | WAVE NO. | Vs [knots] | Vm [m/s] | n1 | n2 |
| 2400 | 8200 | 15 | 1,386 | 6,660 | 8,226 |
| 2410 | 8200 | 17 | 1,571 | 7,654 | 8,894 |
| 2420 | 8210 | 15 | 1,386 | 6,660 | 9,025 |
| 2430 | 8210 | 17 | 1,571 | 7,654 | 9,386 |
| 2440 | 8220 | 15 | 1,386 | 6,660 | 9,380 |
| 2450 | 8220 | 17 | 1,571 | 7,653 | 10,313 |
| 2460 | 8230 | 15 | 1,386 | 6,660 | 10,700 |
| 2470 | 8230 | 17 | 1,571 | 7,654 | |
| 2480 | 8240 | 15 | 1,386 | 6,660 | 10,013 |
| 2490 | 8240 | 17 | 1,571 | 7,653 | 11,000 |
| 2500 | 8250 | 15 | 1,386 | 6,660 | 9,508 |
| 2510 | 8250 | 17 | 1,571 | 7,654 | 10,020 |
| 2520 | 8260 | 15 | 1,386 | 6,660 | 7,995 |
| 2530 | 8260 | 17 | 1,571 | 7,654 | 8,837 |
| 2471 | 8230 | 17 | 1,571 | 7,653 | 11,491 |
| 2531 | 8260 | 17 | 1,571 | 7,654 | 8,837 |
| 2532 | 8260 | 17 | 1,571 | 7,654 | 8,837 |
| 2533 | 8260 | 17 | 1,571 | 7,654 | 8,838 |
| 2534 | 8260 | 17 | 1,571 | 7,654 | |
| 2501 | 8250 | 15 | 1,386 | 6,660 | 9,509 |
| 2535 | 8260 | 17 | 1,571 | 7,654 | 8,837 |

### 6.4.4 Propulsion in Irregular Waves

Propulsion in irregular waves was performed for 1 speed and 1 propeller revolution setting trying to get as close as possible to the calculated tow force $F_D$ for the 2 wave spectra presented in section 6.3.1. The test program is presented in Table 9 below.

Table 9: Test program in irregular waves

| With Mewis Duct Fitted | | | | |
|---|---|---|---|---|
| TEST NO. | WAVE NO. | Vs [knots] | Vm [m/s] | n |
| 3000 | 8000 | 15 | 1,385841 | 7,9912 |
| 3010 | 8010 | 15 | 1,385841 | 7,9919 |
| Without Mewis Duct Fitted | | | | |
| 3100 | 8000 | 15 | 1,385841 | 7,9947 |
| 3110 | 8010 | 15 | 1,385841 | 7,9946 |

# 7 Results and Analysis

## 7.1 Surge Decay Test

To ensure the spring setup did not affect the surge motion due to encounter period in head waves with period $T_0$ and frequency $\omega_0$, the natural period $T_N$ in surge was compared to the encounter periods $T_e$ from the runs in waves. The natural period in surge was found to be $T_N$ = 13.6 [s], see section 6.4.1. The calculated encounter frequency in each condition is presented in Table 10. The encounter period is calculated in head waves according to Faltinsen (1990):

$$T_e = 2\pi / \omega_e \tag{7.1}$$

where the encounter frequency is calculated as

$$\omega_e = \omega_0 + \omega_0^2 \cdot \frac{V}{g} \tag{7.2}$$

The results show that the periods do not coincide and should therefore not be a problem.

Table 10: Calculated encounter period in regular waves

| Vm = 1,386 [m/s] | | | | |
|---|---|---|---|---|
| Run | $T_0$ | $\omega_0$ | $\omega_e$ | $T_e$ |
| 2210 | 1,666 | 3,771 | 6,049 | 1,039 |
| 2230 | 1,932 | 3,252 | 4,946 | 1,270 |
| 2250 | 2,152 | 2,920 | 4,285 | 1,466 |
| 2270 | 2,158 | 2,912 | 4,269 | 1,472 |
| 2290 | 2,270 | 2,768 | 3,995 | 1,573 |
| 2310 | 2,453 | 2,561 | 3,612 | 1,740 |
| 2330 | 2,645 | 2,375 | 3,279 | 1,916 |
| 2251 | 2,152 | 2,920 | 4,285 | 1,466 |
| 2271 | 2,158 | 2,912 | 4,269 | 1,472 |
| Vm = 1,571 [m/s] | | | | |
| 2200 | 1,666 | 3,771 | 5,781 | 1,087 |
| 2220 | 1,932 | 3,252 | 4,746 | 1,324 |
| 2240 | 2,152 | 2,920 | 4,124 | 1,524 |
| 2260 | 2,158 | 2,912 | 4,109 | 1,529 |
| 2280 | 2,270 | 2,768 | 3,850 | 1,632 |
| 2300 | 2,453 | 2,561 | 3,488 | 1,801 |
| 2320 | 2,645 | 2,375 | 3,173 | 1,980 |

## 7.2 Calm Water Propulsion

The main purpose of the analysis of the calm water measurements are to make a basis for comparison with the further results for propulsion in waves. The results are also compared to the original results by MARINTEK, Alterskjær (2012), to indicate the reliability of the measurements.

### 7.2.1 Initial Results

Interpolated results in model scale at the self-propulsion point in still water are presented in Table 11 below. The tow force $F_D$ used is the calculated tow force from MARINTEK's results in 2012, Alterskjær (2012). Model resistance $R_{Tm}$ is an estimated value using $F_{T=0} / R_{Tm} = 1.04$ . The value is an assumption based on that $F_{T=0} / R_{Tm}$ is known to be a value between 1.01-1.04, Holtrop (2001), and is calculated for camparison with the original results from MARINTEK, Alterskjær (2012) and in order to obtain reasonable values for the thrust deduction t. It should be noted that this do not affect the relative difference of t with and without the duct remarkably. The measured values are available in appendix D. Three different revolutions were measured for $V_S$ = 16 and 17 [knots] with the duct fitted and Figure 16 shows that linearity of thrust with the loading is a reasonable assumption. Only two points was measured for 15 [knots] but the results seems to correspond to the assumption as well.

Table 11: Interpolated results in still water

| **With** Mewis Duct Fitted | | | | | | | | |
|---|---|---|---|---|---|---|---|---|
| $V_S$ [kn] | $V_m$ [m/s] | t* [-] | $F_{T=0}$ [N] | $R_{Tm}$ [N] | $F_D$ [N] | n [Hz] | T [N] | Q [Nm] |
| 15 | 1,3858 | 0,1113 | 44,5457 | 42,8324 | 19,2127 | 6,7330 | 28,5061 | 0,9048 |
| 16 | 1,4782 | 0,1314 | 49,7215 | 47,8092 | 21,3632 | 7,2161 | 32,6502 | 1,0383 |
| 17 | 1,5706 | 0,1172 | 56,9474 | 54,7571 | 23,5970 | 7,7398 | 37,7789 | 1,2044 |
| **Without** Mewis Duct Fitted | | | | | | | | |
| $V_S$ [kn] | $V_m$ [m/s] | t* [-] | $F_{T=0}$ [N] | $R_{Tm}$ [N] | $F_D$ [N] | n [Hz] | T [N] | Q [Nm] |
| 15 | 1,3858 | 0,1055 | 43,3462 | 41,6790 | 18,7967 | 6,8633 | 27,4463 | 0,9055 |
| 16 | 1,4782 | 0,0789 | 50,0173 | 48,0935 | 20,9017 | 7,3705 | 31,6087 | 1,0443 |
| 17 | 1,5706 | 0,0974 | 55,8450 | 53,6972 | 23,0882 | 7,8729 | 36,2898 | 1,1977 |

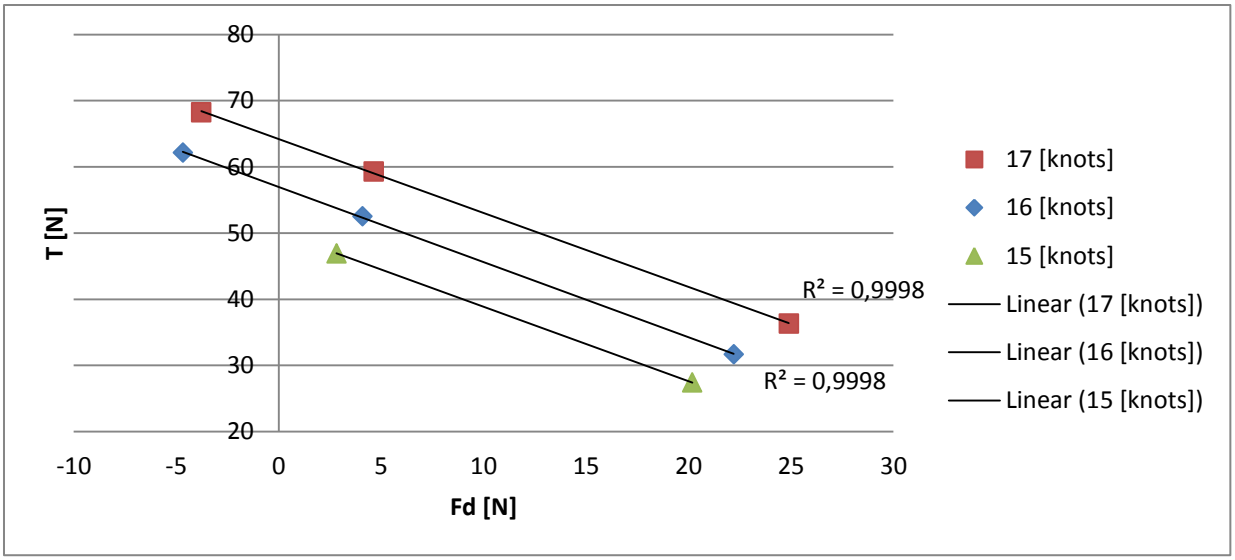


Figure 16: T-F diagram illustrating the linearity between thrust and tow force

The plots in Figure 17 and Figure 18 below present the estimated model resistance $R_{Tm}$ from the current setup and the $R_{Tm}$ calculated in MARINTEK's model tests, Alterskjær (2012), at the same model speeds. It show that the $R_{Tm}$ are still higher for the curren setup with the $F_{T=0} / R_{Tm} = 1.04$ used. There may be several reasons for this, and some of them are discussed in a later section.

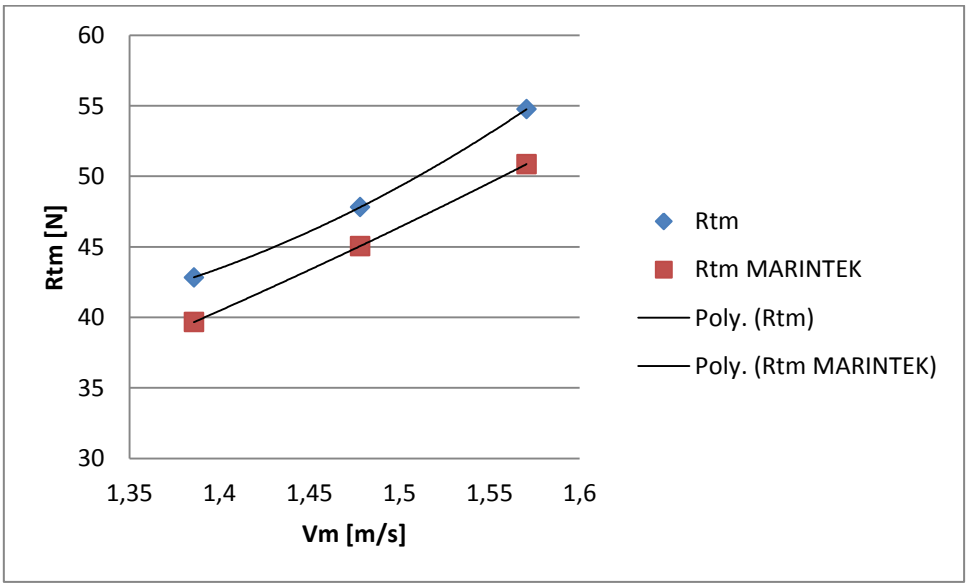


Figure 17: Model resistance calculated with Becker Mewis Duct in calm water

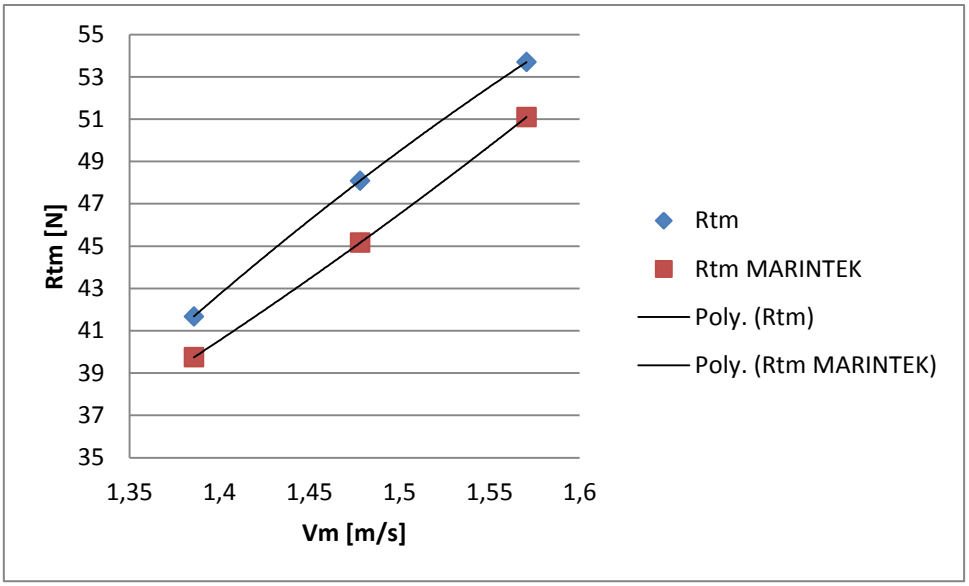


Figure 18: Model resistance calculated without Becker Mewis Duct in calm water

### 7.2.2 Propulsive Factors

Table 12 presents results of propulsive factors used in the calculations. Thrust deduction t is calculated using the estimated $R_{Tm}$ as input. From the table and Figure 19 it is clear that the wake fraction follows a slightly decreasing trend with increasing ship velocity, reflecting the increasing Reynolds number, which corresponds to the statement in Holtrop (2001). It also show a clear consistent increase over the different speeds with the Mewis Duct fitted. The calculated wake fraction from Alterskjær (2012) is also included in the figure. The data for the current setup are higher and has a larger increase for the tests with the Mewis Duct.

The thrust deduction can be seen in Figure 20. The figure also presents the thrust deduction for the same speeds from Alterskjær (2012). It shows an increase with the duct fitted, but seems to be very scattered. This will be investigated and explained further in a later section. Large difference in the thrust deduction with the duct fitted result in a decrease in the difference of the hull efficiency, following the formula for hull efficiency in section 5.2.4, and further to the propulsive efficiency.

Table 12: Calculated propulsive factors in still water

**With** Mewis Duct Fitted

| $V_m$ [m/s] | t [-] | $K_T$ [-] | J [-] | J0 [-] | w [-] | $K_{Q0}$ [-] | $Q_0$ [Nm] | $K_Q$ [-] |
|---|---|---|---|---|---|---|---|---|
| 1,3858 | 0,1714 | 0,1940 | 0,8624 | 0,5140 | 0,4040 | 0,0269 | 0,9449 | 0,0258 |
| 1,4782 | 0,1900 | 0,1934 | 0,8583 | 0,5152 | 0,3997 | 0,0269 | 1,0829 | 0,0258 |
| 1,5706 | 0,1752 | 0,1945 | 0,8502 | 0,5128 | 0,3968 | 0,0270 | 1,2514 | 0,0260 |

**Without** Mewis Duct Fitted

| $V_m$ [m/s] | t [-] | $K_T$ [-] | J [-] | J0 [-] | w [-] | $K_{Q0}$ [-] | $Q_0$ [Nm] | $K_Q$ [-] |
|---|---|---|---|---|---|---|---|---|
| 1,3858 | 0,1663 | 0,1797 | 0,8460 | 0,5440 | 0,3570 | 0,0254 | 0,9250 | 0,0248 |
| 1,4782 | 0,1397 | 0,1795 | 0,8403 | 0,5445 | 0,3521 | 0,0254 | 1,0656 | 0,0248 |
| 1,5706 | 0,1565 | 0,1806 | 0,8359 | 0,5421 | 0,3514 | 0,0255 | 1,2218 | 0,0250 |

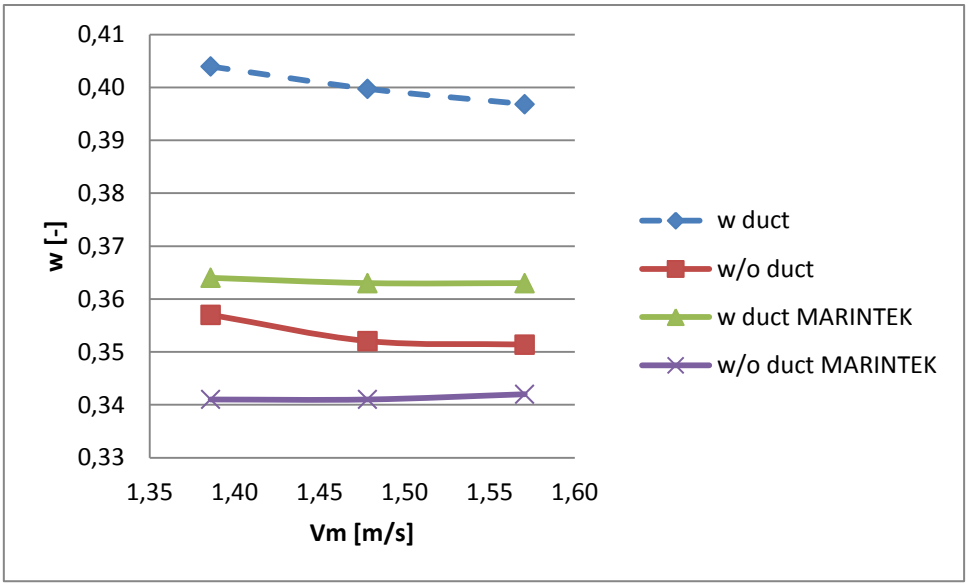


Figure 19: Wake fraction versus model velocity in calm water

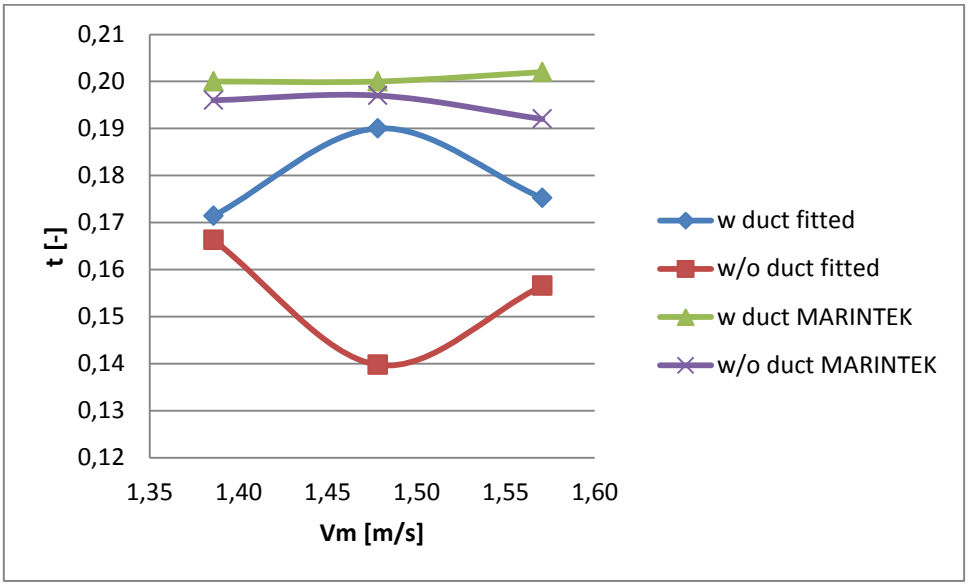


Figure 20: Thrust deduction versus model velocity in calm water

### 7.2.3 Propulsive Efficiency

Table 13 presents the calculated propulsive efficiency and its components. The relative rotative efficiency $\eta_R$ and the open water efficiency $\eta_0$ follow roughly the expected values, and $\eta_0$ corresponds with the usual range of 0.6-0.8 for conventional propellers in design condition and 0.5-0.6 for ducted propellers as stated in Steen and Minsaas (2012).

The hull efficiency $\eta_H$ reflects the inaccurate results for the thrust deduction t, and are uncharacteristically high compared to results in Alterskjær (2012) where $\eta_H$ was calculated to be around 1.25-1.26 with the Mewis Duct fitted and around 1.22-1.23 without. This can also be influenced by bias errors in the thrust and tow force measurements. Further this results in the propulsive efficiency $\eta_D$ being higher than the expected values and does not follow a clear trend with the velocity as can be seen from Figure 21. The efficiency still seems to be higher with the Mewis Duct fitted. Results from Alterskjær (2012) are also included in the plot.

Table 13: Propulsive efficiency in still water

| **With** Mewis Duct Fitted | | | | | |
|---|---|---|---|---|---|
| $V_m$ [m/s] | $\eta_R$ [-] | $\eta_H$ [-] | $\eta_0$ [-] | $\eta_D$ [-] | |
| 1,3858 | 1,0443 | 1,3901 | 0,5891 | 0,8551 | |
| 1,4782 | 1,0430 | 1,3494 | 0,5901 | 0,8304 | |
| 1,5706 | 1,0391 | 1,3675 | 0,5881 | 0,8356 | |
| Mean | | | | 84,04 % | |
| **Without** Mewis Duct Fitted | | | | | |
| $V_m$ [m/s] | $\eta_R$ [-] | $\eta_H$ [-] | $\eta_0$ [-] | $\eta_D$ [-] | Diff. $\eta_D$ [%] |
| 1,3858 | 1,0215 | 1,2966 | 0,6131 | 0,8121 | 5,033 % |
| 1,4782 | 1,0204 | 1,3277 | 0,6135 | 0,8312 | -0,093 % |
| 1,5706 | 1,0201 | 1,3004 | 0,6117 | 0,8114 | 2,892 % |
| Mean | | | | 81,82 % | |
| Diff. | | | | 2,64 % | |

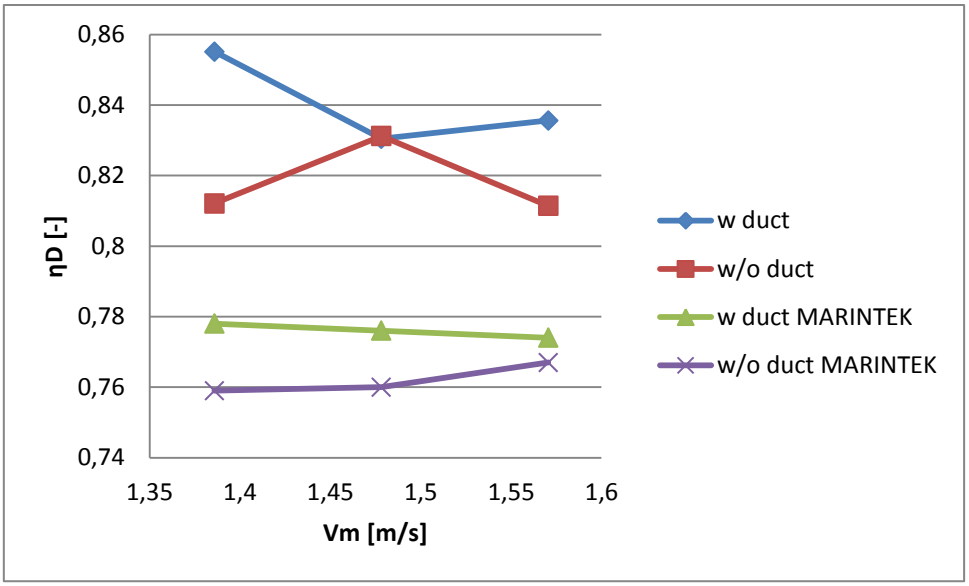


Figure 21: Propulsive efficiency versus model velocity in calm water

### 7.2.4 Powering Prediction

From the previous measurements by MARINTEK, the brake power $P_B$ was used as the main reference to determine the gain with the Mewis Duct fitted. The brake power at the design waterline was found to be 4.1% lower with the duct fitted at 16.8 [knots], Alterskjær (2012). A power difference around 3-5% was predicted for different speeds. For comparison the brake power was calculated and scaled to ship scale for the current setup, and the results are presented in Table 14 and Figure 22. The brake power was calculated for the tow force corresponding to the self-propulsion point. The calculation method differs from the original tests where the delivered power was calculated according to Alterskjær (2012) following the MARINTEK extrapolation method, and the final delivered power was calculated as:

$$P_D = \frac{2\pi}{1000} \cdot \rho \cdot D^5 \cdot (\frac{RPM}{60})^3 \cdot \frac{K_Q}{\eta_R} \tag{7.3}$$

The delivered power was calculated for the current setup according to ITTC (2011_2):

$$P_D = \frac{\rho_S}{\rho_M} . \lambda^{3.5} \cdot 2\pi \cdot n_M \cdot Q / 1000 \tag{7.4}$$

The brake power was calculated using the same mechanical efficiency $\eta_M = 0.98$ as in the previous tests, Alterskjær (2012).

$$P_B = \frac{P_D}{\eta_M} \tag{7.5}$$

The table and the figure show a decrease in the brake power with the Mewis Duct fitted and in an order of around 2%.

Table 14: Powering prediction results in still water

| **With** Mewis Duct Fitted | | | | |
|---|---|---|---|---|
| Vs [knots] | Vm [m/s] | Pd | Pb | Diff. |
| 15 | 1,385831 | 6522,682 | 6655,798 | |
| 16 | 1,478219 | 8021,921 | 8185,634 | |
| 17 | 1,570608 | 9980,4 | 10184,08 | |
| **Without** Mewis Duct Fitted | | | | |
| 15 | 1,385831 | 6653,966 | 6789,761 | 1,97 % |
| 16 | 1,478219 | 8240,457 | 8408,629 | 2,65 % |
| 17 | 1,570608 | 10095,87 | 10301,91 | 1,14 % |
| Mean | | | | 1,92 % |

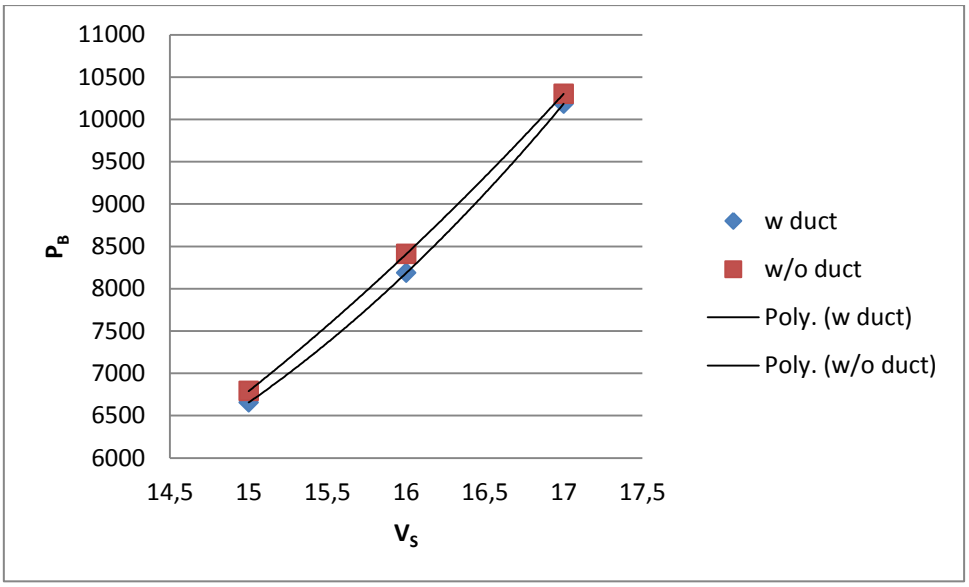


Figure 22: Difference in brake power in still water with and without Becker Mewis Duct fitted

## 7.3 Propulsion in Regular Waves

### 7.3.1 Pitch and Heave Motion in Regular Waves

To present the relative pitch and heave motions in regular waves, the response amplitude operators (RAO) have been calculated and plotted versus the wave length to ship lengt ratio λ/L. Figure 23 show RAO for heave for $V_S$ = 15 [knots] and $V_S$ = 17 [knots]. Large motions can be observed for λ/L around 1-1.5, peaking around λ/L = 1.1 and 1.3 for $V_S$ = 15 and 17 [knots] respectively.

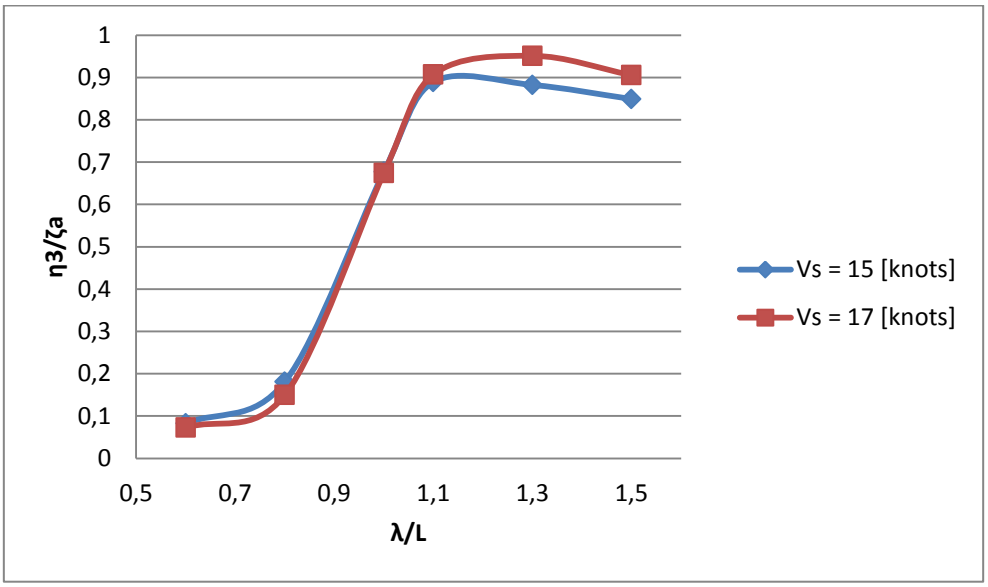


Figure 23: RAO for heave

Figure 24 show RAO for pitch for $V_S$ = 15 [knots] and $V_S$ 17 [knots]. A peak can be observed around λ/L = 1.3.

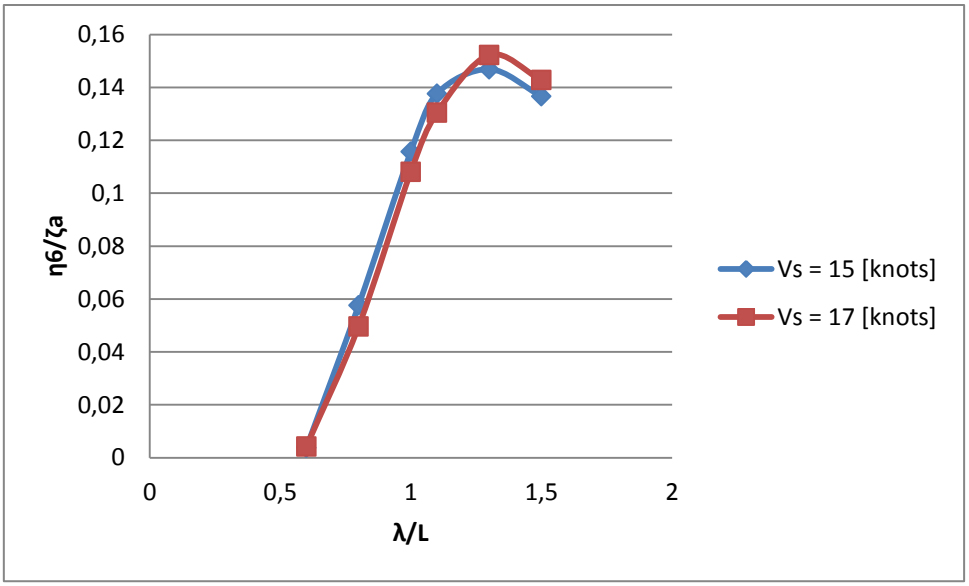


Figure 24: RAO for pitch

### 7.3.2 Initial Results

Interpolated results in model scale for propulsion in regular waves at the self-propulsion point are presented in Table 15 for 15 [knots] and Table 16 for 17 [knots] below. The tow force $F_D$ used is the calculated tow force from MARINTEK's results in 2012, Alterskjær (2012). Model resistance $R_{Tm}$ is estimated using $F_{T=0} / R_{Tm} = 1.04$. The measured values are available in appendix D.

Table 15: Interpolated results in regular waves at Vs = 15 [knots]

**With** Mewis Duct Fitted, 1.386 [m/s] (15 [kn] full scale)

| H [m] | λ/L [-] | t* [-] | $F_{T=0}$ [N] | $R_{Tm}$ [N] | $F_D$ [N] | n [Hz] | T [N] | Q [Nm] |
|---|---|---|---|---|---|---|---|---|
| 0,13 | 0,6 | 0,1187 | 59,6377 | 58,4684 | 19,2127 | 7,9533 | 45,8700 | 1,4225 |
| 0,13 | 0,8 | 0,1883 | 66,0864 | 64,7906 | 19,2127 | 8,6051 | 57,7507 | 1,7815 |
| 0,13 | 1 | 0,1867 | 79,8652 | 78,2992 | 19,2127 | 9,5442 | 74,5716 | 2,2974 |
| 0,17 | 1 | 0,2385 | 101,4654 | 99,4759 | 19,2127 | 11,0857 | 108,0193 | 3,2842 |
| 0,13 | 1,1 | 0,2102 | 77,4419 | 75,9235 | 19,2127 | 9,3545 | 73,7223 | 2,2660 |
| 0,13 | 1,3 | 0,1851 | 65,3899 | 64,1077 | 19,2127 | 8,4379 | 56,6651 | 1,7574 |
| 0,13 | 1,5 | 0,1157 | 57,8937 | 56,7586 | 19,2127 | 7,7918 | 43,7440 | 1,3725 |

**Without** Mewis Duct Fitted, 1.386 [m/s] (15 [kn] full scale)

| H [m] | λ/L [-] | t* [-] | $F_{T=0}$ [N] | $R_{Tm}$ [N] | $F_D$ [N] | n [Hz] | T [N] | Q [Nm] |
|---|---|---|---|---|---|---|---|---|
| 0,13 | 0,6 | 0,1602 | 55,5965 | 54,5064 | 18,7967 | 8,0725 | 43,8211 | 1,4152 |
| 0,13 | 0,8 | 0,1944 | 63,8563 | 62,6042 | 18,7967 | 8,7630 | 55,9336 | 1,7883 |
| 0,13 | 1 | 0,1284 | 80,5654 | 78,9857 | 18,7967 | 9,6303 | 70,8708 | 2,2457 |
| 0,17 | 1 | 0,2183 | 101,2084 | 99,2239 | 18,7967 | 11,2753 | 105,4270 | 3,2742 |
| 0,13 | 1,1 | 0,1423 | 81,8498 | 80,2449 | 18,7967 | 9,6195 | 73,5182 | 2,3106 |
| 0,13 | 1,3 | 0,1069 | 67,9572 | 66,6247 | 18,7967 | 8,6029 | 55,0462 | 1,7514 |
| 0,13 | 1,5 | 0,1223 | 56,7476 | 55,6349 | 18,7967 | 8,0149 | 43,2409 | 1,3932 |

Table 16: Interpolated results in regular waves at Vs = 17 [knots]

**With** Mewis Duct Fitted, 1.571 [m/s] (17 [kn] full scale)

| H [m] | λ/L [-] | t* [-] | $F_{T=0}$ [N] | $R_{Tm}$ [N] | $F_D$ [N] | n [Hz] | T [N] | Q [Nm] |
|---|---|---|---|---|---|---|---|---|
| 0,13 | 0,6 | 0,1678 | 69,6203 | 68,2552 | 23,5970 | 8,8616 | 55,3010 | 1,7278 |
| 0,13 | 0,8 | 0,2286 | 74,7578 | 73,2920 | 23,5970 | 9,4470 | 66,3253 | 2,0680 |
| 0,13 | 1 | 0,1546 | 96,4129 | 94,5225 | 23,5970 | 10,3846 | 86,1271 | 2,6712 |
| 0,17 | 1 | 0,2083 | 114,3303 | 112,0886 | 23,5970 | 11,5842 | 114,6110 | 3,5131 |
| 0,13 | 1,1 | 0,1612 | 99,4685 | 97,5182 | 23,5970 | 10,4791 | 90,4500 | 2,7901 |
| 0,13 | 1,3 | 0,1573 | 87,2347 | 85,5242 | 23,5970 | 9,8521 | 75,5194 | 2,3487 |
| 0,13 | 1,5 | 0,2115 | 70,0579 | 68,6843 | 23,5970 | 9,0504 | 58,9232 | 1,8525 |

**Without** Mewis Duct Fitted, 1.571 [m/s] (17 [kn] full scale)

| H [m] | λ/L [-] | t* [-] | $F_{T=0}$ [N] | $R_{Tm}$ [N] | $F_D$ [N] | n [Hz] | T [N] | Q [Nm] |
|---|---|---|---|---|---|---|---|---|
| 0,13 | 0,6 | 0,1369 | 68,5430 | 67,1990 | 23,0882 | 8,9891 | 52,6659 | 1,7116 |
| 0,13 | 0,8 | 0,1667 | 75,8627 | 74,3752 | 23,0882 | 9,5779 | 63,3306 | 2,0424 |
| 0,13 | 1 | 0,1555 | 92,9878 | 91,1645 | 23,0882 | 10,5490 | 82,7702 | 2,6370 |
| 0,17 | 1 | 0,2287 | 118,9292 | 116,5973 | 23,0882 | 12,4294 | 124,2579 | 3,8704 |
| 0,13 | 1,1 | 0,1530 | 99,2907 | 97,3438 | 23,0882 | 10,7582 | 89,9718 | 2,8362 |
| 0,13 | 1,3 | 0,0602 | 91,8148 | 90,0145 | 23,0882 | 10,0342 | 73,1327 | 2,3341 |
| 0,13 | 1,5 | 0,0651 | 75,5003 | 74,0199 | 23,0882 | 9,1884 | 56,0609 | 1,8124 |

### 7.3.3 Propulsive Factors

Table 17 presents results of calculated propulsive factors in regular waves at 15 [knots]. Thrust deduction t is calculated using the estimated $R_{Tm}$ as input.

Table 17: Calculated propulsive factors in regular waves at Vs = 15 [knots]

**With** Mewis Duct Fitted, 1.386 [m/s] (15 [kn] full scale)

| H [m] | λ/L [-] | t [-] | $K_T$ [-] | J [-] | J0 [-] | w [-] | $K_{Q0}$ [-] | $Q_0$ [Nm] | $K_Q$ [-] |
|---|---|---|---|---|---|---|---|---|---|
| 0,13 | 0,6 | 0,1442 | 0,2237 | 0,7301 | 0,4503 | 0,3833 | 0,0301 | 1,4734 | 0,0291 |
| 0,13 | 0,8 | 0,2108 | 0,2406 | 0,6748 | 0,4132 | 0,3876 | 0,0319 | 1,8254 | 0,0311 |
| 0,13 | 1 | 0,2077 | 0,2525 | 0,6084 | 0,3867 | 0,3643 | 0,0331 | 2,3321 | 0,0326 |
| 0,17 | 1 | 0,2570 | 0,2711 | 0,5238 | 0,3449 | 0,3416 | 0,0350 | 3,3266 | 0,0345 |
| 0,13 | 1,1 | 0,2308 | 0,2599 | 0,6207 | 0,3703 | 0,4035 | 0,0338 | 2,2912 | 0,0335 |
| 0,13 | 1,3 | 0,2077 | 0,2455 | 0,6882 | 0,4023 | 0,4153 | 0,0324 | 1,7831 | 0,0319 |
| 0,13 | 1,5 | 0,1417 | 0,2222 | 0,7452 | 0,4534 | 0,3916 | 0,0300 | 1,4071 | 0,0292 |

**Without** Mewis Duct Fitted, 1.386 [m/s] (15 [kn] full scale)

| H [m] | λ/L [-] | t [-] | $K_T$ [-] | J [-] | J0 [-] | w [-] | $K_{Q0}$ [-] | $Q_0$ [Nm] | $K_Q$ [-] |
|---|---|---|---|---|---|---|---|---|---|
| 0,13 | 0,6 | 0,1851 | 0,2074 | 0,7193 | 0,4853 | 0,3252 | 0,0284 | 1,4312 | 0,0281 |
| 0,13 | 0,8 | 0,2168 | 0,2247 | 0,6626 | 0,4481 | 0,3238 | 0,0302 | 1,7949 | 0,0301 |
| 0,13 | 1 | 0,1507 | 0,2357 | 0,6029 | 0,4239 | 0,2969 | 0,0314 | 2,2502 | 0,0313 |
| 0,17 | 1 | 0,2371 | 0,2558 | 0,5150 | 0,3794 | 0,2633 | 0,0334 | 3,2878 | 0,0333 |
| 0,13 | 1,1 | 0,1642 | 0,2451 | 0,6036 | 0,4033 | 0,3319 | 0,0323 | 2,3143 | 0,0323 |
| 0,13 | 1,3 | 0,1311 | 0,2294 | 0,6749 | 0,4377 | 0,3514 | 0,0307 | 1,7583 | 0,0306 |
| 0,13 | 1,5 | 0,1481 | 0,2076 | 0,7245 | 0,4849 | 0,3307 | 0,0284 | 1,4120 | 0,0280 |

Figure 25 show the thrust deduction plotted against the wave length/ship length ratio λ/L at $V_S$ = 15 [knots] in full scale and wave height H = 4.03 [m], (0.13 [m] model scale). The plot indicates no clear trend; hence no conclusion can be drawn from it. According to Faltinsen et al. (1980) it has been found that for increasing wave height the thrust deduction decreases, while from Table 17 it rather show the opposite trend, with increased values of t for H=0.17 [m] for both with and without the Mewis Duct fitted.

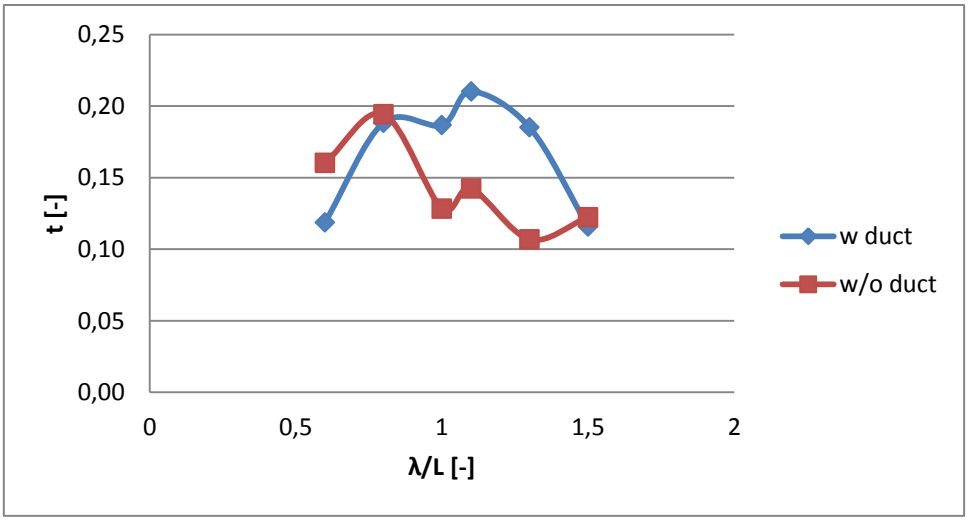


Figure 25: Thrust deduction versus wave length for $V_S$=15 [knots]

Figure 26 show the effective wake plotted against the wave length/ship length ratio at $V_S$ = 15 [knots] in full scale and wave height H = 4.03 [m] (0.13 [m] model scale). There is a dump in the values at approximately λ/L = 1. The results corresponds roughly with analysis by Nakamura and Naito (1975), where they showed that wave induced motions increases the velocities of the wake, and is more noticeable around the pitch natural period. From the pitch RAO in section 7.3.1 one can see there is a peak around λ/L = 1.3. It also show a consistent increase of the wake fraction for the tests with the Mewis Duct fitted, as in the still water results.

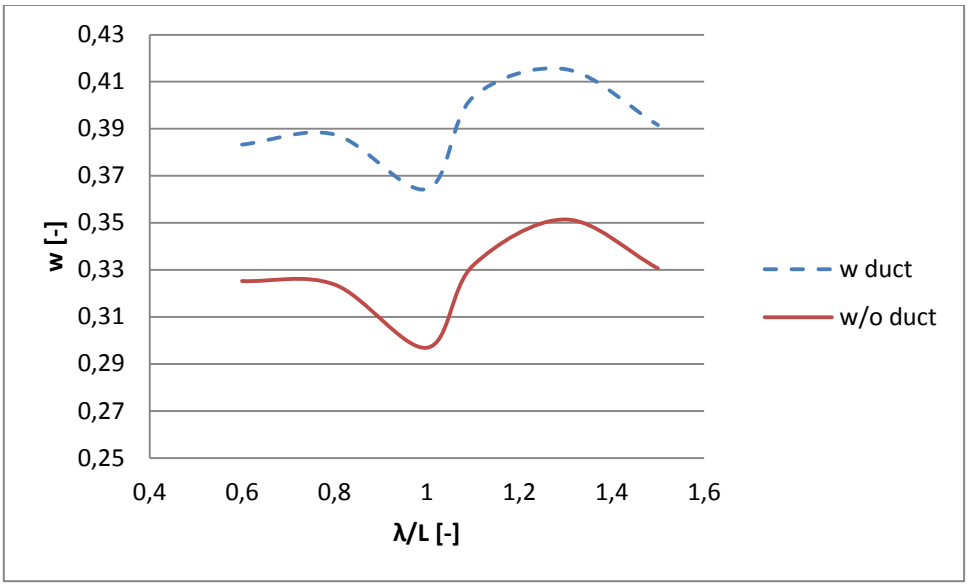


Figure 26: Effective wake versus wave length for Vs=15 [knots]

Table 18 presents results of calculated propulsive factors in waves regular at 17 [knots]. Thrust deduction t is calculated using the estimated $R_{Tm}$ as input.

Table 18: Calculated propulsive factors in regular waves at Vs = 17 [knots]

**With** Mewis Duct Fitted, 1.571 [m/s] (17 [kn] full scale)

| H [m] | λ/L [-] | t [-] | $K_T$ [-] | J [-] | J0 [-] | w [-] | $K_{Q0}$ [-] | $Q_0$ [Nm] | $K_Q$ [-] |
|---|---|---|---|---|---|---|---|---|---|
| 0,13 | 0,6 | 0,1925 | 0,2172 | 0,7426 | 0,4643 | 0,3748 | 0,0294 | 1,7879 | 0,0284 |
| 0,13 | 0,8 | 0,2507 | 0,2292 | 0,6966 | 0,4381 | 0,3710 | 0,0307 | 2,1189 | 0,0299 |
| 0,13 | 1 | 0,1765 | 0,2463 | 0,6337 | 0,4004 | 0,3681 | 0,0325 | 2,7081 | 0,0320 |
| 0,17 | 1 | 0,2279 | 0,2634 | 0,5681 | 0,3622 | 0,3624 | 0,0342 | 3,5514 | 0,0338 |
| 0,13 | 1,1 | 0,1827 | 0,2541 | 0,6280 | 0,3832 | 0,3897 | 0,0332 | 2,8249 | 0,0328 |
| 0,13 | 1,3 | 0,1800 | 0,2400 | 0,6680 | 0,4145 | 0,3794 | 0,0318 | 2,3883 | 0,0313 |
| 0,13 | 1,5 | 0,2348 | 0,2219 | 0,7271 | 0,4541 | 0,3754 | 0,0299 | 1,8960 | 0,0292 |

**Without** Mewis Duct Fitted, 1.571 [m/s] (17 [kn] full scale)

| H [m] | λ/L [-] | t [-] | $K_T$ [-] | J [-] | J0 [-] | w [-] | $K_{Q0}$ [-] | $Q_0$ [Nm] | $K_Q$ [-] |
|---|---|---|---|---|---|---|---|---|---|
| 0,13 | 0,6 | 0,1624 | 0,2010 | 0,7321 | 0,4990 | 0,3184 | 0,0277 | 1,7320 | 0,0274 |
| 0,13 | 0,8 | 0,1902 | 0,2129 | 0,6871 | 0,4735 | 0,3109 | 0,0290 | 2,0565 | 0,0288 |
| 0,13 | 1 | 0,1775 | 0,2294 | 0,6238 | 0,4377 | 0,2983 | 0,0307 | 2,6438 | 0,0306 |
| 0,17 | 1 | 0,2475 | 0,2481 | 0,5294 | 0,3966 | 0,2510 | 0,0326 | 3,9010 | 0,0324 |
| 0,13 | 1,1 | 0,1747 | 0,2398 | 0,6117 | 0,4150 | 0,3216 | 0,0318 | 2,8459 | 0,0317 |
| 0,13 | 1,3 | 0,0849 | 0,2240 | 0,6558 | 0,4495 | 0,3147 | 0,0301 | 2,3482 | 0,0300 |
| 0,13 | 1,5 | 0,0915 | 0,2048 | 0,7162 | 0,4909 | 0,3145 | 0,0281 | 1,8361 | 0,0277 |

Figure 27 show the thrust deduction plotted against the wave length/ship length ratio λ/L at $V_S$ = 17 [knots] in full scale and wave height H = 4.03 [m], (0.13 [m] model scale). Same as the results for $V_S$ = 15 [knots], even though thrust deduction seems higher for the Mewis Duct fitted, the plotted results are too scattered and no certain conclusion can be drawn. From the table and the figure one can see that some of the thrust deduction values are remarkable smaller than the others both for $V_S$ = 15 [knots] and $V_S$ = 17 [knots]. This is discussed further in a later section.

Figure 28 show the effective wake plotted against the wave length/ship length ratio at $V_S$ = 17 [knots] and wave height H = 4.03 [m] (0.13 [m] model scale). The effective wake follows roughly the same trend as discussed for $V_S$ = 15 [knots] and clearly show a consistent increase with the Mewis Duct fitted.

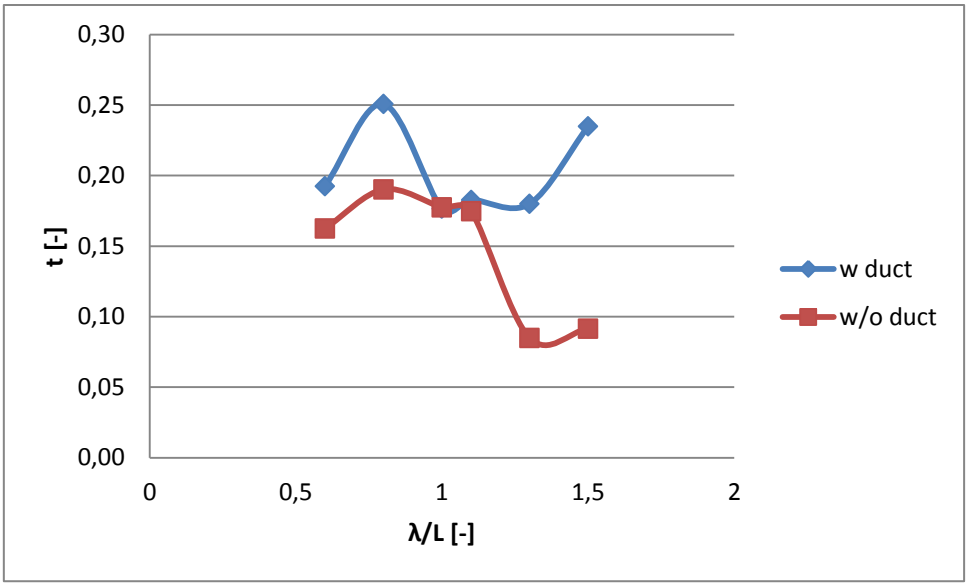


Figure 27: Thrust deduction versus wave length for Vs=17 [knots]

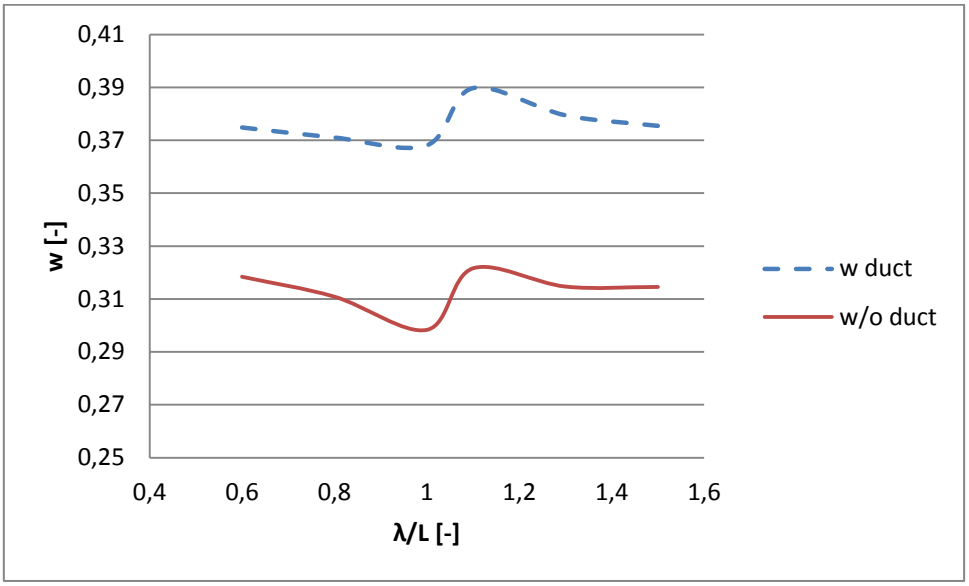


Figure 28: Effective wake versus wave length for Vs=17 [knots]

### 7.3.4 Propulsive Efficiency

Table 19 presents the calculated propulsive efficiency and its components in regular waves at $V_S$ = 15 [knots]. The relative rotative efficiency $\eta_R$ and the open water efficiency $\eta_0$ follows reasonable values with a clear reduction of $\eta_0$ around $\lambda/L = 1$, and most noticeable for the highest wave H = 0.17 [m] in model scale. The hull efficiency $\eta_H$ also follows a decreasing trend towards $\lambda/L = 1$ for the tests performed with the Mewis Duct fitted, but are more scattered without and no trend is clear. No relative difference of the propulsive efficiency $\eta_D$ with and without the duct fitted can be concluded with, which can be seen from Figure 29.

Table 19: Propulsive efficiency in regular waves at Vs = 15 [knots]

**With** Mewis Duct Fitted, 1.386 [m/s] (15 [kn] full scale)

| H [m] | λ/L [-] | $\eta_R$ [-] | $\eta_H$ [-] | $\eta_0$ [-] | $\eta_D$ [-] |
|---|---|---|---|---|---|
| 0,13 | 0,6 | 1,0358 | 1,3877 | 0,5325 | 0,7653 |
| 0,13 | 0,8 | 1,0247 | 1,2887 | 0,4966 | 0,6558 |
| 0,13 | 1 | 1,0151 | 1,2465 | 0,4697 | 0,5944 |
| 0,17 | 1 | 1,0129 | 1,1286 | 0,4254 | 0,4863 |
| 0,13 | 1,1 | 1,0111 | 1,2896 | 0,4526 | 0,5901 |
| 0,13 | 1,3 | 1,0146 | 1,3551 | 0,4857 | 0,6678 |
| 0,13 | 1,5 | 1,0252 | 1,4108 | 0,5354 | 0,7743 |

**Without** Mewis Duct Fitted, 1.386 [m/s] (15 [kn] full scale)

| H [m] | λ/L [-] | $\eta_R$ [-] | $\eta_H$ [-] | $\eta_0$ [-] | $\eta_D$ [-] | Diff. $\eta_D$ [%] |
|---|---|---|---|---|---|---|
| 0,13 | 0,6 | 1,0113 | 1,2077 | 0,5645 | 0,6894 | 9,92 % |
| 0,13 | 0,8 | 1,0037 | 1,1582 | 0,5304 | 0,6166 | 5,98 % |
| 0,13 | 1 | 1,0020 | 1,2079 | 0,5072 | 0,6139 | -3,28 % |
| 0,17 | 1 | 1,0042 | 1,0355 | 0,4621 | 0,4805 | 1,18 % |
| 0,13 | 1,1 | 1,0016 | 1,2510 | 0,4866 | 0,6098 | -3,34 % |
| 0,13 | 1,3 | 1,0039 | 1,3397 | 0,5206 | 0,7001 | -4,85 % |
| 0,13 | 1,5 | 1,0135 | 1,2728 | 0,5641 | 0,7276 | 6,03 % |

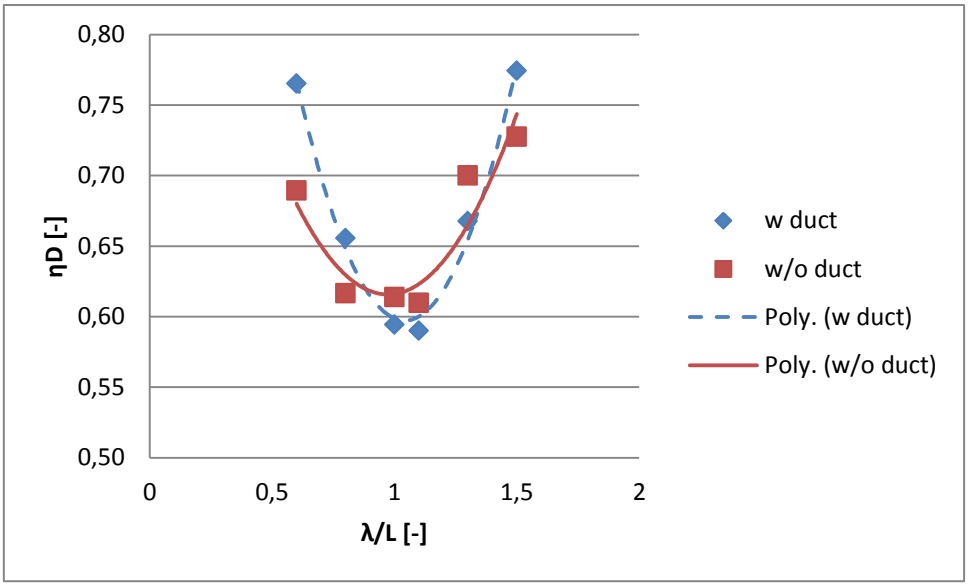


Figure 29: Propulsive efficiency versus wave length to ship length ratio in regular waves at Vs = 15 [knots]

Table 20 presents the calculated propulsive efficiency and its components in regular waves at $V_S$ = 17 [knots]. As for $V_S$ = 15 [knots], no conclusion can be drawn from the values in the table and Figure 30 showing the propulsive efficiency $\eta_D$ with and without the Mewis Duct.

Table 20: Propulsive efficiency in regular waves at Vs = 17 [knots]

| **With** Mewis Duct Fitted, 1.571 [m/s] (17 [kn] full scale) | | | | | | |
|---|---|---|---|---|---|---|
| H [m] | λ/L [-] | | $\eta_R$ [-] | $\eta_H$ [-] | $\eta_0$ [-] | $\eta_D$ [-] |
| 0,13 | | 0,6 | 1,0348 | 1,2917 | 0,5455 | 0,7291 |
| 0,13 | | 0,8 | 1,0246 | 1,1912 | 0,5210 | 0,6359 |
| 0,13 | | 1 | 1,0138 | 1,3032 | 0,4838 | 0,6391 |
| 0,17 | | 1 | 1,0109 | 1,2109 | 0,4440 | 0,5435 |
| 0,13 | | 1,1 | 1,0125 | 1,3392 | 0,4661 | 0,6320 |
| 0,13 | | 1,3 | 1,0169 | 1,3214 | 0,4979 | 0,6690 |
| 0,13 | | 1,5 | 1,0235 | 1,2252 | 0,5361 | 0,6722 |

| **Without** Mewis Duct Fitted, 1.571 [m/s] (17 [kn] full scale) | | | | | | | |
|---|---|---|---|---|---|---|---|
| H [m] | λ/L [-] | | $\eta_R$ [-] | $\eta_H$ [-] | $\eta_0$ [-] | $\eta_D$ [-] | Diff. $\eta_D$ [%] |
| 0,13 | | 0,6 | 1,0119 | 1,2288 | 0,5764 | 0,7166 | 1,71 % |
| 0,13 | | 0,8 | 1,0069 | 1,1751 | 0,5539 | 0,6554 | -3,07 % |
| 0,13 | | 1 | 1,0026 | 1,1721 | 0,5206 | 0,6117 | 4,29 % |
| 0,17 | | 1 | 1,0079 | 1,0047 | 0,4798 | 0,4859 | 10,61 % |
| 0,13 | | 1,1 | 1,0034 | 1,2166 | 0,4983 | 0,6083 | 3,74 % |
| 0,13 | | 1,3 | 1,0061 | 1,3353 | 0,5317 | 0,7143 | -6,77 % |
| 0,13 | | 1,5 | 1,0131 | 1,3254 | 0,5694 | 0,7645 | -13,73 % |

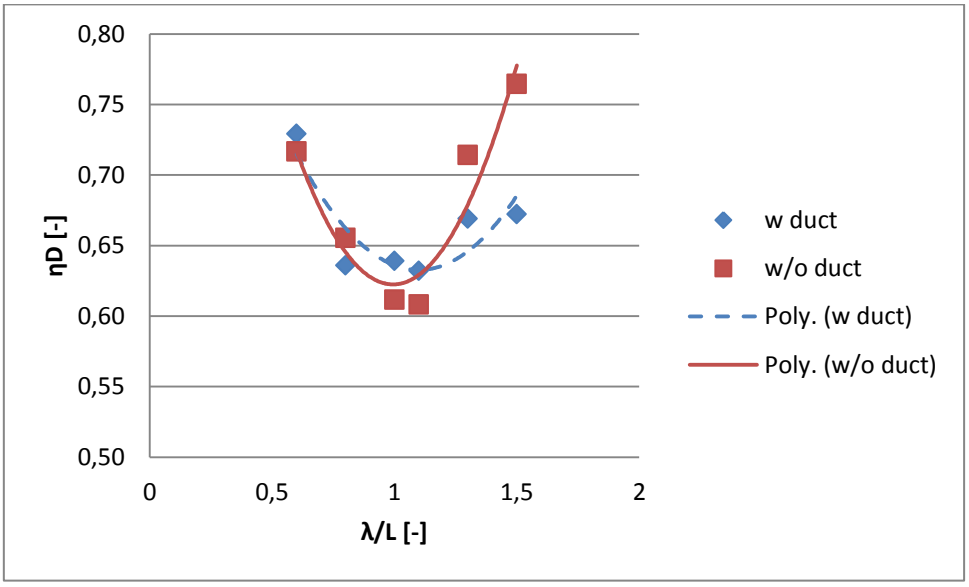


Figure 30: Propulsive efficiency versus wave length to ship length ratio in regular waves at Vs = 17 [knots]

### 7.3.5 Powering Prediction

Table 21 below presents the calculated and scaled delivered power $P_D$ and brake power $P_B$ in waves at $V_S$ = 15 [knots] with and without the Mewis Duct fitted. The results are calculated at the tow force corresponding to the self-propulsion point. The results show a mean decrease in the brake power with the Mewis Duct fitted of 1.94%. The table show somewhat scattered results, and no trend in the difference can be seen regarding wavelength or height. Results of the brake power with and without the Mewis Duct fitted are also presented in Figure 31 disregarding the run with H = 5.27 [m]. The brake power follows a clear trend with the wave length, and peak around λ/L = 1 can be observed.

Table 21: Powering prediction in waves at Vs = 15 [knots]

| **With** Mewis Duct Fitted, $V_S$ = 15 [knots] | | | |
|---|---|---|---|
| H [m] | λ/L [-] | $P_D$ [kW] | Pb [kW] |
| 4,03 | 0,6 | 12112,87 | 12360,07 |
| 4,03 | 0,8 | 16413,16 | 16748,12 |
| 4,03 | 1 | 23476,4 | 23955,51 |
| 5,27 | 1 | 38979,87 | 39775,38 |
| 4,03 | 1,1 | 22695,46 | 23158,63 |
| 4,03 | 1,3 | 15876,8 | 16200,82 |
| 4,03 | 1,5 | 11450,34 | 11684,02 |

| **Without** Mewis Duct Fitted, 15 [knots] | | | | |
|---|---|---|---|---|
| H [m] | λ/L [-] | $P_D$ [kW] | Pb [kW] | Diff. |
| 4,03 | 0,6 | 12231,52 | 12481,14 | 0,97 % |
| 4,03 | 0,8 | 16778,32 | 17120,74 | 2,18 % |
| 4,03 | 1 | 23154,49 | 23627,03 | -1,39 % |
| 5,27 | 1 | 39525,91 | 40332,56 | 1,38 % |
| 4,03 | 1,1 | 23797,26 | 24282,92 | 4,63 % |
| 4,03 | 1,3 | 16131,98 | 16461,2 | 1,58 % |
| 4,03 | 1,5 | 11955,48 | 12199,47 | 4,23 % |
| Mean | | | | 1,94 % |

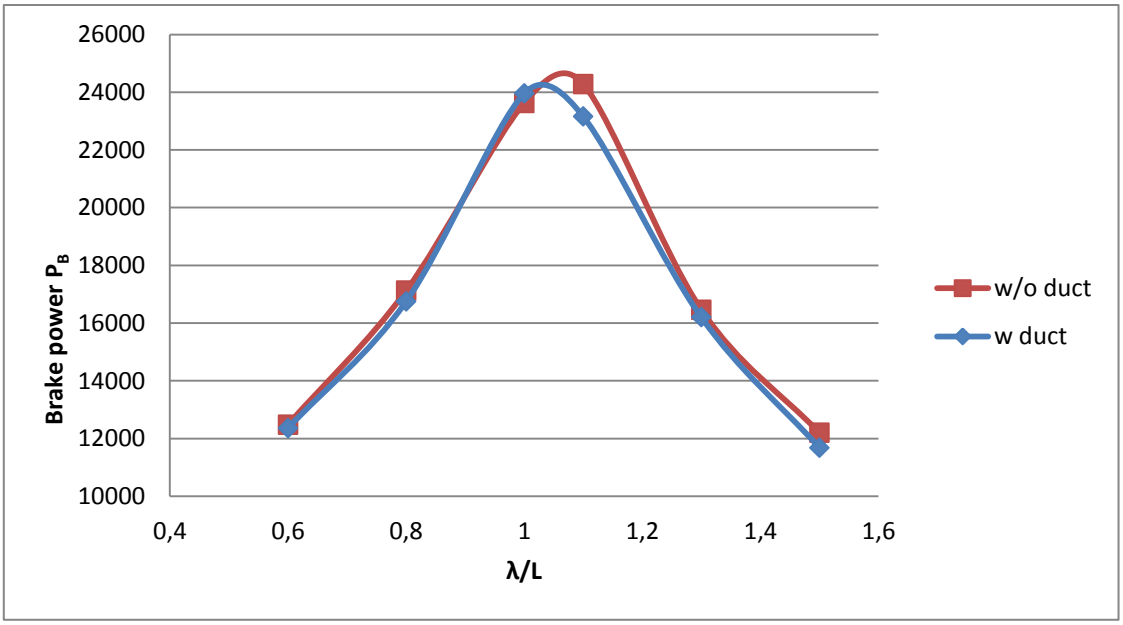


Figure 31: Brake power versus wave length to ship length ratio for H = 4.03 [m] at VS = 15 [knots]

Table 22 below presents the calculated and scaled delivered power $P_D$ and brake power $P_B$ in waves at $V_S$ = 17 [knots] with and without the Mewis Duct fitted. The results show a mean decrease in the brake power with the Mewis Duct fitted of 3%, but the run in wave height 5.27 [m] influences the result significantly and should probably be disregarded. Without that run a mean of less than 1% is observed. From this, it seems that the gain that can be obtained with the use of a Mewis Duct in waves is better pronounced for the lower vessel speed. Figure 32 presents the brake power with and without the Mewis Duct fitted plotted against the wave length to ship length ratio at $V_S$ = 17 [knots] disregarding the run in wave height 5.27 [m].

Table 22: Powering prediction in waves at Vs = 17 [knots]

| **With** Mewis Duct Fitted, $V_S$ = 17 [knots] | | | | |
|---|---|---|---|---|
| H [m] | λ/L [-] | $P_D$ [kW] | Pb [kW] | |
| 4,03 | 0,6 | 16393,02 | 16727,57 | |
| 4,03 | 0,8 | 20917,09 | 21343,97 | |
| 4,03 | 1 | 29699,88 | 30306,00 | |
| 5,27 | 1 | 43572,24 | 44461,47 | |
| 4,03 | 1,1 | 31303,42 | 31942,27 | |
| 4,03 | 1,3 | 24774,12 | 25279,71 | |
| 4,03 | 1,5 | 17950,16 | 18316,49 | |
| **Without** Mewis Duct Fitted, 17 [knots] | | | | |
| H [m] | λ/L [-] | $P_D$ [kW] | Pb [kW] | Diff. |
| 4,03 | 0,6 | 16473,39 | 16809,59 | 0,49 % |
| 4,03 | 0,8 | 20944,52 | 21371,96 | 0,13 % |
| 4,03 | 1 | 29784,03 | 30391,87 | 0,28 % |
| 5,27 | 1 | 51506,42 | 52557,57 | 15,40 % |
| 4,03 | 1,1 | 32668,21 | 33334,91 | 4,18 % |
| 4,03 | 1,3 | 25076,02 | 25587,78 | 1,20 % |
| 4,03 | 1,5 | 17829,3 | 18193,16 | -0,68 % |
| Mean | | | | 3,00 % |

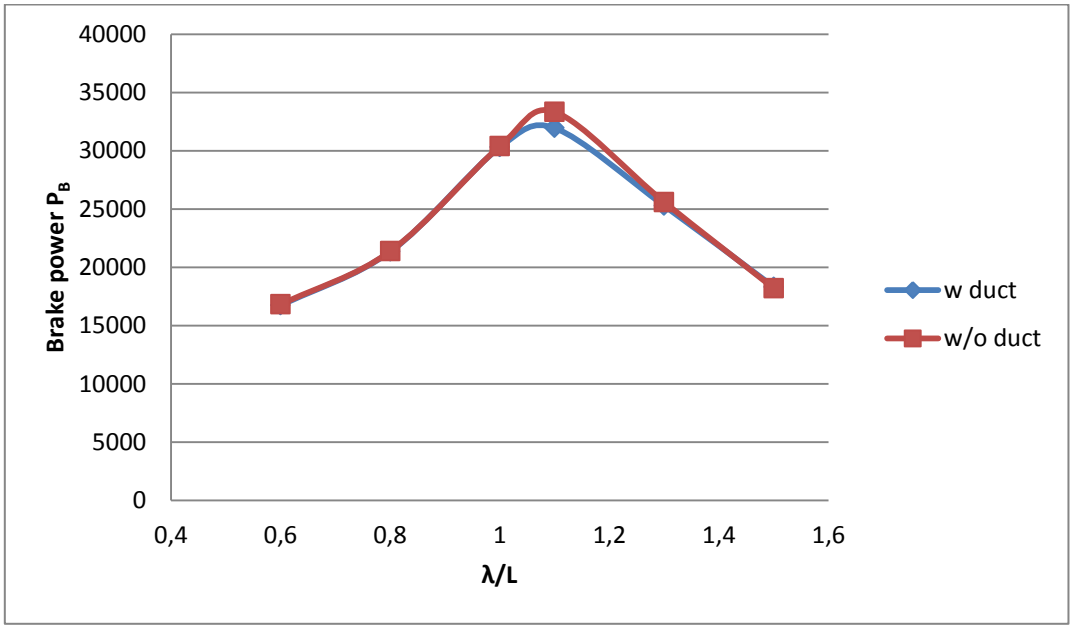


Figure 32: Brake power versus wave length to ship length ratio for H = 4.03 [m] at VS = 17 [knots]

## 7.4 Propulsion in Irregular Waves

For the irregular wave tests one carriage speed was used in all runs, $V_M$=1.386 [m/s] corresponding to 15 [knots] in full scale. As stated earlier, the irregular wave tests was performed at one propeller revolution setting trying to hit as close as possible to the calculated tow force $F_D$. As no resistance tests was conducted, the thrust deduction t had to be taken as a mean from previous results. A sensitivity study regarding the influence of minor changes in the thrust deduction t on the propulsive efficiency $\eta_D$ has been followed through.

### 7.4.1 Initial Results

Table 23 below presents the measured values from the propulsion in the irregular spectra 8000, $H_S$=0.113 [m] and $T_P$=2.156 [m] in model scale. The table show that the tow force are somewhat scattered, and does not correspond directly to the correct propulsion point, but results show that the thrust and torque are considerable higher at the given propeller revolution for the tests with the Mewis Duct.

Table 23: Measured values in the irregular wave spectrum Hs = 0.113 [m], Tp = 2.156 [m]

| **With** Mewis Duct Fitted, Hs=0.113 | | | |
|---|---|---|---|
| n | Q | T | F |
| 7,9912 | 1,460608 | 46,69511 | 10,5191 |
| 7,9917 | 1,459707 | 46,66101 | 13,1586 |
| 7,992 | 1,462307 | 46,83921 | 11,9425 |
| **Without** Mewis Duct Fitted, Hs=0.113 | | | |
| n | Q | T | F |
| 7,9947 | 1,381905 | 43,00921 | 12,051 |
| 7,9949 | 1,382105 | 43,02761 | 14,9117 |
| 7,9948 | 1,383405 | 43,09171 | 13,4935 |

Table 24 below presents the measured values from the propulsion in the irregular spectra 8010, $H_S$=0.161 [m] and $T_P$=2.156 [m] in model scale. The tow force corresponds better with the calculated tow force, but still has some scatter. The results show the same indication of increase of thrust and torque with the Mewis Duct fitted.

Table 24: Measured values in the irregular wave spectrum Hs = 0.161 [m], Tp = 2.156 [m]

| **With** Mewis Duct Fitted, Hs=0.161 | | | |
|---|---|---|---|
| n | Q | T | F |
| 7,9919 | 1,455007 | 46,56531 | 17,3322 |
| 7,992 | 1,456507 | 46,62281 | 21,3575 |
| 7,992 | 1,458507 | 46,70441 | 20,7463 |
| **Without** Mewis Duct Fitted, Hs=0.161 | | | |
| n | Q | T | F |
| 7,9946 | 1,376805 | 42,76601 | 19,1919 |
| 7,9947 | 1,381405 | 42,92351 | 23,5745 |
| 7,9949 | 1,379405 | 42,85921 | 22,5598 |

### 7.4.2 Propulsive Efficiency

Table 25 and Table 26 below present results of thrust deduction t, effective wake w and the propulsive efficiency $\eta_D$ and its components for $H_S$=0.113 [m] and $H_S$=0.161 [m] respectively. The t values used is averaged values from the previous results by MARINTEK, Alterskjær (2012). Using those values in the calculation result in approximately 2% higher propulsive efficiency with the Mewis Duct for $H_S$=0.113 and 2.4% for $H_S$=0.161. This does not mean a conclusion can be drawn from the results, as the thrust deduction used are from still water results. However it indicates the efficiency gain if the thrust deduction keeps the same relative difference in waves with and without the Mewis Duct as in still water. A simplification is made and the thrust deduction is assumed equal for both wave heights in these calculations, and reference is made to Nakamura and Naito (1975) where they showed that the thrust deduction had a relatively small change and only increased slightly with the wave height.

Table 25: Propulsive efficiency in the irregular wave spectrum Hs = 0.113 [m], Tp = 2.156 [m]

| **With** Mewis Duct Fitted, Hs=0.113 | | | | | | |
|---|---|---|---|---|---|---|
| t | w | $\eta_R$ | $\eta_H$ | $\eta_0$ | $\eta_D$ | diff. |
| 0,2 | 0,38594 | 1,02501 | 1,302804 | 0,528618 | 0,70591 | 2,08 % |
| 0,2 | 0,385323 | 1,025087 | 1,301496 | 0,529016 | 0,705786 | 2,04 % |
| 0,2 | 0,38783 | 1,026324 | 1,306827 | 0,527274 | 0,707195 | 2,18 % |
| **Without** Mewis Duct Fitted, Hs=0.113 | | | | | | |
| t | w | $\eta_R$ | $\eta_H$ | $\eta_0$ | $\eta_D$ | |
| 0,195 | 0,332153 | 1,016368 | 1,205365 | 0,56421 | 0,691211 | |
| 0,195 | 0,332367 | 1,016571 | 1,205753 | 0,564062 | 0,69139 | |
| 0,195 | 0,333304 | 1,016789 | 1,207447 | 0,563466 | 0,691778 | |

Table 26: Propulsive efficiency in the irregular wave spectrum Hs = 0.161 [m], Tp = 2.156 [m]

| **With** Mewis Duct Fitted, Hs=0.161 | | | | | | |
|---|---|---|---|---|---|---|
| t | w | $\eta_R$ | $\eta_H$ | $\eta_0$ | $\eta_D$ | diff. |
| 0,2 | 0,383888 | 1,026767 | 1,298466 | 0,529991 | 0,706596 | 2,37 % |
| 0,2 | 0,384696 | 1,026702 | 1,30017 | 0,529431 | 0,706731 | 2,36 % |
| 0,2 | 0,385878 | 1,026691 | 1,302672 | 0,528619 | 0,706997 | 2,40 % |
| **Without** Mewis Duct Fitted, Hs=0.161 | | | | | | |
| t | w | $\eta_R$ | $\eta_H$ | $\eta_0$ | $\eta_D$ | |
| 0,195 | 0,328714 | 1,015627 | 1,199191 | 0,566417 | 0,689857 | |
| 0,195 | 0,330932 | 1,015156 | 1,203166 | 0,564993 | 0,690084 | |
| 0,195 | 0,329969 | 1,015452 | 1,201438 | 0,565599 | 0,690032 | |

### 7.4.3 Influence of Thrust Deduction

A sensitivity analysis of the influence of change in the thrust deduction t on the propulsive efficiency $\eta_D$ was carried out for the irregular wave data and the results are presented in Table 27 below. Different values of thrust deduction was chosen with basis in still water and regular wave data. Mean values from the runs in irregular waves with and without the Mewis Duct fitted was compared. The basis of the values chosen for t was:

- The averaged values of all the runs in regular waves with and without the Mewis Duct fitted.
- The Averaged values from regular waves with wave length to ship length ratio $\lambda/L$ = 0.8-1.1 with and without the Mewis Duct fitted.
- Values obtained by curve fitting of the regular wave values at $V_S$ = 15 [knots] using a polynomial of second degree. The values at $\lambda/L$ = 0.8-1.1 was used.
- Values from the still water results for $V_S$ = 15 [knots] with and without the Mewis Duct fitted.
- Values from the still water results from the tests performed by MARINTEK with and without the Mewis Duct fitted, Alterskjær (2012).

The table show that values of thrust deduction with around the same difference with and without the Mewis Duct gives about the same result. Relative small changes in the propulsive efficiency is made from relative large changes in the thrust deduction, as can be seen in Figure 33, but as the values of interest are the differences with and without the Mewis Duct fitted, which is expected around 2-5 % or even smaller in waves, it show the necessity to obtain accurate values for all the parameters involved. Both positive and negative values of the

difference is obtained. The uncertainty in the measurements are discussed further in a later section.

Table 27: Influence of changes in thrust deduction on the propulsive efficiency with and without Becker Mewis Duct

| | Average from reg. waves | | Average from reg. waves with λ/L 0.8-1.1 | | Curve fitted values from reg. waves | | Still water for Vs = 15 [knots] | | Still water from MARINTEK | |
|---|---|---|---|---|---|---|---|---|---|---|
| | t | $\eta_D$ | t | $\eta_D$ | t | $\eta_D$ | t | $\eta_D$ | t | $\eta_D$ |
| w duct | 0,2032 | 0,7037 | 0,218 | 0,6906 | 0,1979 | 0,7084 | 0,1714 | 0,7318 | 0,2 | 0,7065 |
| w/o duct | 0,1687 | 0,7133 | 0,1948 | 0,6909 | 0,147 | 0,7319 | 0,1663 | 0,7154 | 0,195 | 0,6907 |
| Difference | | -1,36 % | | -0,03 % | | -3,33 % | | 2,24 % | | 2,24 % |

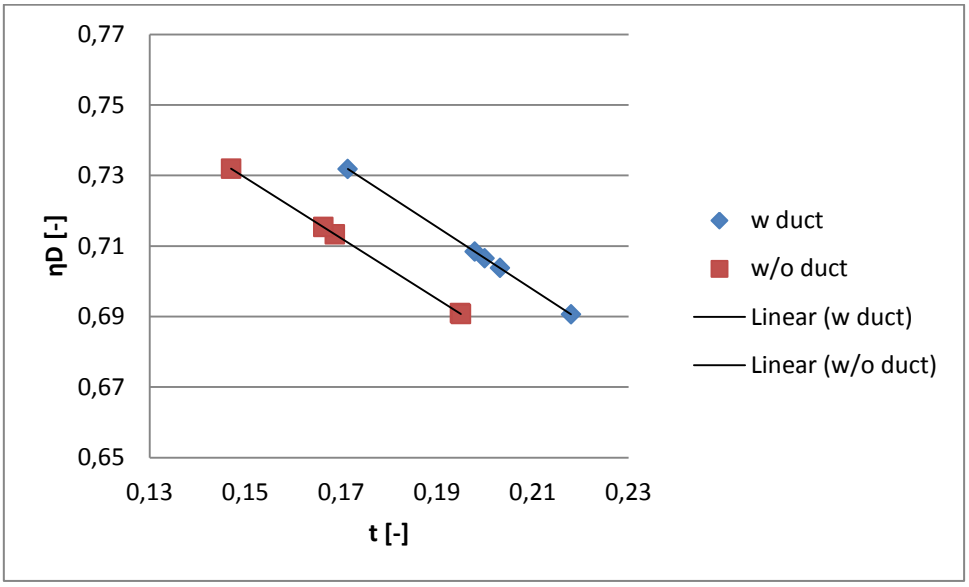


Figure 33: Influence of thrust deduction on the propulsive efficiency

## 7.5 Repeatability

Repeatability of the test will indicate the accuracy of the performed tests, and hence indicate if the results are reliable. The replication level of the repeated measurements indicate how large part of the set-up that is held the same. The important part in the current set-up was to ensure that as mutch as possible of the test-setup was held the same, thus moving most of the errors to bias error in the measurement.

Ideally, if time and money was of no concern, every test condition would be repeated a sufficient amount of times to ensure the accuracy. Realistically this is not possible, hence one condition is repeated and the standard deviation is assumed representative for the other conditions.

### 7.5.1 Precision Limit

Precision limits are calculated according to ITTC (2002). The standard deviation s is calculated as:

$$s^2 = [1/(n-1)]\sum_{k=1}^{n}(q_k - \bar{q})^2 \tag{7.6}$$

where $q_k$ is the observed quantity, n is the number of observations and $\bar{q}$ is the mean value:

$$\bar{q} = \sum_{k=1}^{n}\frac{q_k}{n} \tag{7.7}$$

Precision limits are now calculated as:

$$P(M) = \frac{s \cdot t}{\sqrt{n}} \qquad \text{for multiple sample precision} \tag{7.8}$$

$$P(S) = s \cdot t \qquad \text{for single sample precision} \tag{7.9}$$

where the weight t is determined following Student's t distribution for a 95% confidence interval shown in Figure 34 taken from Steen (2012):

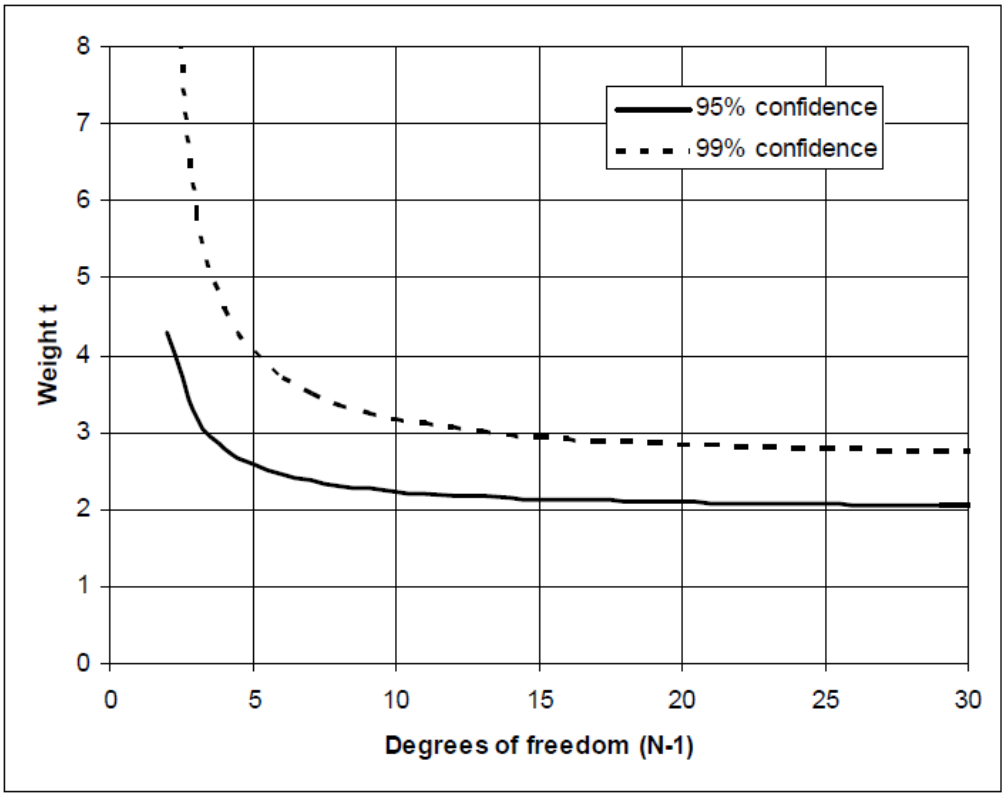


Figure 34: The weight t for estimating confidence intervals using Student's t distribution, Steen (2012)

For the M3030 A, one of the calm wave conditions were repeated, and a total of five runs were performed (run 2530, 2531, 2532, 2533 and 2535). Wave 8260 was used (Reg H=0.13, T=2.640), and a ship velocity 17 knots (1.571 [m/s] model scale). This is a wave with a long period and hence for simplicity the results are assumed to be roughly representative for still water conditions as well, as the uncertainty in still water measurements should definitely not be higher. The results are presented in Table 28 and Table 29 below.

Table 28: Calculation of precision limit for multiple and single runs for the measured values

| | $n_1$ | $T_1$ | $Q_1$ | $F_{D1}$ | $n_2$ | $T_2$ | $Q_2$ | $F_{D2}$ |
|---|---|---|---|---|---|---|---|---|
| | 7,6537 | 32,3312 | 1,0937 | 45,2931 | 8,8372 | 50,6473 | 1,661 | 28,1691 |
| | 7,6536 | 32,1258 | 1,0873 | 43,8093 | 8,8371 | 50,6541 | 1,6604 | 27,8787 |
| | 7,6541 | 31,7898 | 1,0789 | 44,272 | 8,8372 | 50,7151 | 1,6627 | 28,0534 |
| | 7,6541 | 32,0557 | 1,086 | 44,1948 | 8,8376 | 50,583 | 1,6592 | 28,1352 |
| | 7,6541 | 32,2346 | 1,0911 | 44,0041 | 8,8371 | 50,6185 | 1,6625 | 29,2261 |
| Avg | 7,65392 | 32,10742 | 1,0874 | 44,31466 | 8,83724 | 50,6436 | 1,66116 | 28,2925 |
| s^2 | 6,2E-08 | 0,04254 | 3,19E-05 | 0,33134 | 4,3E-08 | 0,00238 | 2,153E-06 | 0,28499 |
| s | 0,00025 | 0,20624 | 0,00565 | 0,57562 | 0,00021 | 0,04883 | 0,00147 | 0,53385 |
| P(M) | 0,00031 | 0,25609 | 0,00701 | 0,71473 | 0,00026 | 0,06063 | 0,00182 | 0,66286 |
| % | 0,004 % | 0,798 % | 0,645 % | 1,613 % | 0,003 % | 0,120 % | 0,110 % | 2,343 % |
| P(S) | 0,00069 | 0,57263 | 0,01568 | 1,59819 | 0,00058 | 0,13558 | 0,00407 | 1,48220 |
| % | 0,009 % | 1,783 % | 1,442 % | 3,606 % | 0,007 % | 0,268 % | 0,245 % | 5,239 % |

Table 28 shows that the measured quantities have a reasonable accuracy for single runs, and the tow force $F_D$ is more uncertain than the other quantities which agree with Holtrop and Hooijmans (2002) where they stated that a higher scatter had been observed for the tow force F than the other signals. The accuracy is higher for the second thrust and torque measurements, whilst lower for the second tow force. This can be explained by the fact that higher values with difference of around the same order give a lower relative uncertainty.

Table 29: Calculation of precision limit for multiple and single runs for the calculated t*, w and propulsive efficiency

| | t* | w | $\eta_R$ | $\eta_H$ | $\eta_0$ | $\eta_D$ |
|---|---|---|---|---|---|---|
| | 0,0651 | 0,3145 | 1,0131 | 1,3639 | 0,5694 | 0,7868 |
| | 0,1402 | 0,3152 | 1,0135 | 1,2555 | 0,5688 | 0,7237 |
| | 0,1430 | 0,3169 | 1,0129 | 1,2546 | 0,5674 | 0,7210 |
| | 0,1332 | 0,3137 | 1,0131 | 1,2630 | 0,5689 | 0,7280 |
| | 0,1961 | 0,3089 | 1,0113 | 1,1632 | 0,5664 | 0,6663 |
| Avg | 0,1355 | 0,3138 | 1,0128 | 1,2600 | 0,5682 | 0,7251 |
| s^2 | 0,0022 | 0,0000 | 0,0000 | 0,0051 | 0,0000 | 0,0018 |
| s | 0,0467 | 0,0030 | 0,0008 | 0,0711 | 0,0012 | 0,0427 |
| P(M) | 0,0580 | 0,0037 | 0,0011 | 0,0883 | 0,0015 | 0,0530 |
| % | 42,776 % | 1,183 % | 0,104 % | 7,008 % | 0,272 % | 7,311 % |
| P(S) | 0,1296 | 0,0083 | 0,0024 | 0,1975 | 0,0035 | 0,1185 |
| % | 95,650 % | 2,645 % | 0,233 % | 15,671 % | 0,609 % | 16,348 % |

From Table 29 it can be seen that the accuracy of the effective wake $w$, the relative rotative efficiency $\eta_R$, and the open water efficiency $\eta_0$ is well within reasonable values for single runs. The calculated thrust deduction factor $t^*$ show a very large precision limit of 42.776% for the multiple runs and as high as 95.65% for single runs. Two of the values are completely off in different directions from the others.

The precision limit was also calculated for the brake power $P_B$, and the results are presented in Table 30 below. With a precision limit of 6.2% for single runs it indicates that there are error sources in the model set-up with significant influence. With the differences with and without the Mewis Duct fitted of around 1- 3% depending on wave condition and speed, no certain conclusion can be made regarding the decrease in brake power. Further it should be noticed from the table that only one of the values of brake power are far from the others. If more repeated runs had been made one could disregard such outliers if the deviation was large enough in order to minimize the error and obtain a more certain outcome.

Table 30: Calculation of precision limit for multiple and single runs for brake power

| | $P_B$ |
|---|---|
| | 18193,162 |
| | 18236,565 |
| | 18336,540 |
| | 18335,645 |
| | 19187,762 |
| Avg | 18457,935 |
| s^2 | 170362,188 |
| s | 412,750 |
| P(M) | 512,496 |
| % | 2,777 % |
| P(S) | 1145,976 |
| % | 6,209 % |

### 7.5.2 Error Propagation in the calculated thrust deduction

To further investigate the error in the thrust deduction t* it is useful to look at the error propagation. The thrust deduction equation is given as stated earlier:

$$t^* = 1 - \frac{\delta F_D}{\delta T} = 1 - \frac{F_1 - F_2}{T_2 - T_1} \tag{7.10}$$

To indicate the influence each of the input parameter have on the resulting thrust deduction t*, influence coefficients have been calculated according to Steen (2012):

The reduction equation of the result for which the uncertainty is sought can be written in general as:

$$X = f_r(Y_1, Y_2, ..., Y_N) \tag{7.11}$$

Here $f_r$ is the functional relation and $Y_i$ is the parameters X depends on. Assuming a small change in parameter $Y_i$ results in a small change in X, a Taylor expansion gives:

$$X = X + \sum_{i=1}^{N} \frac{\partial X}{\partial Y_i} \Delta Y_i + \frac{1}{2} \frac{\partial^2 X}{\partial Y_i^2} \Delta Y_i^2 + O(\Delta Y_i^3) \simeq X + \sum_{i=1}^{N} \frac{\partial X}{\partial Y_i} \Delta Y_i \tag{7.12}$$

Here $X$ is the result from the measurement. The influence coefficients are from this defined as:

$$\kappa_i = \frac{\partial X}{\partial Y_i} \tag{7.13}$$

Partial differentiation of the function for t*, and with the averaged values of the measurements in the 5 repeated runs as input, gives:

$$\frac{\partial t^*}{\partial F_1} = -\frac{1}{T_2 - T_1} = -0.0466 \tag{7.14}$$

$$\frac{\partial t^*}{\partial F_2} = \frac{1}{T_2 - T_1} = 0,0466 \tag{7.15}$$

$$\frac{\partial t^*}{\partial T_1} = -\frac{F_1 - F_2}{(T_2 - T_1)^2} = -0,0539 \tag{7.16}$$

$$\frac{\partial t^*}{\partial T_2} = \frac{F_1 - F_2}{(T_2 - T_1)^2} = 0,0539 \tag{7.17}$$

This indicates that changes in the thrust have slightly more influence on the end result than changes in the tow force.

From this the elemental errors can be calculated as:

$$e_i = \kappa_i \cdot \Delta Y_i \tag{7.18}$$

where for the precision elemental error $\Delta Y_i$ is the precision error from the repeated measurements, and the combined effect gives:

$$e = \sqrt{\sum_{i=1}^{N} e_i^{\,2}} = 0,1208 \tag{7.19}$$

This gives a relative precision error of $e / X = 89,10\ \%$, corresponding roughly to the precision limit calculated directly from the 5 measurements in section 7.5.1. The tow force and the thrust are both relatively large quantities compared to the resulting thrust deduction. As it is calculated from dividing the difference in the values at two different conditions, even small deviations in the input values will result in large differences in the output. The scatter in the measured tow force seems to be the main reason for the variation in the thrust deduction.

This again propagates to the hull efficiency $\eta_H$ with a precision limit of 15.67% for single runs:

$$\eta_H = \frac{1-t}{1-w} \tag{7.20}$$

and further to the resulting propulsive efficiency $\eta_D$ with a precision limit of 16.35% for single runs:

$$\eta_D = \eta_R \eta_0 \eta_H \tag{7.21}$$

The bias error in the measurement can be investigated in a similar way, but then $\Delta Y_i$ need to be estimated, which is a more complex and time consuming process.

# 8 Discussion of Error Sources

The main results in this thesis are based on relative differences with and without the Mewis Duct fitted during the test runs. Therefore keeping the test conditions as equal as possible for the compared runs was of high priority, thus moving most of the precision error to bias error in the measurements. After the tests were completed, some deviation from the original tests with M3030 A, and the Mewis Duct model was observed, and a discussion of possible error sources could provide useful information in that regard. Most notably the tow force in calm water was higher than the original tests with the same rate of revolution and model speed, which indicates an increase of resistance.

Before the tests were conducted the model went through reparation of some surface cracks which could have an impact on the resistance.

After the decision to change waterline, the model draught was a bit larger compared to the DWL, resulting in a larger wetted surface and increased frictional resistance. The weight measured after the test was 2342 [kg] against 2324.6 [kg] at DWL. This is a small detail and result in a minor bias.

The large size of the model resulted in the necessity of a custom setup with the wires from the mid ship beam fastened to a platform behind the model. Despite of careful mounting and test runs this still resulted in a minor yaw angle and uneven towing force SB/PB which could affect the total tow force measurement.

# 9 Conclusion and Recommendations

In this thesis, the efficiency of a Mewis Duct in waves has been investigated with the use of model tests in the large towing tank at MARINTEK in Trondheim. A "load-varying" self-propulsion method was used, allowing for calculations without the need for results from a resistance test, and hence saves time spent in the tank. The model used was M3030 A, which was originally used to model test the Mewis Duct in still water, and the results was made available for the work on this thesis. Still water, regular and irregular wave conditions was tested in this work.

Some of the results in still water for the current setup were compared to the original results. The model resistance was found to be higher than for the original tests, which was expected from what is known from ageing of the hull, but in a larger order than expected even with the correction applied assuming lower resistance without the propeller present. It could be affected by bias in the tow force measurements, or the execution of the model setup. The effective wake was found to be somewhat larger for the current setup and the difference with and without the duct fitted was larger. The thrust deduction was found to be lower for the current setup, and the results was scattered. The scatter is most likely due to uncertainty in the tow force measurements. This again resulted in the propulsive efficiency being scattered, but it still seems to be higher with the Mewis Duct fitted with an average difference around 2.6%. Brake power was also calculated, and was around 2% lower with the duct fitted compared to 3-5% for different speeds in the original tests.

The wake field into the propeller is an important part of the Mewis Duct, and modification of the wake field in waves is expected to be of importance. The effective wake maintained the relative difference with and without the Mewis Duct in all the wave conditions for both speeds tested. This indicates that the velocity change in the wake field does not affect the efficiency gain with the Mewis Duct compared to still water.

The thrust deduction in waves was very varying, as in the still water measurements. This resulted in both positive and negative difference in the propulsive efficiency with and without the Mewis Duct fitted. No clear trend following the wave length could be seen. The thrust deduction is not necessarily the most important parameter affecting the Mewis Duct in waves, but the scatter influenced the end result in a large degree.

The calculated brake power in waves followed a clear trend with the wave length, peaking around $\lambda/L = 1$. The relative difference with and without the Mewis Duct was in the order of

around 2% for $V_S$ = 15 [knots] and below 1% for $V_S$ = 17 [knots]. This indicates that the energy savings with the Mewis Duct is still preserved in waves, or at least not severely influenced by waves.

A sensitivity study of the thrust deduction on the propulsive efficiency based on these results from irregular waves was carried out. The results showed that the magnitude of the thrust deduction had relatively little influenc on the end result, but as the differences in thrust deduction with and without the Mewis Duct fitted was varying a lot, both negative and positive efficiency gain with the duct fitted was obtained. This shows the necessity of obtaining accurate values for all the parameters involved in the calculation to get certain results.

An uncertainty analysis was performed based on five repeated runs in one of the wave conditions. The precision limit for the measured quantities and the calculated quantities of interest was calculated. It showed relatively small uncertainty for rate of revolutions, thrust and torque, but the tow force contained more scatter. Influence coefficients calculated for the thrust deduction indicated a large dependency of accurate measurements of thrust and tow force. High uncertainty in the tow force measurement resulted in large scatter in the thrust deduction, and further to the resulting propulsive efficiency. This shows that no certain conclusion regarding the difference in propulsive efficiency in waves can be stated. Precision limit calculated for the brake power show a higher uncertainty than the predicted relative differences with and without the Mewis Duct. This means that a certain conclusion cannot be made from the test results. The analysis indicates that the energy savings with the Mewis Duct are very hard to measure accurate, and with the load-varying propulsion method, accurate measurements of tow force is of high importance. The inaccurate measurements also influence the interpolation to the self-propulsion point. The savings are not necessarily influenced by waves, but further study is needed to be certain.

The two different rates of revolutions for different loading conditions were measured in one run. In order to obtain more accurate measurements of the tow force, the loading conditions should be measured in separate runs to get longer time series to average. More than two loading conditions could also be used in order to verify the linearity of thrust versus tow force. Constant increments of the rate of revolutions could also provide more stable results.

The regular MARINTEK procedure for propulsion tests could provide more accurate results, as the experience with the load-varying method is rather little for the facility. More time would be required for this, as a set of resistance tests would be needed.

A more comprehensive uncertainty analysis including investigation of the bias in the measurements can be carried out, and with several repeated conditions, and also using former test results. This is complex and time consuming.

## References


Alterskjær, S.A. (2012). "Model Tests with Becker Mewis Duct® for Solvang 84k LPG Carrier", BMS 10185 Ship Owners Report, MARINTEK.

Carlton, J. S. (2007). "Marine Propellers and Propulsion (2nd Edition)", Elsevier

DNV (2010). "Environmental Conditions and Environmental Loads", Recommended Practice, Det Norske Veritas, DNV-RP-C205.

Faltinsen, Minsaas, Liapis and Skjørdal. (1980). "Prediction of Resistance and Propulsion of a ship in a seaway", Thirteenth Symposium on Naval Hydrodynamics, Tokyo, Japan

Holtrop, J. (2001). "Extrapolation of propulsion tests for ships with appendages and complex propulsors", Marine Technology, Vol. 38, No. 3:p. 145–157.

Holtrop, J and Hooijmans, P. (2002). "Quasi-Steady Model Experiments on Hybrid Propulsion Arrangements", MARIN, Wageningen, The Netherlands.

ITTC (2002). "Propulsion, Performance Uncertainty Analysis, Example for Propulsion Test", ITTC –Recommended Procedures and Guidelines.

ITTC (2011_1). "Prediction of Power Increase in Irregular Waves from Model Test", ITTC – Recommended Procedures and Guidelines.

ITTC (2011_2). "Propulsion/Bollard Pull Test", ITTC –Recommended Procedures and Guidelines.

Langeland, A.O. (2013). "EMIP II- Mewis Duct performance on Grieg Star I- class vessels", Bergen, Norway.

Mewis, F. (2009). "A Novel Power-Saving Device for Full-Form Vessels", Mewis Ship Hydrodynamics (MSH), Dresden, Germany.

Mewis, F. (2010). "Mewis Duct – a new Energy-Saving Device", Presentation.

Mewis, F. and Guiard, T. (2011). "Mewis Duct® – New Developments, Solutions and Conclusions", Second International Symposium on Marine Propulsors smp'11, Hamburg, Germany.

Mewis, F. (2012). “Propulsionsversuche mit und ohne Mewis Duct®”, Schiff & Hafen, May 2012 Nr. 5, Hamburg, Germany.

Molland, A.F., Turnock, S.R., Hudson, D.A. (2011). “Ship resistance and propulsion: practical estimation of ship propulsive power”, Cambridge University Press, New York.

Nakamura, S. and Naito, S. (1975). “Propulsive Performance of a Container Ship in Waves”, J.S.N.A., Kansai, Japan.

Rolls Royce (2009). “Promas High efficiency propulsion system”, Fact sheet, Rolls-Royce AB, Kristinehamn, Sweden.

Schneekluth, H. (1986) “Wake equalizing ducts”, The Naval Architect, London, UK.

Steen, S. and Minsaas, K. (2012). “Propeller Theory”, Lecture notes, Marine Technology Centre, Trondheim, Norway.

Steen, S. (2012). “Experimental Methods in Marine Hydrodynamics”, Lecture notes, Marine Technology Centre, Trondheim, Norway.

Topphol, R.A. (2012). “The Efficiency of a Mewis Duct in Waves”, Project Thesis, NTNU, Trondheim, Norway.

# APPENDIX A: Results from pendulum test in pitch

**SHIFTING WEIGHTS**

Version: 1
Last update: 2011.02.21

| | | | | |
|---|---|---|---|---|
| Project No. | 846002.19 | Ettervipping etter kjøring med nytt depl | 08.03.2013 | **Date:** |
| Title | M3030A-NTNU | VIPPING PITCH | kl.14.30 | |
| Client | Sverre Steen | | T.I. | **Sign.:** |
| **EMPTY CRADLE** | Mass | | 387,100 | kg |
| | Moment of inertia about COG | | 202,242 | kg m2 |
| | Distance from knife to COG (+ downwards) | | 0,496 | m |
| | Distance from knife to base line (+ downwards) | | 0,450 | m |
| **ADDITIONAL WEIGHTS** | Mass per weight (2 of) | | 15,000 | kg |
| | Horizontal distance from knife | | 3,000 | m |
| | Vertical distance from knife to weights (+ downwards) | | 0,005 | m |
| **MODEL** | Mass | | 2342,000 | kg |
| **OSCILLATION PERIODS** | Oscillation period without additional weights | | 8,467 | s |
| | Oscillation period with additional weights | | 8,641 | s |
| **RESULTS** | Moment of inertia about knife | | 6126,530 | kg m2 |
| | Distance from knife to COG (+ downwards) | | 0,072 | m |
| | Moment of inertia about COG | | 6114,372 | kg m2 |
| | KG | | 0,378 | m |
| | Radii of gyration | | 1,616 | m |

# SHIFTING WEIGHTS

Version: 1
Last update: 2011.02.21

| | | | | | |
|---|---|---|---|---|---|
| Project No. | 846002.19 | Ettervipping etter kjøring med nytt depl | | 08.03.2013 | **Date:** |
| Title | M3030A-NTNU | TOMVIPPE | FOR PITCH | kl.10.00 | |
| Client | Sverre Steen | | | T.I. | **Sign.:** |

| | | | |
|---|---|---|---|
| **EMPTY CRADLE** | Mass | 0,000 | kg |
| | Moment of inertia about COG | 0,000 | kg m2 |
| | Distance from knife to COG (+ downwards) | 0,000 | m |
| | Distance from knife to base line (+ downwards) | 0,000 | m |
| **ADDITIONAL WEIGHTS** | Mass per weight (2 of) | 15,000 | kg |
| | Horizontal distance from knife | 3,000 | m |
| | Vertical distance from knife to weights (+ downwards) | 0,005 | m |
| **MODEL** | Mass | 387,100 | kg |
| **OSCILLATION PERIODS** | Oscillation period without additional weights | 2,497 | s |
| | Oscillation period with additional weights | 3,447 | s |
| **RESULTS** | Moment of inertia about knife | 297,637 | kg m2 |
| | Distance from knife to COG (+ downwards) | 0,496 | m |
| | Moment of inertia about COG | 202,242 | kg m2 |
| | KG | -0,496 | m |
| | Radii of gyration | 0,723 | m |

dato: 8/3-2013 kl 1430
sign: T. I

M 3030A NTNU

Etterstøping med nytt dekpl.

Vipping i pith

| uten tilleggslodd (~~10~~ 5 sving) | | m tilleggslodd 2x15kg (~~10~~ 5 sving) | |
|---|---|---|---|
| ~~8,454~~ | | ~~8,643~~ | |
| ~~8,470~~ | | 8,643 | |
| 8,466 | middel = 8,46675 | 8,640 | middel = 8,6415 |
| 8,468 | | ~~8,638~~ | |
| 8,466 | | 8,640 | |

Ballansert i vippa målt fra sp 0: 3510 millimeter (38 mm bakk sp 10)

Vekt: 2342 kg

Dette gir

treghetsmoment (I) : 6114,372 kgm2

KG : 0,378 m

treghetsradie (R) : 1,616 m

(Etterbøying eller forsøk)

dato: 8/3-2013 kl. 1000
sign:

M 3030A (NTNU
Tomvippe for pitch

| uten tilleggslodd (10 sving) | | m tilleggslodd 2x15kg (10 sving) | |
|---|---|---|---|
| ~~2,497~~ | | ~~3,447~~ | |
| ~~2,497~~ | | 3,447 | |
| 2,497 | middel = 2,497 | 3,447 | middel = 3,447 |
| 2,497 | | 3,447 | |
| 2,497 | | ~~3,446~~ | |

Ballansert i vippa målt fra sp 0: _____ millimeter

Vekt: 387,1 kg

tomvippe 185,1
2x100kg 200,-
ballenveledd 2,-
387,1

Dette gir

treghetsmoment (I) : 202,242 kgm2

KG : ÷0,496 m

treghetsradie (R) : 0,723 m

# APPENDIX B: Instrument calibration

| bjelkegiver | 8671 |
|---|---|

| | |
|---|---|
| **Dato:** | 2012-03-01 |
| **Tid:** | 10:36:00 |
| **Operatoer:** | MKo |
| **Gyldig til:** | |
| **Kalibreringsenhet:** | 20208 |
| **MGC:** | 1089 |
| **Målefrekvens [Hz]:** | 25 |
| **Målelengde [s]:** | 3 |

| | |
|---|---|
| **Slot:** | 5.1 |
| **ML-type:** | ML801 |
| **AP-type:** | AP810 |
| **Brotype:** | SG full bridge |
| **Brospenning [V]:** | 5 |
| **Filtertype:** | Bess |
| **Filterfrekvens [Hz]:** | 5 |
| **Målemetode:** | Net |
| **ML-serienummer:** | 040054081101 |
| **AP-serienummer:** | 104127001 |
| **Fysisk enhet:** | kg |
| **Skalering:** | 9.8066 |
| **Elektrisk enhet:** | mV/V |
| **Måleenhet:** | N |

| | Sensitivity: | Span: |
|---|---|---|
| **Kalibrering org.** | **1.0000 mV/V** | **2769.9254 N** |
| **Kalibrering mod.** | **1.0000 mV/V** | **2769.9254 N** |

| | | |
|---|---|---|
| **Stigningsfaktor:** | 2769.925353 N/(mV/V) | +/- NaN N/(mV/V) |
| **Nullpunkt:** | 0.000865 mV/V | |
| **Største målefeil:** | 0.222772 N | |

| |
|---|
| **Beskrivelse av giver:** |
| **Notater til kalibreringen:** |

v. 3.8.1

| bjelkegiver | 8672 |
|---|---|

| | |
|---|---|
| **Dato:** | 2012-03-01 |
| **Tid:** | 10:50:00 |
| **Operatoer:** | MKo |
| **Gyldig til:** | |
| **Kalibreringsenhet:** | 20208 |
| **MGC:** | 1089 |
| **Målefrekvens [Hz]:** | 25 |
| **Målelengde [s]:** | 3 |

| | |
|---|---|
| **Slot:** | 5.1 |
| **ML-type:** | ML801 |
| **AP-type:** | AP810 |
| **Brotype:** | SG full bridge |
| **Brospenning [V]:** | 5 |
| **Filtertype:** | Bess |
| **Filterfrekvens [Hz]:** | 5 |
| **Målemetode:** | Net |
| **ML-serienummer:** | 040054081101 |
| **AP-serienummer:** | 104127001 |
| **Fysisk enhet:** | kg |
| **Skalering:** | 9.8066 |
| **Elektrisk enhet:** | mV/V |
| **Måleenhet:** | N |

| | **Sensitivity:** | **Span:** |
|---|---|---|
| Kalibrering org. | **1.0000 mV/V** | **2774.6565 N** |
| Kalibrering mod. | **1.0000 mV/V** | **2774.6565 N** |

| | | |
|---|---|---|
| **Stigningsfaktor:** | 2774.656465 N/(mV/V) | +/- NaN N/(mV/V) |
| **Nullpunkt:** | 0.004674 mV/V | |
| **Største målefeil:** | 0.161343 N | |

| |
|---|
| **Beskrivelse av giver:** |
| **Notater til kalibreringen:** |

v. 3.8.1

| Dynamometer | | Thrust | Moment | Kalib |
|---|---|---|---|---|
| marintek nr | Dyn.nr | Span 2mv/v | Span 2mv/v | Dato |
| 20025 | 77 | 124.9223 | -6.0972 | 05.10.2012 |
| 20026 | 78 | 128.4928 | -5.5276 | 31.08.2012 |
| 20027 | 108 | 125.3709 | -6.0169 | 31.08.2012 |
| 20028 | 185 | 126.4874 | -5.883 | 31.08.2012 |
| 20029 | 186 | 130.1179 | -5.585 | 07.08.2012 |
| 20030 | 12 | 292.9958 | -14.3521 | 09.11.2012 |
| 20031 | 103 | 290.9525 | -12.1305 | 09.11.2012 |
| 20032 | 180 | 285.0361 | -12.1848 | 07.08.2012 |
| 20033 | 210 | 296.8082 | -12.718 | 09.11.2012 |
| 20034 | 211 | 291.4244 | -12.6785 | 15.01.2013 |
| 20035 | 136 | 500.0068 | -18.687 | 14.08.2012 |
| 20324 | | 294.8288 | -12.2373 | 05.10.2012 |
| 20325 | | 291.9568 | -12.2352 | 08.08.2012 |
| 20326 | | 493.4209 | -18.4668 | 08.08.2012 |

Annet fortegn på momentet dersom det er venstregående propell.
Alle dynamometrene er kalibrert med MGC+
Ac forsterker ext 5v 1mv/v

| | | Span 2mv/v | |
|---|---|---|---|
| 20046 | Towrope | 79.746 | 07.02.2012 |
| 20236 | Rtm | 492.4287 | 26.10.2012 |

| Sidekraftmåler | | Span 2mv/v | |
|---|---|---|---|
| 20059 | FP | -354.015 | 07.02.2012 |
| 20060 | AP | -342.981 | 07.02.2012 |

| Dysedynamometer | | Span 2mv/v | |
|---|---|---|---|
| 20039 | | 689.6922 | 23.02.2012 |
| 20040 | 22 | -201.3612 | 23.02.2012 |
| 20041 | 23 | -200.402 | 14.02.2012 |
| 20042 | 27 | -223.3325 | 22.02.2012 |
| 20043 | 19 | -422.538 | 16.10.2012 |
| 20044 | | 148.1724 | 14.03.2012 |
| 20045 | | 153.4118 | 14.03.2012 |
| 20049 | | 692.1631 | 12.03.2012 |
| 8575 | | 637.9015 | 16.10.2012 |

| | | Thrust | Moment | |
|---|---|---|---|---|
| Friprøvebåt | | Span 2mv/v | Span 2mv/v | |
| 20048 | Frip dyn | -516.919 | 18.05 | 31.03.2011 |

| Trimgivere | | Span 80mv/v | | |
|---|---|---|---|---|
| 6042 | Fp | -349.5458 | mm/v vender bakover | 13.03.2012 |
| 6042 | Fp | 323.9223 | mmv vender forover | 13.03.2012 |
| 6044 | Ap | -337.5956 | mm/v vender forover | 13.03.2012 |
| 6044 | Ap | 317.8351 | mm/v vender bakover | 13.03.2012 |

| Kalibreringsdato:11.09.2012 | | | Kalibreringsdato:11.09.2012 | | | Kalibreringsdato:21.09.2010 | | |
|---|---|---|---|---|---|---|---|---|
| 20001 | mmH2O | Pa | 20003 | mmH2O | Pa | 20004 | mmH2O | Pa |
| CS | 197.723 | 1939.000 | CS | 98.638 | 967.308 | CS | 103.007 | 1010.154 |
| CP | 198.486 | 1946.483 | CP | 98.982 | 970.682 | CP | 102.376 | 1003.966 |
| SP | 199.543 | 1956.848 | SP | 99.068 | 971.525 | SP | 100.599 | 986.539 |
| CT | 200.832 | 1969.489 | CT | 98.846 | 969.348 | CT | 102.888 | 1008.987 |
| CB | 197.158 | 1933.460 | CB | 99.312 | 973.918 | CB | 93.915 | 920.992 |
| TB | 197.607 | 1937.863 | TB | 100.849 | 988.991 | TB | 101.804 | 998.356 |

# APPENDIX C: Irregulare wave calibration

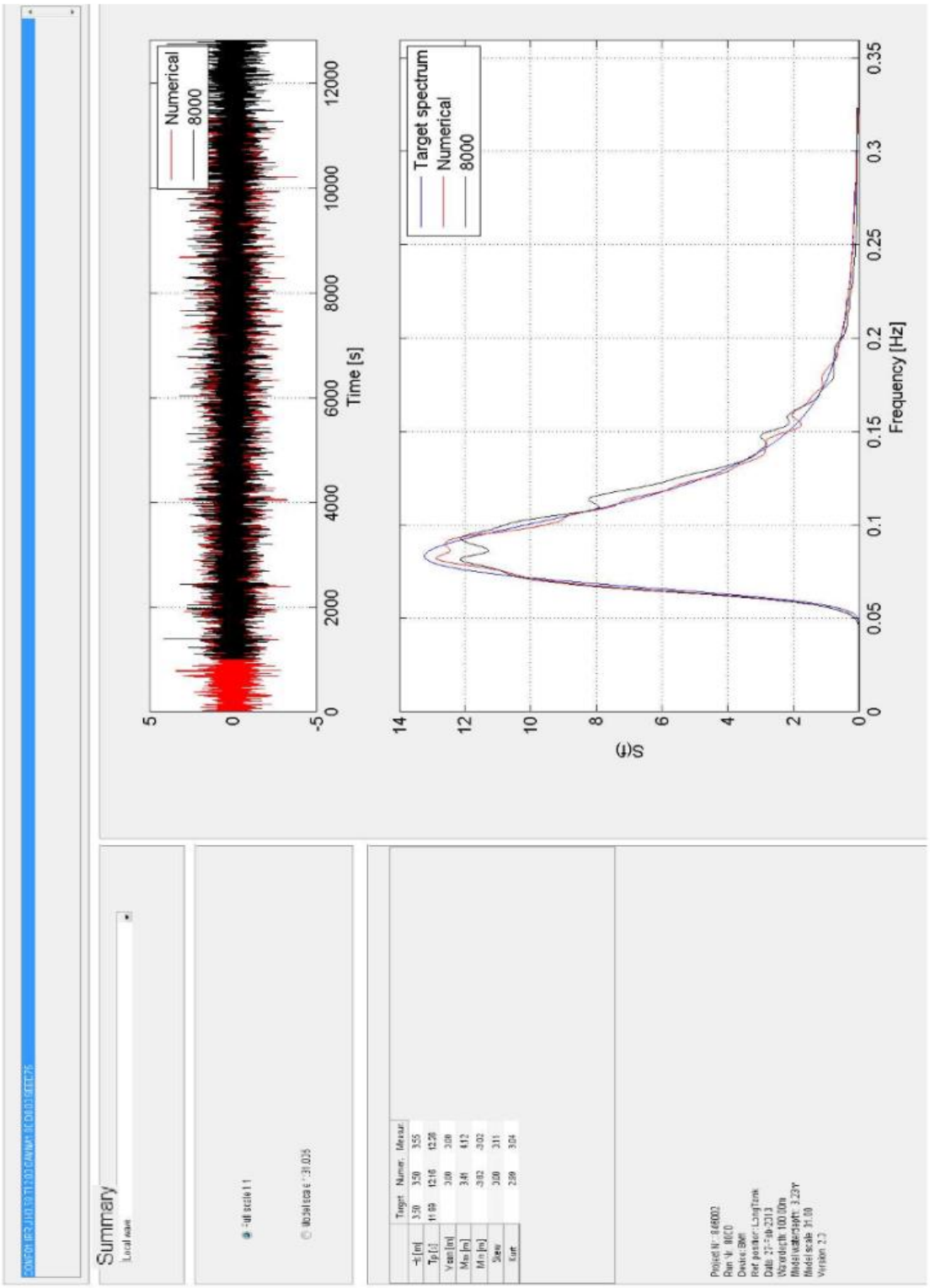

COMP01 IRR J H5.00 T12.00 GAMMA1.00 D0.00 SEED75

View Selector

Local wave

Scale

Full scale 1:1

Model scale 1:31.005

Summary

| | Target | Numer. | Measur. |
|---|---|---|---|
| Hs [m] | 5.00 | 5.00 | 5.05 |
| Tp [s] | 11.99 | 12.16 | 10.87 |
| Mean [m] | | 0.00 | 0.00 |
| Max [m] | | 4.87 | 6.35 |
| Min [m] | | -5.45 | -4.31 |
| Skew | | 0.00 | 0.14 |
| Kurt | | 2.99 | 3.07 |

Project Nr.: 846002
Run Nr.: 8010
Device: BM1
Ref. position: LongTank
Date: 27-Feb-2013
Waterdepth: 100.00m
Model waterdepth: 3.23m
Model scale: 31.00
Version: 2.0

Local wave

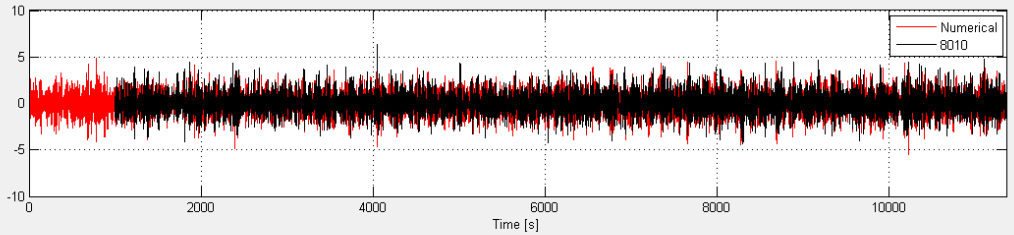


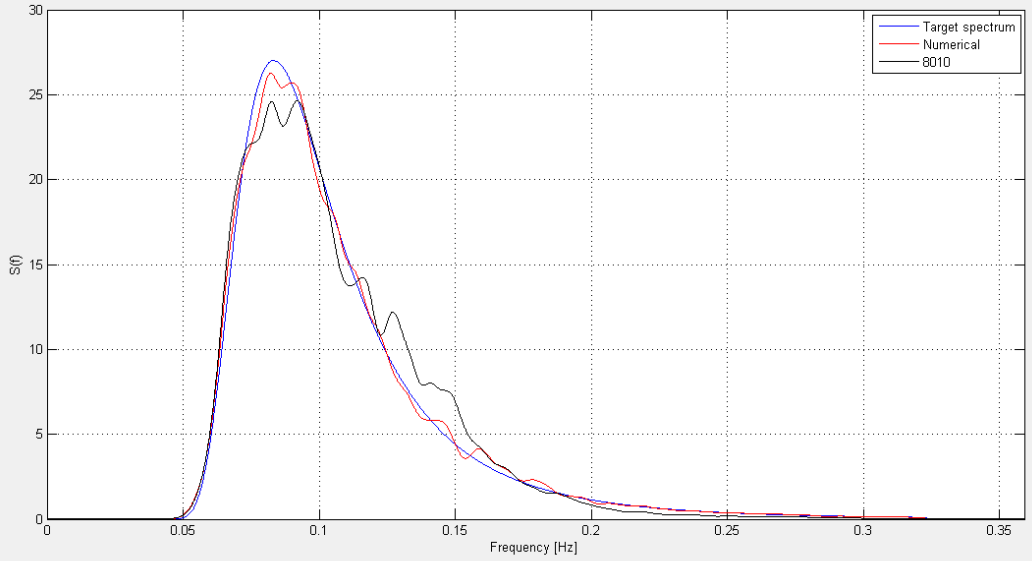

## APPENDIX D: Measured values in the self-propulsion tests

Measured values in calm water propulsion with the Mewis-Duct fitted:

| TEST NO. | $V_m$ [m/s] | $n_1$ [Hz] | $T_1$ [N] | $Q_1$ [Nm] | $Q_{corr}$ [Nm] | $T_{corr}$ [N] | $F_{D1}$ [N] |
|---|---|---|---|---|---|---|---|
| 6100 | 1,385831 | 6,6584 | 27,4219 | 0,8862 | 0,871507 | 27,41381 | 20,1834 |
| 6111 | 1,478219 | 7,1541 | 31,6941 | 1,0239 | 1,008761 | 31,67953 | 22,2062 |
| 6120 | 1,570608 | 7,6508 | 36,3271 | 1,1753 | 1,159714 | 36,30604 | 24,8972 |

| TEST NO. | $V_m$ [m/s] | $n_2$ [Hz] | $T_2$ [N] | $Q_2$ [Nm] | $Q_{corr}$ [Nm] | $T_{corr}$ [N] | $F_{D2}$ [N] |
|---|---|---|---|---|---|---|---|
| 6100 | 1,385831 | 7,9921 | 46,9563 | 1,4833 | 1,467407 | 46,94821 | 2,8234 |
| 6111 | 1,478219 | 8,4872 | 52,5504 | 1,6597 | 1,643362 | 52,53583 | 4,0914 |
| 6120 | 1,570608 | 9,0383 | 59,2818 | 1,8727 | 1,855866 | 59,26074 | 4,6333 |

Measured values in calm water propulsion without the Mewis-Duct fitted:

| TEST NO. | $V_m$ [m/s] | $n_1$ [Hz] | $T_1$ [N] | $Q_1$ [Nm] | $Q_{corr}$ [Nm] | $T_{corr}$ [N] | $F_{D1}$ [N] |
|---|---|---|---|---|---|---|---|
| 6200 | 1,385831 | 6,6599 | 24,6051 | 0,8326 | 0,817906 | 24,59701 | 21,3452 |
| 6210 | 1,478219 | 7,1556 | 28,4322 | 0,961 | 0,94586 | 28,41763 | 23,8411 |
| 6220 | 1,570608 | 7,6532 | 32,8404 | 1,1056 | 1,090012 | 32,81934 | 26,2208 |

| TEST NO. | $V_m$ [m/s] | $n_2$ [Hz] | $T_2$ [N] | $Q_2$ [Nm] | $Q_{corr}$ [Nm] | $T_{corr}$ [N] | $F_{D2}$ [N] |
|---|---|---|---|---|---|---|---|
| 6200 | 1,385831 | 7,9947 | 43,3001 | 1,4086 | 1,392705 | 43,29201 | 4,6233 |
| 6210 | 1,478219 | 8,4896 | 48,2456 | 1,5731 | 1,556759 | 48,23103 | 5,5905 |
| 6220 | 1,570608 | 9,027 | 54,5426 | 1,7804 | 1,763576 | 54,52154 | 6,6314 |

Measured values for propulsion in regular waves with the Mewis-Duct fitted:

| TEST NO. | $V_m$ [m/s] | $n_1$ [Hz] | $T_1$ [N] | $Q_1$ [Nm] | $Q_{corr}$ [Nm] | $T_{corr}$ [N] | $F_{D1}$ [N] |
|---|---|---|---|---|---|---|---|
| 2200 | 1,385841 | 6,66 | 26,58 | 0,8501 | 0,835406 | 26,57191 | 36,22 |
| 2210 | 1,57062 | 7,652 | 35,3 | 1,134 | 1,118413 | 35,27894 | 40,26 |
| 2220 | 1,385841 | 6,66 | 26,9116 | 0,8573 | 0,842606 | 26,90351 | 44,25 |
| 2230 | 1,57062 | 7,652 | 35,58 | 1,142 | 1,126413 | 35,55894 | 47,329 |
| 2240 | 1,385841 | 6,659 | 27,137 | 0,8657 | 0,851007 | 27,12891 | 57,8 |
| 2251 | 1,57062 | 9,0201 | 58,9247 | 1,8666 | 1,849782 | 58,90364 | 46,613 |
| 2260 | 1,385841 | 6,659 | 27,1942 | 0,8825 | 0,867807 | 27,18611 | 80,7642 |
| 2271 | 1,57062 | 9,0247 | 59,2661 | 1,8751 | 1,858278 | 59,24504 | 67,4282 |
| 2280 | 1,385841 | 6,658 | 27,2281 | 0,8826 | 0,867908 | 27,22001 | 55,9423 |
| 2290 | 1,57062 | 7,6514 | 35,84 | 1,1678 | 1,152214 | 35,81894 | 69,4228 |
| 2300 | 1,385841 | 6,6585 | 27,0304 | 0,8797 | 0,865007 | 27,02231 | 43,369 |
| 2310 | 1,57062 | 7,6517 | 35,8777 | 1,1684 | 1,152813 | 35,85664 | 57,0195 |
| 2320 | 1,385841 | 6,7083 | 27,8442 | 0,9032 | 0,888463 | 27,83611 | 33,2794 |
| 2330 | 1,57062 | 7,6518 | 35,8607 | 1,1666 | 1,151013 | 35,83964 | 41,7984 |

| TEST NO. | $V_m$ [m/s] | $n_2$ [Hz] | $T_2$ [N] | $Q_2$ [Nm] | $Q_{corr}$ [Nm] | $T_{corr}$ [N] | $F_{D2}$ [N] |
|---|---|---|---|---|---|---|---|
| 2200 | 1,385841 | 8,19 | 49,41 | 1,546 | 1,529929 | 49,40191 | 16,1 |
| 2210 | 1,57062 | 8,934 | 56,52 | 1,781 | 1,764259 | 56,49894 | 22,6 |
| 2220 | 1,385841 | 9,023 | 64,3856 | 2 | 1,983179 | 64,37751 | 13,834 |
| 2230 | 1,57062 | 9,38 | 65,1976 | 2,05 | 2,032858 | 65,17654 | 24,4831 |
| 2240 | 1,385841 | 9,375 | 71,7968 | 2,2297 | 2,212563 | 71,78871 | 21,4761 |
| 2251 | 1,57062 | 10,3103 | 84,6661 | 2,6445 | 2,626521 | 84,64504 | 24,85 |
| 2260 | 1,385841 | 10,6972 | 100,9327 | 3,0904 | 3,072073 | 100,9246 | 24,615 |
| 2271 | 1,57062 | 11,4873 | 112,5361 | 3,4695 | 3,450461 | 112,515 | 25,2563 |
| 2280 | 1,385841 | 10,0096 | 85,0277 | 2,6234 | 2,605691 | 85,01961 | 10,2895 |
| 2290 | 1,57062 | 10,9957 | 100,452 | 3,1079 | 3,089304 | 100,4309 | 15,2248 |
| 2300 | 1,385841 | 9,5024 | 74,4078 | 2,3086 | 2,291348 | 74,39971 | 4,7605 |
| 2310 | 1,57062 | 10,0146 | 78,4703 | 2,4547 | 2,436987 | 78,44924 | 21,1281 |
| 2320 | 1,385841 | 7,993 | 46,7053 | 1,4783 | 1,462406 | 46,69721 | 16,6013 |
| 2330 | 1,57062 | 8,8346 | 55,3831 | 1,7609 | 1,744249 | 55,36204 | 26,405 |

Measured values for propulsion in regular waves without the Mewis-Duct fitted:

| TEST NO. | $V_m$ [m/s] | $n_1$ [Hz] | $T_1$ [N] | $Q_1$ [Nm] | $Q_{corr}$ [Nm] | $T_{corr}$ [N] | $F_{D1}$ [N] |
|---|---|---|---|---|---|---|---|
| 2400 | 1,385841 | 6,6602 | 23,6961 | 0,8061 | 0,791406 | 23,68801 | 35,7039 |
| 2410 | 1,57062 | 7,6539 | 31,7544 | 1,0801 | 1,064511 | 31,73334 | 41,1546 |
| 2420 | 1,385841 | 6,66 | 24,0878 | 0,8159 | 0,801206 | 24,07971 | 44,4579 |
| 2430 | 1,57062 | 7,6535 | 31,9547 | 1,0854 | 1,069812 | 31,93364 | 49,2518 |
| 2440 | 1,385841 | 6,6599 | 24,2142 | 0,8214 | 0,806706 | 24,20611 | 59,4681 |
| 2450 | 1,57062 | 7,6533 | 32,0933 | 1,0894 | 1,073812 | 32,07224 | 65,9027 |
| 2460 | 1,385841 | 6,6599 | 24,1262 | 0,8202 | 0,805506 | 24,11811 | 82,3554 |
| 2471 | 1,57062 | 7,6534 | 32,1935 | 1,0928 | 1,077212 | 32,17244 | 94,1144 |
| 2480 | 1,385841 | 6,6602 | 24,2847 | 0,822 | 0,807306 | 24,27661 | 61,0289 |
| 2490 | 1,57062 | 7,6534 | 32,3169 | 1,0949 | 1,079312 | 32,29584 | 71,9374 |
| 2500 | 1,385841 | 6,6601 | 24,0896 | 0,8166 | 0,801906 | 24,08151 | 46,4505 |
| 2510 | 1,57062 | 7,6538 | 32,2843 | 1,0955 | 1,079912 | 32,26324 | 61,4953 |
| 2520 | 1,385841 | 6,6599 | 24,256 | 0,8212 | 0,806506 | 24,24791 | 35,4661 |
| 2530 | 1,57062 | 7,6537 | 32,3312 | 1,0937 | 1,078112 | 32,31014 | 45,2931 |

| TEST NO. | $V_m$ [m/s] | $n_2$ [Hz] | $T_2$ [N] | $Q_2$ [Nm] | $Q_{corr}$ [Nm] | $T_{corr}$ [N] | $F_{D2}$ [N] |
|---|---|---|---|---|---|---|---|
| 2400 | 1,385841 | 8,2264 | 46,0234 | 1,4993 | 1,483196 | 46,01531 | 16,954 |
| 2410 | 1,57062 | 8,8943 | 51,2006 | 1,6824 | 1,665695 | 51,17954 | 24,371 |
| 2420 | 1,385841 | 9,025 | 59,9099 | 1,9281 | 1,911278 | 59,90181 | 15,5999 |
| 2430 | 1,57062 | 9,386 | 60,221 | 1,9626 | 1,945453 | 60,19994 | 25,697 |
| 2440 | 1,385841 | 9,3795 | 66,9388 | 2,1413 | 2,124158 | 66,93071 | 22,2307 |
| 2450 | 1,57062 | 10,313 | 78,6586 | 2,5276 | 2,509618 | 78,63754 | 26,5782 |
| 2460 | 1,385841 | 10,7 | 95,3004 | 2,9848 | 2,96647 | 95,29231 | 26,7189 |
| 2471 | 1,57062 | 11,4907 | 106,1806 | 3,3405 | 3,321458 | 106,1595 | 37,0476 |
| 2480 | 1,385841 | 10,013 | 80,0742 | 2,5282 | 2,510488 | 80,06611 | 13,1808 |
| 2490 | 1,57062 | 10,9997 | 94,4784 | 2,9914 | 2,9728 | 94,45734 | 19,2891 |
| 2500 | 1,385841 | 9,5082 | 69,4824 | 2,2111 | 2,193843 | 69,47431 | 5,9112 |
| 2510 | 1,57062 | 10,0195 | 72,9015 | 2,3441 | 2,326382 | 72,88044 | 23,3252 |
| 2520 | 1,385841 | 7,9946 | 42,9641 | 1,4003 | 1,384405 | 42,95601 | 19,0467 |
| 2530 | 1,57062 | 8,8372 | 50,6473 | 1,661 | 1,644347 | 50,62624 | 28,1691 |

## APPENDIX D: Results of model tests of the Mewis Duct

The table below is reproduced from Mewis (2012).

| No. | Towing Tank | Ship type | DWT | V [kts] | CB | CTh | Power reduction Design T | Ballast T |
|---|---|---|---|---|---|---|---|---|
| **1** | HSVA | BC | 118k | 14,5 | 0,847 | 2,27 | 6,9 | 6 |
| **2** | SVA | BC | 12k | 15,5 | 0,794 | 1,88 | 8 | 7,4 |
| **3** | HSVA | BC | 45k | 15,2 | 0,802 | 1,43 | 6 | 5,4 |
| **4** | SSPA | BC | 41k | 15,2 | 0,795 | 2,1 | 6 | 11 |
| **5** | SSPA | VLCC | 318k | 16 | 0,813 | 2,24 | 6,4 | 7,8 |
| **5a** | HMRI | „ | „ | „ | „ | „ | 6,2 | 7 |
| **6** | SSPA | BC | 180k | 15,2 | 0,847 | 1,98 | 5 | 8,5 |
| **7** | HSVA | COT | 158k | 14,6 | 0,821 | 1,4 | 3,9 | - |
| **8** | HSVA | HLC | 20.5k | 17,5 | 0,765 | 1,83 | 1,5 | - |
| **9** | HSVA | BC | 57k | 14,4 | 0,848 | 2,05 | 5,4 | 7,2 |
| **10** | HSVA | BC | 163k | 14,5 | 0,817 | 2,25 | 5,2 | 6,6 |
| **11** | HSVA | BC | 75k | 16 | 0,879 | 1,86 | 4,5 | 7,1 |
| **12** | SVA | RoRo | 38.5k | 20,2 | 0,687 | 1,1 | 2,7 | 3,4 |
| **13** | MARINTEK | BC | 37.5k | 15 | 0,776 | 2,32 | 7,6 | 7,8 |
| **13a** | MARIN | „ | „ | „ | „ | „ | 6,5 | 6,2 |
| **14** | MARINTEK | BC | 40k | 15 | 0,808 | 2,75 | 9 | 10 |
| **15** | MARIN | VLCC | 306k | 15,3 | 0,821 | 2,1 | 8,7 | 7,6 |
| **16** | SVA | BC | 45k | 15,6 | 0,8 | 1,98 | 6,5 | 8,9 |
| **17** | HSVA | BC | 151k | 15,6 | 0,815 | 2,24 | 5,3 | - |
| **18** | MARINTEK | BC | 35k | 14,2 | 0,83 | 2,31 | 6,5 | 9 |
| **19** | SVA | COT | 74.7k | 15 | 0,856 | 1,74 | 4,9 | 5,4 |
| **20** | SVA | BC | 82k | 16,8 | 0,876 | 2 | 5,1 | - |
| **21** | HSVA | BC | 286k | 15,4 | 0,85 | 2,14 | 7,6 | 10,2 |
| **22** | HSVA | MPC | 31k | 18 | 0,755 | 1,16 | 3,6 | 3,3 |
| **23** | HSVA | MPV | 47,8 | 15,5 | 0,795 | 1,37 | 2,4 | - |
| **24** | SSPA | BC | 82k | 14,5 | 0,87 | 1,79 | 5,7 | 10,5 |
| **25** | HMRI | VLCC | 318k | 16 | 0,814 | 2,18 | 6 | - |
| **26** | FORCE | BC | 35k | 14 | 0,818 | 1,43 | 1,8 inval. | 4,6 inval. |
| **26a** | SSPA | „ | „ | „ | „ | „ | 4,5 | - |
| **27** | MARINTEK | BC | 205k | 14,6 | 0,832 | 2,17 | 7,2 | - |
| **28** | SSPA | BC | 180k | 15,4 | 0,852 | 2,36 | 4,8 | 7,2 |
| **29** | HSVA | BC | 52k | 15,5 | 0,791 | 2,56 | 9,6 | 9,7 |
| **30** | HMRI | VLCC | 318k | 16 | 0,814 | 2,2 | 6,3 | - |
| **31** | SSPA | COT | 114k | 15,2 | 0,834 | 2,37 | 5,1 | - |
| **32** | FORCE | BC | 32k | 13,7 | 0,82 | 2,31 | 6,8 | - |
| **33** | SSPA | T | 150k | 14 | 0,774 | 1,74 | 4,7 | - |
| **34** | SVA | BC | 37,5 | 14,5 | 0,833 | 2,79 | 7,8 | 8,9 |
| **35** | HSVA | BC | 63,5k | 14,5 | 0,86 | 1,45 | 0,9 | 2,5 |
| **36** | SVA | BC | 49,6k | 14,5 | 0,795 | 1,74 | 5,6 | 9 |

| | | | | | | | | |
|---|---|---|---|---|---|---|---|---|
| **37** | SVA | BC | 57k | 13,9 | 0,861 | 2,86 | 8,1 | - |
| **38** | SSPA | BC | 53k | 14 | 0,848 | 2,5 | 3,4 | 3,7 |
| **39** | MOERI | BC | 157k | 15 | 0,819 | 2,11 | 5,6 | 6 |
| **40** | SVA | BC | 58k | 13,9 | 0,841 | 2,37 | 10,2 | - |
| **41** | HSVA | BC | 40k | 15 | 0,803 | 1,9 | 6,3 | - |
| **42** | FORCE | BC | 52k | 15,4 | 0,772 | 1,57 | 4,7 | 6,2 |
| **43** | MARINTEK | T | 74,7 | 14,6 | 0,843 | 2,45 | 4,5 | - |
| **44** | HSVA | BC | 36 | 14,1 | 0,82 | 1,63 | 6,1 | 7,2 |
| **45** | SSPA | BC | 105 | 14,2 | 0,817 | 2,37 | 5,6 | 5,7 |
| **46** | SSPA | T | 316 | 16 | 0,813 | 1,78 | 7,1 | 7,2 |
| **47** | SVA | BC | 35k | 14 | 0,805 | 1,35 | 3,2 | 5,2 |
| **48** | FORCE | BC | 113k | 14,6 | 0,834 | 2,29 | 6,6 | - |
| | | | average design/ballast | | | | 5,8 | 7,1 |
| | | | average of all tests | | | | 6,3 | |